

Doctoral Dissertation

Architectural Design Approach Facilitating Energy Simulation as  
Design Performance Modeling

建築設計初期段階におけるエネルギーシミュレーションの効率化  
に関する研究

温 麗維

Graduate School of Science and Engineering

Yamaguchi University

August 2017

# Contents

Abstract.....	V
Acknowledgements.....	VIII
List of Figures.....	IX
List of Tables.....	XV
List of publications.....	XVII
<b>1. Introduction.....</b>	<b>1</b>
1.1 General context.....	3
1.1.1 Urgency of energy efficiency and CO <sub>2</sub> emissions reduction.....	3
1.1.2 Why the building sector.....	4
1.1.3 Increasing demand on energy efficiency and environmental performance.....	5
1.1.4 Integrated design.....	8
1.2 Design performance modeling.....	10
1.2.1 The definition of DPM and a comparison between DPM and BEM.....	10
1.2.2 Barriers to integrate DPM into the design process.....	13
1.2.3 Previous studies for addressing these barriers.....	15
1.3 Research objective of this study.....	17
1.4 Construction of this study.....	18
1.5 Confirm the inputs this study selected to support their default values assignment.....	23
1.5.1 A review on ten simple tools.....	23
1.5.2 The necessary inputs and their organization approaches.....	27

Reference.....	33
<b>2. A method for creating recommended window-to-wall ratios (WWR) maps to provide information on optimal window area for DPM.....</b>	<b>39</b>
2.1 General statement.....	40
2.2 Method for creating recommended WWR maps.....	42
2.3 Case study.....	44
2.3.1 Distribution of optimal WWR under different design conditions.....	44
2.3.1.1 Basic simulation conditions .....	44
2.3.1.2 Variable design conditions.....	49
2.3.1.3 Investigation Results.....	55
2.3.1.4 Discussion.....	69
2.3.2 Recommended WWR maps based on optimization calculation.....	74
2.3.2.1 Optimization scheme.....	74
2.3.2.2 Recommended WWR maps.....	78
2.4 Summary.....	83
Appendix A.....	86
Appendix B.....	88
Appendix C.....	92
Reference.....	96
<b>3 A method for creating response surface to provide information on optimal window geometry.....</b>	<b>100</b>
3.1 General statement.....	101

3.2 Method for creating response surface.....	102
3.2.1 Dynamic daylighting simulation.....	103
3.2.2 Energy simulation.....	104
3.2.3 Estimation on the total electric energy consumption.....	104
3.3 Case study.....	106
3.3.1 Basic condition.....	106
3.3.2 Dynamic daylighting simulation.....	109
3.3.3 Energy simulation.....	113
3.3.4 Total electric energy consumption.....	115
3.4 Validation of the proposed method.....	117
3.4.1. Estimation of cDA using the link between DF and cDA.....	117
3.4.2. Estimation of the total electric energy consumption using the proposed method.....	118
3.5 Summary.....	121
Appendix.....	123
Reference.....	125
<b>4 Target air change rate and natural ventilation potential maps for assisting with preliminary natural ventilation design.....</b>	<b>127</b>
4.1 General statement.....	128
4.2 Theory.....	130
4.2.1 Definition of the target air change rate.....	130
4.2.2 Simple method for estimating the target air change rate.....	132
4.2.3 Application of the target air change rate in preliminary design of natural ventilation....	136
4.3 Validating the robustness of the target air change rate using a case study of China.....	136

4.3.1	Base simulation conditions.....	136
4.3.2	Variable design conditions.....	138
4.3.3	Simulation results.....	140
4.4	Case study.....	143
4.4.1	Base conditions for maps creation.....	143
4.4.2	Target air change rate and natural ventilation potential maps in China.....	143
4.5	Summary.....	152
	Appendix A.....	154
	Appendix B.....	155
	Reference.....	160
<b>5</b>	<b>Conclusion and future work.....</b>	<b>164</b>
5.1	Key findings of this study.....	165
5.2	Future work.....	170

# Abstract

Facing the increasing demand on energy efficiency and sustainability certificate, building energy/performance simulations are increasingly required to be integrated into the early design stages because that the design decisions made in these stages significantly impact the final performance of buildings. These simulations performed in the concept and schematic design stages for informing design decisions are named as design performance modeling (DPM) by American Institute of Architects (AIA). However, the numerous uncertainties on design parameters during the early design stages complicate the integration of DPM. In addition, insufficient intelligence approaches which can be used to inform design decisions based on the analysis results also impedes the exertion of the effect of DPM in guiding the design towards better performance. The main purpose of this thesis is to develop flexible approaches for facilitating the high accuracy and efficiency implementation of DPM towards performance-based design decisions making. To achieve this goal, we conduct the study in two aspects. The first aspect is to develop approaches for assigning robust default values which are defined as tentative values for uncertain design parameters required by DPM for discussing a target design variable. The other aspect is to develop an efficient approach for performing DPM and informing the corresponding design decisions. This thesis is constituted as follows.

Chapter 1 firstly presents the research background, purpose, and the construction of this thesis. The following review study in this Chapter focuses on simple building performance evaluation tools which are supposed as tools for performing DPM in this study. The reason is that these simple tools can be used to perform DPM with less detailed building information as inputs. The necessary inputs of ten simple tools and their organization measures are reviewed to search the inputs which are difficult to be accessed in design practice. An additional criterion is that these inputs have an influential impact on the evaluation results. Consequently, window configuration including rough window area and window geometry, and natural ventilation information including air change rate and rough natural

ventilation strategies are selected as the support objects of this thesis.

Chapter 2 describes an approach developed for supporting the default value assignment of rough window area which is represented as window-to-wall ratio (WWR) and generally required in the beginning stages of design process. It is realized by the creation of recommended WWR maps based on the analysis results of integrated simulation investigations and optimizations. A case study is conducted to create recommended WWR maps in Japan. The novelty of the proposed maps is to show architects with the recommended setting direction of WWR towards which building performance becomes better in contrast to global optimal default values. According to the integrated simulation results from case study, the distribution of the optimal WWR under varying design conditions exhibits three overall patterns: (i) As the WWR decreases, the CO<sub>2</sub> emissions decrease. (ii) An appropriate WWR value exists (30-50 %) at which the CO<sub>2</sub> emissions are minimized. (iii) As the WWR increases, the CO<sub>2</sub> emissions decrease. Therefore, three options of a small, moderate, or large default WWR value are available from the created maps according to the characteristic of new projects.

With the design progressing, the default WWR value mentioned in Chapter 2 can be replaced by the actual design value. Therefore, Chapter 3 develops an efficient approach for performing DPM to assist the determination of optimal window geometry including window height, window width and window location in the floor. A procedure for creating the response surfaces between window geometries and building performance by combining the analysis results of dynamic daylighting simulation which is performed to analyze the daylight use and energy simulation is developed. The response surfaces can not only show architects with the optimal solution but also help architects to understand to what extent they can widen or narrow the window geometry without significantly decreasing the building performance. The novelty of the proposed procedure is to address the enormous number of simulations for exploring the surface features. It is realized by the adoption of the link between daylight factor (DF) and continuous daylight autonomy (cDA). In case studies, the

daylighting simulation tool of DAYSIM and energy simulation tool of EnergyPlus are used to create response surfaces. With the proposed link, the number of dynamic daylighting calculation which trends to time consuming is limited to be only one. In addition, the lighting electric saving can also be calculated using the results from DAYSIM and EnergyPlus simulations. The impact of COPs for the cooling/heating systems on the features of the response surface can be easily determined. Higher COP results in a narrow selectable design range of window geometry in case where the same percentage of building performance degradation is acceptable. The proposed method is also validated in this Chapter.

Chapter 4 describes a developing approach from an earlier study for supporting the data filling associated with natural ventilation. This approach is achieved by showing the maps of target air change rate. It is defined as an air change rate at which the increase in cooling effect from natural ventilation reaches the maximum value. The ultimate purpose of this Chapter is to create the world target air change rate maps for facilitating the early natural ventilation design. However, it is necessary to confirm the robustness of target air change rate under the representative conditions of building model and construction specifications in advance of the maps creation for a country. Therefore, this Chapter reports the availability of this method in China. Case studies are firstly conducted to examine the robustness of the target air change rate using a typical Chinese office building model with representative operation conditions in five climate zones of China. Then, the target air change rate and natural ventilation potential maps from China are created based on the verified method to inform the air change rate and rough natural ventilation strategy. For example, well organized natural ventilation strategies with an air change rate above 3ac/h are required in the Hot Summer and Warm Winter zone and Temperate zone under moderate internal gains condition. These strategies are particularly suggested for cities in the Temperate zone due to the higher available cooling potential.

For final conclusions, Chapter 5 summarized the main findings of this study and recommended key areas for further studies.



# Acknowledgements

First of all, I would like to express my deepest gratitude to my supervisor Professor Makoto Koganei, for giving me the opportunity to conduct this study and complete my thesis in the Human Environmental Engineering laboratory of Faculty of Engineering, Yamaguchi University. He always encourages me to challenge in research and provides lots of support. I would like to particular thank Associate Professor Kyosuke Hiyama in Meiji University who directly supervised me in the first one and half years of my doctoral study in Yamaguchi University. The work in this thesis could not completed without the continuous support, patience, invaluable advice, knowledge, and meaningful discussion provided by Associate Professor Kyosuke Hiyama.

I would like to express my thanks to my vice-supervisors, Professor Kazuhiro Fukuyo and Professor Hideaki Izumi, for their penetrating advice in the construction of this thesis. I also express my thanks to other members of the dissertation examination committee Professor Masanori Fujita and Assistant Professor Hyun-tae Kim for their valuable suggestions and comments in revising this thesis to improve the quality of my thesis.

I also want to express my sincere gratefulness to all members in my laboratory including Yoshinao Sato, Hirotsugu Okada, Kentaro Miyauchi, Miki Nagamoto, Mika Nomura, Mitusyuki Kudo, Kaho Shiraishi, Yusuke Morita, Fangzhou Lu for their care in dairy life. It is a pleasure time to conduct the research together with them. I also want to thank Associate Professor Ryoichi Kuwahara for his constructive advice in the revision stage of my thesis.

At last but not the least, I would like to express my thanks to my beloved parents and husband, Dr. Yang Wu, for their love, support, and encouragement throughout the duration my doctoral study.

# List of Figures

Figure 1.1 (a) Historical CO <sub>2</sub> emissions and predicted CO <sub>2</sub> emissions ranges for representative concentration pathways (RCPs) until 2100. (b) The increase in global mean surface temperature when the global CO <sub>2</sub> emissions reach a given net cumulative total. Source: IPCC (2014) report.....	3
Figure 1.2 United States energy consumption by sector. (b) United States CO <sub>2</sub> emissions by sector. Source: U.S. Energy Information Administration (eia 2017), accessed at February.....	4
Figure 1.3 Japan energy consumption by sector. (b) Japan CO <sub>2</sub> emissions by sector. Source (a): Japan Energy white paper 2016, accessed at February. Source (b): Greenhouse Gas Inventory Office of Japan, accessed at February.....	5
Figure 1.4 Design stages and energy models types. Source: AIA 2012 pp.8.....	10
Figure 1.5 Time (fee) spend within the phases of the design process for business as usual and integrated project delivery. Source: AIA 2012 pp.28.....	13
Figure 1.6 Research flow chart of this study.....	22
Figure 1.7 Reliable sources of BP data.....	30
Figure 2.1 Flow chart of recommended WWR map creation.....	43
Figure 2.2 3D model of the building model.....	45
Figure 2.3 Plan view of the building model.....	45
Figure 2.4 Correlation between lighting output and input power of adopted continuous dimming control system.....	48
Figure 2.5 Locations of the daylight sensors in zones 1 and 2.....	49
Figure 2.6 Three cities (Sapporo, Tokyo, and Naha) selected for simulation.....	51
Figure 2.7 Activity schedules for a weekday.....	52

Figure 2.8 Space depth of the building.....	53
Figure 2.9 Variations in the window-to-wall Ratio (WWR).....	55
Figure 2.10 Distribution of optimal WWR for three cities and four main orientations of a small-scale building with medium internal gains: (a) Sapporo; (b) Tokyo; (c)Naha.....	55
Figure 2.11 The effects of WWR on the CO <sub>2</sub> emissions corresponding to cooling, heating, and lighting energy use for four orientations in a small-scale building with medium internal gains in Sapporo: (a) South; (b) North; (c) East; (d) West.....	58
Figure 2.12 The effects of WWR on the CO <sub>2</sub> emissions corresponding to cooling, heating, and lighting energy use for four orientations in a small-scale building with medium internal gains in Tokyo: (a) South; (b) North; (c) East; (d) West.....	59
Figure 2.13 The effects of WWR on the CO <sub>2</sub> emissions corresponding to cooling, heating, and lighting energy use for four orientations in a small-scale building with medium internal gains in Naha: (a) South; (b) North; (c) East; (d) West.....	60
Figure 2.14 Distribution of optimal WWR for three cities at low, medium, and high internal gains for an east-facing orientation in a small-scale building: (a) Sapporo; (b) Tokyo; (c) Naha.....	61
Figure 2.15 Distribution of optimal WWR for three cities at low, medium, and high internal gains for a south-facing orientation in a small-scale building: (a) Sapporo; (b) Tokyo; (c) Naha.....	62
Figure 2.16 Distribution of optimal WWR for three cities at low, medium, and high internal gains for a north-facing orientation in a small-scale building: (a) Sapporo; (b) Tokyo; (c) Naha.....	62
Figure 2.17 Distribution of optimal WWR for three cities at low, medium, and high internal gains for a west-facing orientation in a small-scale building: (a) Sapporo; (b) Tokyo; (c) Naha.....	63
Figure 2.18 Distribution of optimal WWR for three cities and four main orientations for a large-scale building with medium internal gains: (a) Sapporo; (b) Tokyo; (c) Naha.....	63
Figure 2.19 Distribution of optimal WWR for three cities at low, medium, and high internal gains for	

an east-facing orientation in a large-scale building: (a) Sapporo; (b) Tokyo; (c) Naha.....	65
Figure 2.20 Distribution of optimal WWR for three cities at low, medium, and high internal gains for a south-facing orientation in a large-scale building: (a) Sapporo; (b) Tokyo; (c) Naha.....	65
Figure 2.21 Distribution of optimal WWR for three cities at low, medium, and high internal gains for a north-facing orientation in a large-scale building: (a) Sapporo; (b) Tokyo; (c) Naha.....	66
Figure 2.22 Distribution of optimal WWR for three cities at low, medium, and high internal gains for a west-facing orientation in a large-scale building: (a) Sapporo; (b) Tokyo; (c) Naha.....	66
Figure 2.23 Representative simulation results for the lighting power density of 5 W/m <sup>2</sup> (a) Distribution of optimal WWR for three cities for a south-facing orientation in a small-scale building with medium internal gains; (b) Distribution of optimal WWR in four main orientations for a small-scale building with medium internal gains located in Tokyo; (c) Distribution of optimal WWR at low, medium, and high internal gains for an east-facing orientation in a small-scale building located in Tokyo; (d) Distribution of optimal WWR for small- and large-scale buildings for a north-facing orientation with medium internal gains located in Naha.....	67
Figure 2.24 The impact of glazing type on optimal WWR configuration (north-facing orientation of Sapporo in small-scale building with medium internal gains under lighting power density of 5 W/m <sup>2</sup> ).....	76
Figure 2.25 Recommended WWR map for a lighting power density of 10 W/m <sup>2</sup> (The four disconnected circle sections represent the four main orientations: top stands for north, bottom for south, left for west, and right for east).....	79
Figure 2.26 Recommended WWR map for a lighting power density of 5 W/m <sup>2</sup> (The four disconnected circle sections represent the four main orientations: top stands for north, bottom for south, left for west, and right for east).....	81
Figure 2.A.1 Distribution of optimal WWR in a small-scale building (Double Low-E glazing; Lighting	

power density of 5 W/m <sup>2</sup> ; Top: Sapporo, Middle: Tokyo, Bottom: Naha; (a) Low internal gains, (b) Medium internal gains, (c) High internal gains).....	86
Figure 2.A.2 Distribution of optimal WWR in a large-scale building (Double Low-E glazing; Lighting power density of 5 W/m <sup>2</sup> ; Top: Sapporo, Middle: Tokyo, Bottom: Naha; (a) Low internal gains, (b) Medium internal gains, (c) High internal gains).....	87
Figure 2.B.1 Distribution of optimal WWR in a small-scale building (Double Clear glazing; Lighting power density of 10 W/m <sup>2</sup> ; Top: Sapporo, Middle: Tokyo, Bottom: Naha; (a) Low internal gains, (b) Medium internal gains, (c) High internal gains).....	88
Figure 2.B.2 Distribution of optimal WWR in a large-scale building (Double Clear glazing; Lighting power density of 10 W/m <sup>2</sup> ; Top: Sapporo, Middle: Tokyo, Bottom: Naha; (a) Low internal gains, (b) Medium internal gains, (c) High internal gains).....	89
Figure 2.B.3 Distribution of optimal WWR in a small-scale building (Double Clear glazing; Lighting power density of 5 W/m <sup>2</sup> ; Top: Sapporo, Middle: Tokyo, Bottom: Naha; (a) Low internal gains, (b) Medium internal gains, (c) High internal gains).....	90
Figure 2.B.4 Distribution of optimal WWR in a large-scale building (Double Clear glazing; Lighting power density of 5 W/m <sup>2</sup> ; Top: Sapporo, Middle: Tokyo, Bottom: Naha; (a) Low internal gains, (b) Medium internal gains, (c) High internal gains).....	91
Figure 2.C.1 Distribution of optimal WWR in a small-scale building (Double Ref-A-H glazing; Lighting power density of 10 W/m <sup>2</sup> ; Top: Sapporo, Middle: Tokyo, Bottom: Naha; (a) Low internal gains, (b) Medium internal gains, (c) High internal gains).....	92
Figure 2.C.2 Distribution of optimal WWR in a large-scale building (Double Ref-A-H glazing; Lighting power density of 10 W/m <sup>2</sup> ; Top: Sapporo, Middle: Tokyo, Bottom: Naha; (a) Low internal gains, (b) Medium internal gains, (c) High internal gains).....	93
Figure 2.C.3 Distribution of optimal WWR in a small-scale building (Double Ref-A-H glazing;	

Lighting power density of 5 W/m <sup>2</sup> ; Top: Sapporo, Middle: Tokyo, Bottom: Naha; (a) Low internal gains, (b) Medium internal gains, (c) High internal gains).....	94
Figure 2.C.4 Distribution of optimal WWR in a large-scale building (Double Ref-A-H glazing; Lighting power density of 5 W/m <sup>2</sup> ; Top: Sapporo, Middle: Tokyo, Bottom: Naha; (a) Low internal gains, (b) Medium internal gains, (c) High internal gains).....	95
Figure 3.1 Flow chart of the calculation steps for creating response surface.....	106
Figure 3.2 Outline of the building model adopted in case study.....	107
Figure 3.3 Redefined window geometry types for case study.....	108
Figure 3.4 The location of illuminance sensors for calculating the link between the DF and cDA...	110
Figure 3.5 Link between the DF and cDA calculated using the type A window geometry (point diagram between the cDA and DF are analyze by DAYSIM).....	111
Figure 3.6 The location of illuminance sensors for calculating the variation in DF due to the change in window geometry.....	112
Figure 3.7 Response surface between the window geometry and cDA.....	112
Figure 3.8 Response surface between the window geometry and cooling load.....	113
Figure 3.9 Response surface between the window geometry and the total electric energy consumption when the COPs of heating/ cooling system are 2.0.....	115
Figure 3.10 Response surface between the window geometry and the total electric energy consumption when the COPs of heating/cooling system are 4.0.....	116
Figure 3.11 Two sensor locations in the cases for the validation.....	118
Figure 3.A.1 The diagrams of DA and cDA.....	124
Figure 4.1 Definition of target air change rate using a simulation result.....	131
Figure 4.2 The image of a mixed-mode (air condition and operate window simultaneously turn....	133
Figure 4.3 The image of natural ventilation mode (air conditioner is off and operate window is	

open).....	134
Figure 4.4 The image of air conditioner mode (air conditioner is on and operate window is off).....	134
Figure 4.5 Geographic and climate divisions in China.....	137
Figure 4.6 Typical office building model used in this study.....	139
Figure 4.7 Maps with a specific internal gains of 10 W/m <sup>2</sup> in China.....	148
Figure 4.8 Maps with a specific internal gains of 20 W/m <sup>2</sup> in China.....	149
Figure 4.9 Maps with a specific internal gains of 40 W/m <sup>2</sup> in China.....	150
Figure 4.10 Maps with a specific internal gains of 80 W/m <sup>2</sup> in China.....	151
Figure 4.B.1 Maps with a specific internal gains of 10 W/m <sup>2</sup> in Japan.....	156
Figure 4.B.2 Maps with a specific internal gains of 20 W/m <sup>2</sup> in Japan.....	157
Figure 4.B.3 Maps with a specific internal gains of 40 W/m <sup>2</sup> in Japan.....	158
Figure 4.B.4 Maps with a specific internal gains of 80 W/m <sup>2</sup> in Japan.....	159

# List of Tables

Table 1.1 Approaches developed in this thesis and their applications in design practice.....	2
Table 1.2 A comparison between DPM and BEM.....	12
Table 1.3 Necessary input data of ten simple tools.....	28
Table 1.4 Necessary Input data without reliable source.....	32
Table 2.1 Thermal properties of the construction elements (layers are listed from outside to inside)...	47
Table 2.2 HVAC system settings.....	48
Table 2.3 Description of design variables.....	50
Table 2.4 Climate characteristic of three cities (Sapporo, Tokyo, and Naha).....	51
Table 2.5 Maximum increase in total CO <sub>2</sub> emissions obtained by replacing the optimal default value with the reference default value (Glazing type: Double Low-E glazing 6mm-13mm-6mm).....	72
Table 2.6 Maximum increase in total CO <sub>2</sub> emissions obtained by replacing the optimal default value with the reference default value (Glazing type: Double Clear glazing 6mm-13mm-6mm).....	72
Table 2.7 Maximum increase in total CO <sub>2</sub> emissions obtained by replacing the optimal default value with the reference default value (Glazing type: Double Ref-A-H glazing 6mm-13mm-6mm).....	72
Table 2.8 Maximum increase in total CO <sub>2</sub> emissions obtained by replacing the optimal default value with a non-optimal value (Double Low-E glazing).....	74
Table 2.9 Basic information of the ten selected locations.....	75
Table 2.10 Selected glazing types (the values in the parentheses indicate the light-to-solar Gain ratio, which is defined as the visible transmittance (VT) divided by the solar heat gain coefficient (SHGC)).....	77
Table 2.11 Optimal glazing types for a lighting power density of 10 W/m <sup>2</sup> .....	82



Table 2.12 Optimal glazing types for a lighting power density of 5 W/m <sup>2</sup> .....	83
Table 3.1 Utilized radiance simulation parameters.....	109
Table 3.2 Material properties of the investigated model.....	110
Table 3.3 Conditions for energy simulation.....	114
Table 3.4 Comparison of the DAYSIM results and the estimated results by the link between the DF and cDA which is obtained from the result of the type A window geometry.....	117
Table 3.5 Comparisons among the estimations for each window type.....	120
Table 4.1 Climate characteristics and the required U values of envelopes in five representative cities.....	139
Table 4.2 Simulation conditions.....	140
Table 4.3 U value of the external wall in each selected city (W/m <sup>2</sup> K).....	140
Table 4.4 Target air change rates under the typical internal gains condition.....	142
Table 4.5 Target air change rates under the high level internal gains condition.....	142
Table 4.6 36 Selected cities for the creation of maps.....	144
Table 4.7 Parameters for evaluating the target air change rate and natural ventilation potential.....	145
Table 4.B.1 Target air change rate and natural ventilation in 46 selected cities of Japan.....	155

# List of Publications

## Refereed Journal Papers

**L. Wen**, K. Hiyama, M. Koganei, A method for creating maps of recommended window-to-wall ratios to assign appropriate default values in design performance modeling: A case study of a typical office building in Japan, *Energy and Buildings*, 145 (2017) 304-317.

[Chapter 2]

K. Hiyama, **L. Wen**, Rapid response surface creation method to optimize window geometry using dynamic daylighting simulation and energy simulation, *Energy and Buildings*, 107 (2015) 417–423.

[Chapter 3]

## Refereed Conference Papers

**L. Wen**, K. Hiyama, INFLUENCE OF DESIGN CONDITIONS ON THE DISTRIBUTION OF OPTIMAL WINDOW TO WALL RATIO FOR A TYPICAL OFFICE BUILDING IN JAPAN. In *Proceedings of Building Simulation and Optimization 2016: Third IBPSA - England Conference, Newcastle*, pp. 60–67.

[2.3.1 in Chapter 2]

**L. Wen**, K. Hiyama, A review: simple tools for evaluating the energy performance in early design stages. *Procedia Engineering (8th International Cold Climate HVAC 2015 Conference, CCHVAC 2015)*, 146 (2016) 32–39.

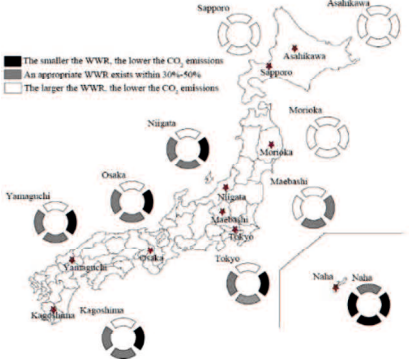
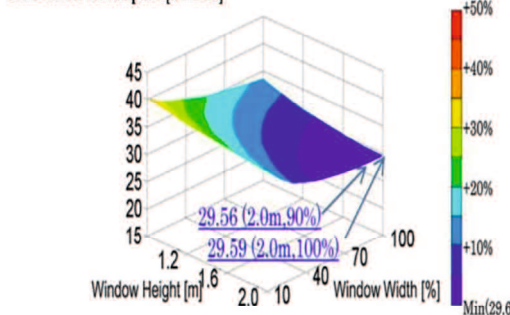
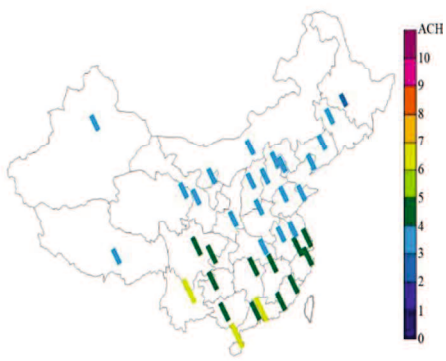
[1.5 in Chapter 1]

# 1.

## Introduction

Facing the challenges of increasing demand of energy efficiency and sustainability certificate, building performance simulations are increasingly required to be integrated into the early design stages because that the design decisions made in these stages significantly impact the final performance of buildings. American Institute of Architects (AIA) which usually publishes exemplary standards for design practice defines the building performance simulations performed in the concept and schematic design stages as design performance modeling (DPM). DPM is mainly employed to inform advisable design decisions and design directions making the design towards better energy and environmental performance. However, the implement of DPM is encountered with two major barriers. Firstly, numerous uncertainties associated with design parameters which are required as inputs by DPM during the early design stages complicate the integration of DPM into the design process. Secondly, insufficient intelligence approaches which can be used to inform design decisions based on the analysis results also impedes the exertion of DPM in guiding designs towards better performance. In this context, the main purpose of this thesis is to develop flexible approaches for facilitating the high accuracy and efficiency implementation of DPM towards performance-based design decisions making. To achieve this goal, we conduct the study in two aspects. The first aspect is to develop approaches for assigning robust default values, which are defined as tentative values, for the uncertain design parameters required as inputs by DPM for discussing a target design variable (Chapter 2 and 4). The other aspect is to develop an approach for assisting the efficient implementation of DPM and informing the corresponding design decisions based on the modeling results (Chapter 3). The approaches developed in this thesis and their application in design practice are summarized in Table 1.1.

Table 1.1. Approaches developed in this thesis and their applications in design practice.

<p><b>Approaches developed in this thesis</b></p>	<p><b>Chapter/Research aspect</b></p>	<p><b>Application in design practice</b></p>
<p><b>Recommend WWR map</b></p> 	<p>Chapter 2/Research aspect 1 (approach for supporting the assignment of uncertain input of WWR in DPM)</p>	<p>According to the critical design conditions, A larger, a moderate, or a smaller recommended default WWR value can be obtained from the proposed maps.</p>
<p><b>Response surface between window geometry and building performance</b></p> <p>Total electric consumption [kWh/m<sup>2</sup>]</p> 	<p>Chapter 3/Research aspect 2 (approach for assisting the implement of DPM to discuss window geometry)</p>	<p>Optimal and accepted range of window geometry (window width and height) can be obtained from the proposed three-dimensional contours.</p>
<p><b>Target air change rate map</b></p> 	<p>Chapter 4/Research aspect 1 (approach for assigning uncertain input of air change rate for natural ventilation in DPM)</p>	<p>Air change rate and rough strategies of natural ventilation can be obtained from the proposed maps based on the conditions of climate and internal gains.</p>

## 1.1 General context

### 1.1.1 Urgency of energy efficiency and CO<sub>2</sub> emissions reduction

Climate changes, such as global warming, sea level increase and snow/ice cover decrease, has become increasingly remarkable in the last three decades. According to the Fifth Assessment Report of Intergovernmental Panel on Climate Change, the increase in averaged combined land and ocean surface temperature was 0.85 °C from 1880 to 2012 (IPCC 2014). These climate changes are mainly caused by human activities, such as economic and population growth. Four scenarios defined in the IPCC report show the predicted amount of anthropogenic greenhouse gas (CO<sub>2</sub>) emissions and the rise in global mean surface temperature, as shown in Figure 1.1. Only the stringent mitigation scenario (RCP 2.6) is capable of maintaining the temperature increase within 2 °C in comparison with the pre-industrial levels. It requires that the amount of CO<sub>2</sub> emissions attains the peak value by 2020. Therefore, immediate and sustained measures for the anthropogenic CO<sub>2</sub> emissions reduction are necessary. These measures are particularly urgent for sectors that heavily rely on fossil fuels combustion.

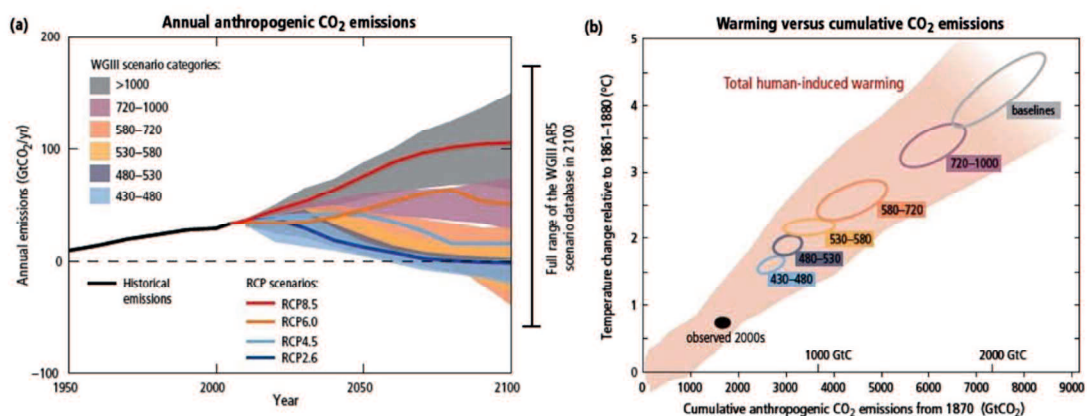


Figure 1.1. (a) Historical CO<sub>2</sub> emissions and predicted CO<sub>2</sub> emissions ranges for representative concentration pathways (RCPs) until 2100. (b) The increase in global mean surface temperature when the global CO<sub>2</sub> emissions reach a given net cumulative total. *Source: IPCC (2014) report.*

### 1.1.2 Why the building sector

Building, industry, and transportation are known as three major energy consumers all over the world. The energy consumption and CO<sub>2</sub> emissions by the building sector in two representative developed countries of United States and Japan are shown in Figures 1.2 and 1.3. It is obvious that both of energy consumption and CO<sub>2</sub> emissions by the building sector in United States are close to 40 % of the total values. In Japan, approximate one third of the final energy consumption and the CO<sub>2</sub> emissions are associated with buildings. In the case of developing countries, the building sector accounted for 37 % of the total energy consumption in China (Ji et al. 2009). It was reported that the corresponding proportion was around 36 % in India (Energy & Special 2015). It was also pointed that these ratios in developing countries would continue to increase due to further population growth, urbanization, and the living standards improvement (Levine et al. 2007).

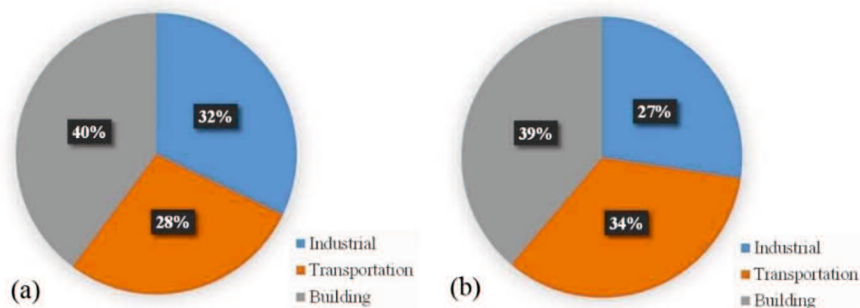


Figure 1.2. (a) United States energy consumption by sector. (b) United States CO<sub>2</sub> emissions by sector. *Source: U.S. Energy Information Administration (eia 2017), accessed at February.*

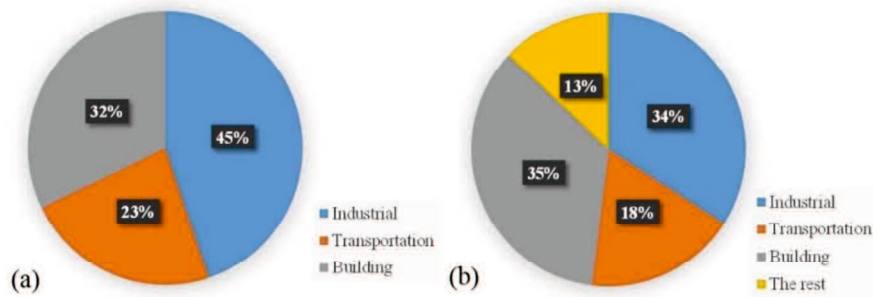


Figure 1.3. (a) Japan energy consumption by sector. (b) Japan CO<sub>2</sub> emissions by sector.

*Source (a): Japan Energy white paper 2016, accessed at February. Source (b): Greenhouse Gas Inventory Office of Japan, accessed at February.*

Moreover, building operations, such as space heating, cooling, and lighting, are greatly dependent on electricity which is commonly generated from fossil fuels combustion. For example, 75 % of the total electricity in United States was used to operate buildings (Viebahn et al. 2013). Thus, energy efficiency in building sector makes a dominant contribution to mitigate anthropogenic CO<sub>2</sub> emissions. With this background, severe energy policies have been regulated and enforced in most of countries around the world.

### 1.1.3 Increasing demand on energy efficiency and environmental performance

In recent years, world-wide attentions have been paid on the rigorous energy saving objective of zero energy building (ZEB) or carbon-neutral building because that buildings are the major sources of global energy and CO<sub>2</sub> emissions as mentioned above. In Japan, MEIT (Ministry of Economy, Trade and Industry) organized the first conference to discuss the development and realization of net zero energy building (NZEB) (新成長戦略 2010). In this conference, two development stages of NZEB

in Japan were schemed. The first stage was the promotion stage of NZEB in which specific buildings in Japan were going to realize NZEB until 2020. The second stage was the popularization stage of NZEB in which general Japanese buildings were going to be designed to meet NZEB until 2030. NZEB is defined as a building in which the income and expenses of primary energy are nearly equal to zero through the usage of advanced technologies and designs by MEIT. In order to realize NZEB, strategies on three aspects are under consideration. The first aspect is to reduce the built-in load of buildings through the adoption of advanced design technologies. The second aspect is to introduce renewable energy into the buildings through passive technologies. Using the efficient systems to server the load of the buildings are employed as the third aspect. These technologies can not only improve the indoor environment but also reduce the energy consumed for serving the necessary load of the buildings. Meanwhile, the energy self-support degree of the buildings can be enhanced through the adoption of renewable energy. It is clear that NZEB is a contrastive concept. The comparison object is a reference building with the same scale which is designed using previous design technologies. In comparison with the reference building, the reduction on total primary energy consumption of the new designed building is required to be over 50 %. Three grades are set to evaluate the levels of NZEB in Japan. ZEB condition is satisfied when the energy saving rate of designed buildings above 100 %. Nearly ZEB and ZEB Ready are defined when the energy saving rates of designed buildings are above 75 % and 50 %, respectively.

ZEB mainly focus on the balance of the income and expenses of primary energy consumption in buildings. However, besides the energy efficiency performance, the environmental performances, such as security, occupant comfort, service performance, outdoor environment condition and like become increasingly important for the current building design. Therefore, it is necessary to combine the energy efficiency performance evaluation with the building environmental performance evaluation for realizing comprehensive Sustainability. CASBEE (Comprehensive Assessment System for Built



Environment Efficiency developed by Japan Institute for Building Environment and Energy Conservation in 2001) and LEED (Leadership in Energy and Environmental Design developed by U.S. Green Building Council in 1998) are two widely-used environmental performance evaluation systems in Japan. CASBEE supported by Japan national and local governments has been defined to enhance the quality of people's lives and reduce the life-cycle resource use and environmental loads associated with the built environment. CASBEE family includes the tools for evaluating the performances of residence building, public building, city block, and urban. In addition, these evaluation types cover the entire life-cycle of buildings including scheme, newly-built, pre-existing, and renovation. Due to the available incentive and business value, the total numbers of registration for CASBEE had attained 18552 until 2016.3.31 (CASBEE). LEED is accepted as the most popular environmental performance evaluation system all around the world. The oversea users of LEED had exceeded 40 % of the total number. Five types of project can be evaluated by LEED are building design and construction, interior design and construction, building operations and maintenance, neighborhood development, and homes. For the same project type, LEED is flexible enough to be applied by buildings designed with different applications from hospitals to data centers. In addition, in order to meet the developments of building design, further improvement has been made to integrate these environmental performance evaluation systems into the multipurpose building design and comprehensive environmental evaluation.

Facing the challenges of increasing demand on energy efficiency and sustainability certificate, the participants involved in building design and construction should precisely understand, predict, and quantify the energy usage and environmental performance of buildings than ever before. In addition, more than the energy usage and environmental performance evaluation process, the ultimate purpose of these increasingly rigorous energy saving objective and demanded sustainability certificate is to encourage and drive the process of building design and construction towards a higher level. It is important to develop the design with the mind of high environmental performance and energy

efficiency early and throughout the design process.

#### **1.1.4 Integrated design**

In twentieth century, the traditional design approach is a sequential process in which one discipline completes its design work then sends it to the next discipline for the following design. For example, architects firstly start the construction design, such as the shape, orientation, and envelope, and then send the design drawings to the engineers for their subsequent work on mechanical system. The performance simulations are introduced into the design process in a later design stage after the main design decisions making to predict the energy consumption of the building.

With the increasing awareness on sustainability, this separate work way of architecture and engineering and performance simulation/modeling is found to be no longer applicable. In this scenario, architects mostly start their work based on the requirements of building application and aesthetics. They leave the works with regards to building performance to mechanical engineers. However, the construction design significantly impacts the building load. The fixed building load will limit the mechanical systems. Therefore, opportunities for improving building performance are missed. It is clear that such conventional process greatly reduces the efficiency of building designs. Conversely, a tiny change in design may influence the performance of several building systems. To achieve the increasing high energy efficiency and environmental performance goals, a more holistic and collaborative design process is required because that the design, performance, and simulation/modeling process are interacted. That is defined as integrated design in which all of the disciplines involved in the building design and construction work as a team from the beginning (Lynn & Bellenger 2010). Architects, engineers, and modelers should strengthen communications to better understand each other and work together.

Multidisciplinary communications have been valued and implemented in the actual design practice in Japan. Engineers generally provide some design advices for architects in previous meetings during their design process. However, majority of suggestions are made mainly based on the experiences and design philosophy from the engineers and design teams. In this situation, the suggestions would be largely changed due to the different advisers and design firms. The building performance simulations/modeling still tend to be carried out after the major design decisions making in design practice to verify that the design conforms with energy efficiency codes. It means that the design decisions are still made according to the rule and thumb. Energy/performance modeling fails in being integrated into design process. This is also the problem which exists in other countries (The American Institute of Architects 2012).

In addition, the importance of design decisions making in the early design stages and the necessary of instantaneous feedback for informing design decisions during the early design stages have been emphasized in many previous studies. It is because that design decisions making in these stages significantly influences the final performance and cost of buildings (Al-Homoud 1997) (Hong et al. 2000) (Granadeiro, Duarte, et al. 2013) (Samuelson et al. 2016). For example, how architects design the building orientation, shape the building, shade the glass, and introduce the daylighting, passive heating and cooling strategies during the early design stages strongly impact the built-in load of the building, such as space heating, cooling, and lighting. Therefore, the early stages of design process owns the most critical opportunities to achieve energy efficiency and high environmental performance in buildings design. It is vital to conduct the collaborative planning, designing and modeling from this early stages for the improvement of the whole building performance and design efficiency. Therefore, it is urgent to facilitate the integration of energy/performance modeling into the early design stages.

## 1.2 Design performance modeling

### 1.2.1 The definition of DPM and a comparison between DPM and BEM

It is widely accepted that the results obtained from building performance simulations can provide useful information for making design decisions and for guiding the design toward high performance (Kim et al. 2011). In addition, as a communicative language, building performance simulations help design participants, such as the architects, engineers, energy modelers, to work together with and understand each other better. In order to realize the increasing demand of sustainability, building energy/performance simulations should be integrated into the design process early and often.

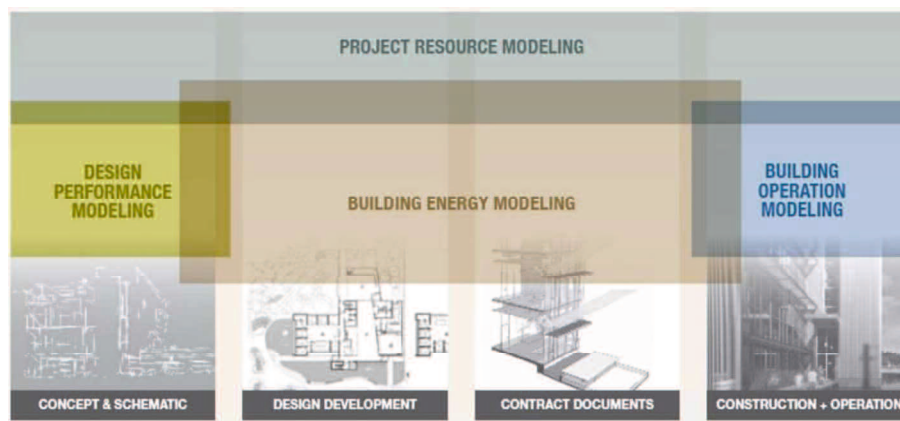


Figure 1.4. Design stages and energy models types. *Source: AIA 2012 pp.8.*

As the model of construction industry American Institute of Architects (AIA) published a design guideline to encourage design teams to integrate computerized simulations into the design process (The American Institute of Architects 2012). In this design guideline, building performance simulations are divided into four categories in accordance with different implement stages, as shown in Figure 1.4. These four categories are design performance modeling in the concept and schematic design stages, building energy modeling in design development and contract document stages, building operation modeling in construction and operation stages, and project resource modeling

throughout the design stages. Among these four simulation categories, the design performance modeling (DPM) and building energy modeling (BEM) are principally associated with the design process. Therefore, DPM and BEM are picked out from the four types modeling.

BEM which is usually performed in a later design stages after design decisions making has been implemented in actual design process. Therefore, a comparison study between DPM and well known BEM is performed for a better understanding of the characteristic of DPM, as summarized in Table 1.2. First, BEM is conducted in the design development and contract documents stages after the production of the building concept and schematic drawing. Whereas, DPM is performed in the concept and schematic stages of design process. Second, BEM intends to verify that the designed project conforms to the energy efficiency code through comparing the predicted energy use of the designed building with the national and local energy codes. However, DPM aims to determine the sensitivities of a wide range of design parameters. This information helps architects to understand the impacts of their strategies on building performance and explore design directions for improving building performance in their designs. Thus, DPM is mainly employed to inform design decisions and design direction towards better building performance. Third, BEM usually requires advanced numerical analysis to obtain the accurate values of building performance. However, it is important to note that DPM should be not complex or time consuming. It is due to that decisions making during early design phases should be in a feasible and timely manner.

It has been mentioned that design, performance, and modeling should be an iterative process. The early modeling works out basic parameters without the consideration of mechanical system. Therefore, as a summary, DPM performed in early design stages works at the basic design parameters including architectural form, window area, shading option, glazing type, R-value of wall and the like by the prediction of a building's energy usage and environmental performance with respect to energy efficiency, daylight penetration, glare control, thermal comfort, natural ventilation and similar factors.

The design decisions based on the results of DPM can improve the overall performance through the comprehension of the interplay between building systems and components, reduction of the energy demand of the building, and proper selection the size of mechanical system.

Table 1.2. A comparison between DPM and BEM.

	Design Performance Modeling (DPM)	Building Energy Modeling (BEM)
Implementation Stages	<ul style="list-style-type: none"> <li>· Concept &amp; Schematic</li> </ul>	<ul style="list-style-type: none"> <li>· Design Development</li> <li>· Contract Document</li> </ul>
Purpose	<ul style="list-style-type: none"> <li>· Determine the sensitivities of design parameters</li> <li>· Inform design decisions</li> </ul>	<ul style="list-style-type: none"> <li>· Predict whole building performance</li> <li>· Demonstrate the project compliance with energy saving codes</li> </ul>
Modeling Characteristics	<ul style="list-style-type: none"> <li>· Simple Model</li> <li>· Require easy and quick analysis</li> </ul>	<ul style="list-style-type: none"> <li>· Complex Model</li> <li>· Require highly accurate analysis</li> </ul>

As a supplement, the images of time/fee spend within different phases of the design process for business as usual (sequential process) and integrated design process is shown in Figure 1.5. The timeline of business as usual is alone the top, and the timeline associated with demanded integrated design process for realizing high performance building is along the bottom. For business as usual, more time is spent in design development, construction document, and construction stages for developing design and implementing simulation. However, for the integrated design process, more time is spent in the early design stages including project brief, predesign, schematic stages. It is clear that the up-front effort and planning will saving the time and cost for revisiting and restarting the design in later phases.

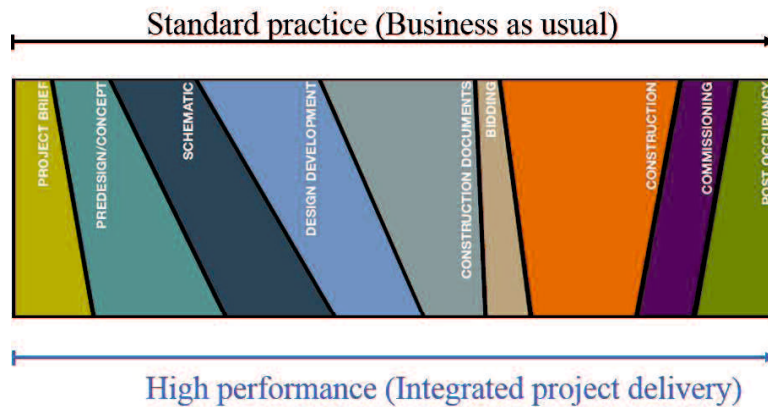


Figure 1.5. Time (fee) spend within the phases of the design process for business as usual and integrated project delivery. *Source: AIA 2012 pp.28.*

### 1.2.2 Barriers to integrate DPM into the design process

Both the DPM and BEM are indispensable for successful high energy efficient building designs. Especially, architects will lose important design opportunities without the design tool of DPM and the instantaneous feedback (Hygh et al. 2012) (Attia et al. 2012) (Samuelson et al. 2016) (Benni et al. 2016). It is strenuous and inefficient to remedy the early design decisions. In conventional design practice, however, architects are more familiar with the manipulation of simulation tools to carry out BEM in later phases of the design process.

The challenges for performing DPM during the early design stages can be summarized into three major aspects. First, the appropriate tools and efficient approach which can be adopted to provide design feedback are insufficient. Although, many sophisticated simulation software which can export a wide range of performance indicators as outputs were developed in the past two decades (Crawley et al. 2008). Majority of the tools are more suitable for the evaluation of the design alternatives after decisions making. It was indicated that only about 10 % of 400 building performance simulation tools listed on DOE software directory were capable of guiding architects in early design stages (Attia &

Herde 2011). In addition, building design is characterized by multi objective, complex, and multidisciplinary. Thus, efficient analysis approaches with the capacity of providing useful information for design decisions making based on the calculation results are insufficient. This also impedes the exertion of the effect of DPM in guiding the design towards better performance. Second, the available time for analysis in early design stages is limited. Simulation requires a large number of input data including design parameters and physical parameters to drive the calculation engine. Collecting these required input data, such as building geometry, envelop materials, is a time-consuming job (Granadeiro, Duarte, et al. 2013). This is especially remarkable for the detailed simulation software which requires hundreds or thousands of input data. Third, some of input data, especially concerned with the design parameters, may not yet be determined in the concept and schematic design stages. In other words, even some of the design parameters are waiting for determination after the analysis of DPM. These uncertainties would greatly reduce the accuracy of DPM results. It will lead to a back seat in design and simulation process. It is contractive to the high-efficiency design through performing DPM. Therefore, these uncertainties in design variables further complicate the integration of DPM into the design process. In addition, lack of information, vast design space, increasing levels of model resolution and rapid change of design are also identified as the barriers of the implement of DPM (Østergård et al. 2016). However, these other barriers can be considered as the outgrowths generated from the three major fundamental aspects.



### **1.2.3 Previous studies for addressing these barriers**

Simple energy/performance evaluation tools with a simplified calculation engine can provide easy and quick assessment of building performance to help architects to explore their designs (Depecker et al. 2001) (Ourghi et al. 2007). In addition, much detailed information as input data are not required by these simple tools. In combination with the challenges mentioned above, simple tools are considered as an effective approach for reducing the labor and time spent on the collection of input data (Wen & Hiyama 2016). However, even a smaller amount of input data required by simple evaluation tools is still difficult to obtain because of the uncertainties and lack of reliable information resources during the early design stage.

Some optimization approaches are proposed based on building performance. However, it is difficult to determine the design direction only in the view of optimal building performance. Thus, it is still necessary to develop more intellectual approaches with the capacity of providing straightforward guidance on decisions making based on the calculation results to further popularize DPM.

A realistic performance modeling process is completed through the introduction of the ranges of uncertainty parameters from underlying approximates (Hopfe et al. 2013). Knowledge based system can provide validity information for the estimation of these uncertainty parameter by means of knowledge reuse and share. National Renewable Energy Laboratory developed a building component library in which the comprehensive data including building components and measures for building simulations were stored (NREL 2017) (Long et al. 2011). This library is also integrated into many simulation software, such as EnergyPlus and Openstudio. The selection of various template from the drop-down list in these software becomes simple and time-saving. However, it is difficult to ensure the reliability and quality of these data in this library because that they are generally originated from architects and engineers.

The optimization of the design variables for a new project from the very beginning stages can

effectively accelerate the implementation of DPM. The previous optimal design can provide valuable insight for the design of a new project. Therefore, the authors proposed a method for assigning a default value in building performance simulations by reusing the optimal design data stored in building information models (BIM) which are widely adopted in current design practice (Hiyama et al. 2014). However, this method greatly depended on the past experiences about the design objectives and design constraints of projects. Thus, the adoption of the proposed method is difficult for architects with insufficient experience in identifying the similarities between a new project and the previous optimal design.

Therefore, how to assign appropriate values for uncertainties during the early design stages is still a pivotal issue for the implement of DPM. In actual practice, architects have to make some assumptions which depend on knowledges, experiences, and guess for these uncertain design variables to perform DPM. However, the quality and availability of these assumption values significantly influence the accuracy of analysis results. DPM with improper input data led to misleading information for design decisions making (Bazjanac et al. 2011). These unreliable design decisions further impact the efficiency of the building design and even the final performance of the building. Thus, technology development is required to support the undetermined input data assignment for improving the accuracy of DPM. In addition, more effective approaches for performing DPM and informing design decisions are simultaneously required. In this context, this thesis concentrates on the measures which can be adopted to facilitate the implementation of DPM.

### **1.3 Research objective of this study**

The main purpose of this thesis is to develop flexible approaches for facilitating the high accuracy and efficiency implementation of DPM towards performance-based design decisions making. To achieve this goal, we conduct the study in two aspects. The first aspect is to develop approaches for assigning robust default values, which are defined as tentative values, for the uncertain design parameters required by DPM for discussing a target design variable. For example, the assignment of default values to the undetermined window properties, such as window area and glass type, is necessary in DPM for the discussion of the building shape which is studied in the beginning of the design stage. It is necessary to note that these adopted default values are still regarded as design variables in the following design stage for optimization. Therefore, the improvement of the whole design is less affected by the measure of using default values. However, to ensure the accuracy of the results from DPM, it is important to minimize the differences between the adopted default values and their corresponding actual values (optimal value) as the design progresses. Therefore, this thesis mainly focus on the development of the algorithms which can generate robust default values for uncertain design variables. In addition, developing a flexible and user-friendly way to provide the relevant information is also an important goal of this investigation. The novelty of the developed approaches in the first aspect is to provide information about the recommended direction for default values setting and the relationship between default values and building performance.

The other aspect is to develop an efficient approach for assisting the implementation of DPM and informing the corresponding design decisions based on the modeling results. The priority of the developed approach for performing DPM is to help architects to address the multiple objectives in design practice. It is hoped that these proposed approaches can facilitate the front loading of the design process through integrating DPM into this process. The practical significance of this thesis is to contribute to ZEB (zero energy building) and sustainability certificate.

## **1.4 Constructions of this study**

The main purpose of this thesis is to develop flexible approaches for facilitating the high accuracy and efficiency implementation of DPM towards performance-based design decisions making. To achieve this goal, we conduct the study in two aspects. The first aspect is to develop approaches for assigning robust default values which are defined as tentative values for uncertain design parameters required by DPM for discussing a target design variable. The other aspect is to develop an efficient approach for performing DPM and informing the corresponding design decisions. The framework of this thesis is organized as follows (see Figure 1.6).

Chapter 1 firstly presents the research background, purpose, and the construction of this thesis. The following review study in this Chapter focuses on simple building performance evaluation tools which are supposed as tools for performing DPM in this study. The reason is that these simple tools can be used to perform DPM with less detailed building information as inputs. The necessary inputs of ten simple tools and their organization measures are reviewed to search the inputs which are difficult to be accessed in design practice. An additional criterion is that these inputs have an influential impact on the evaluation results. Consequently, window configuration including rough window area and window geometry, and natural ventilation information including air change rate and rough natural ventilation strategies are selected as the support objects of this thesis.

Chapter 2 describes an approach developed for supporting the default value assignment of rough window area which is represented as window-to-wall ratio (WWR) and generally required in the beginning stages of design process. It is realized by the creation of recommended WWR maps based on the analysis results of integrated simulation investigations and optimizations. A case study is conducted to create recommended WWR maps in Japan. The novelty of the proposed maps is to show architects with the recommended setting direction of WWR towards which building performance becomes better in contrast to global optimal default values. According to the integrated simulation

results from case study, the distribution of the optimal WWR under varying design conditions exhibits three overall patterns: (i) As the WWR decreases, the CO<sub>2</sub> emissions decrease. (ii) An appropriate WWR value exists (30-50 %) at which the CO<sub>2</sub> emissions are minimized. (iii) As the WWR increases, the CO<sub>2</sub> emissions decrease. Therefore, three options of a small, moderate, or large default WWR value are available from the created maps according to the characteristic of new projects.

With the design progressing, the default WWR value mentioned in Chapter 2 can be replaced by the actual design value. Therefore, Chapter 3 develops an efficient approach for performing DPM to assist the determination of optimal window geometry including window height, window width and window location in the floor. A procedure for creating the response surfaces between window geometries and building performance by combining the analysis results of dynamic daylighting simulation which is performed to analysis the daylight use and energy simulation is developed. The response surfaces can not only show architects with the optimal solution but also help architects to understand to what extent they can widen or narrow the window geometry without significantly decreasing the building performance. The novelty of the proposed procedure is to address the enormous number of simulations for exploring the surface features. It is realized by the adoption of the link between daylight factor (DF) and continuous daylight autonomy (cDA). In case studies, the daylighting simulation tool of DAYSIM and energy simulation tool of EnergyPlus are used to create response surfaces. With the proposed link, the number of dynamic daylighting calculation which trends to time consuming is limited to be only one. In addition, the lighting electric saving can also be calculated using the results from DAYSIM and EnergyPlus simulations. The impact of COPs for the cooling/heating systems on the features of the response surface can be easily determined. Higher COP results in a narrow selectable design range of window geometry in case where the same percentage of building performance degradation is acceptable. The proposed method is also validated in this Chapter.

Chapter 4 describes a developing approach from an earlier study for supporting the data filling

associated with natural ventilation. This approach is achieved by showing the maps of target air change rate. It is defined as an air change rate at which the increase in cooling effect from natural ventilation reaches the maximum value. The ultimate purpose of authors in this Chapter is to create the world target air change rate maps for facilitating the early natural ventilation design. However, it is necessary to confirm the robustness of target air change rate under the representative conditions of building model and construction specifications in advance of the maps creation for a country. Therefore, the Chapter reports the availability of this method in China. Case studies are firstly conducted to examine the robustness of the target air change rate using a typical Chinese office building model with representative operation conditions in five climate zones of China. Then, the target air change rate and natural ventilation potential maps from China are created based on the verified method to inform the air change rate and rough natural ventilation strategy. For example, well organized natural ventilation strategies with an air change rate above 3ac/h are required in the Hot Summer and Warm Winter zone and Temperate zone under moderate internal gains condition. These strategies are particularly suggested for cities in the Temperate zone with warm climate due to the higher available cooling potential.

For final conclusions, Chapter 5 summarized the main findings of this study and recommended key areas for further studies.

In this thesis, the methods proposed in Chapter 2 and 3 with the aim of supporting the determination of window configuration are elaborated by implementing them into case studies of Japan. The method developed from previous study for supporting the preliminary natural ventilation design is employed in China in Chapter 4.

Although, selection of the same region to perform case studies is beneficial to keep the consistency of this thesis. In order to enhance the convincingness of the verification in Chapter 4, China which differed from the target regions in Chapters 2 and 3 was also selected. The main reason for the selection

of Japan and China originates from the characteristics of window configuration and natural ventilation in this study. The additional reason for selecting these two countries is that the data for simulation is accessible for authors. It is necessary to declare that our ultimate goal is to popularize these proposed methods all around the world to facilitate the high efficiency implement of DPM. The case studies shown in this study are only employed to explain the implement procedures of the proposed method.

The most meteorological factors impacting the configuration of window are the outdoor air temperature and the flux of solar radiation (Singh et al. 2015). From sub-frigid climate zone in north to sub-tropics climate zone in south, Japan owns various climate zone due to long and narrow span of Japan archipelago in north-south orientation. In addition, the solar radiation condition in Japan also varies from zone to zone. For example, there is less of solar radiation in Japan Sea side during the winter due to the cloudy, rainy, and snowy days. On the other hand, there is sufficient solar radiation in the Pacific side owing to the frequent sunny days. Therefore, the climate conditions in Japan are complex enough to show the diverse impacts of climate on window configuration.

The meteorological factors which influence natural ventilation design are more complex in comparison with the assignment of window configuration. It was indicated that outdoor air temperature, air humidity, wind direction, wind speed, and air quality impacted the performance of natural ventilation (Tong et al. 2017). Due to the obvious differences in the terrain and topography and the locations of land and sea, various types of climate, including temperate monsoon climate in the north, temperate continental climate in the northwest, plateau-mountain climate in the southwest, and subtropical monsoon climate in the south exist in China. Therefore, in comparison with Japan, China is more suitable to be used as the research object to further verify and develop the method proposed in previous study. In addition, Japan target air change rate maps are also supplemented in the appendix of Chapter 4 as a reference material.

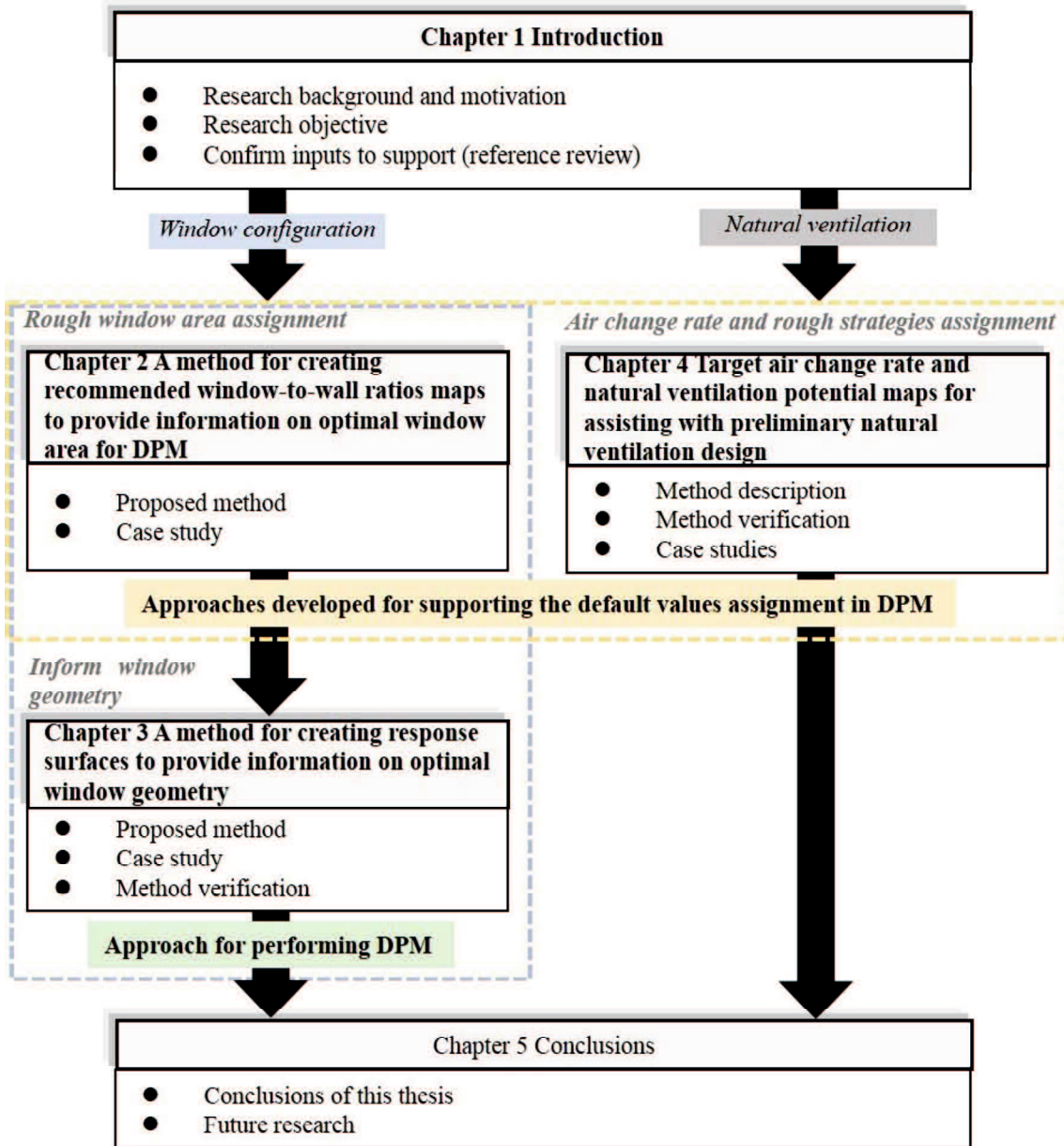


Figure 1.6. Research flow chart of this study.



## **1.5 Confirm the inputs this study selected to support their default values assignment**

In this section, the reason why this thesis focus on the default values assignment associated with design variables of window configuration and natural ventilation is stated. It is based on a review study on the necessary input data of ten simple tools which are supposed to be adopted to perform DPM in this thesis. Simple tools are reviewed because of that these simple tools can be used to perform DPM with less detailed building information as inputs. Thus, the minimum necessary input data can be clarified. In exception of the difficulty in organizing the design variable, another important judgement criterion for support object is that the design variable is sensitivity to design performance (evaluation results).

### **1.5.1 A review on ten simple tools**

The ten simple tools reviewed are  $C_f$ , PAL\*, ERED, WinSim, TEMMI/MCI<sup>3</sup>, FACES, BuildingCalc, CoolVent, DPV and EcoDesigner. The application, characteristics, modeling/calculation features and outputs are firstly introduced. The ten simple tools reviewed in this paper can be divided into three categories: design index, simple analysis program and BIM relevant program. Design index tools, including  $C_f$ , PAL\* and ERED, utilize the envelope performance to represent the approximate energy performance of the whole buildings. Simple analysis program usually exports specific values as evaluation results, such as thermal load, indoor air temperature and airflow rate. However, a simple analysis program requires relatively more inputs compared with design index tool. WinSim, TEMMI/MCI<sup>3</sup>, FACES, BuildingCalc and CoolVent are examples of simple analysis programs. A BIM relevant program combined with BIM software can automatically generate the geometry data for analysis program. Examples of BIM relevant programs are DPV and EcoDesigner.

### *C<sub>f</sub> (shape coefficient)*

$C_f$  (Depecker et al. 2001) was designed as an indicator of the heating consumption for residential buildings in a rigorous climate.  $C_f$  is defined as the rate between the external envelope surface area and the inner volume of the building. The authors performed the trend test on several theoretical buildings and determined that  $C_f$  was proportional to heating consumption. Therefore, it is considered that outdoor temperature is the largest driver for heating consumption of the residential building in rigorous climate. It is worth noting that there is no correlation between  $C_f$  and heating consumption in mildest and sunny climate.

### *PAL\* (Perimeter Annual Load\*)*

Ministry of Land, Infrastructure, Transport and Tourism, Japan (2013) created  $PAL^*$  to describe the thermal insulation performance of the building envelope for non-residential buildings.  $PAL^*$  is defined as the rate between the total annual load of the perimeter zone and the area of the perimeter zone of the building. In Japan, the energy convention plan must be proposed for non-residential buildings whose area exceeds 2000 m<sup>2</sup>.  $PAL^*$  is adopted as an index to quantify the energy conservation level. The standard value of  $PAL^*$  was set according to the application and location of the project. The calculated  $PAL^*$  for the target building should be smaller than the standard value.

### *ERED (Envelop-Related Energy Demand)*

The design indicator  $ERED$  (Granadeiro, Correia, et al. 2013) was developed to indicate the energy consumption of residential buildings. The limitation of  $C_f$ , i.e., it has no correlation with the energy performance in a mildest climate, is addressed by  $ERED$ .  $ERED$  is the sum of the heat transmission through the envelope and the solar gains through the windows calculated using some simple formulas and definitions. This indicator is combined with the envelope shape, envelope materials and window

areas.

#### *WinSim*

To facilitate the selection of windows, *WinSim* (Schultz & Svendsen 1998) was developed to quickly and easily evaluate the thermal performance of windows. An electric analogy model (two-node) is adopted in this program. The calculation object is limited to a simple one-zone room. The outputs of *WinSim* are the annual energy consumption, the amount of transmitted solar energy and total number hours when the building is under overheated conditions.

#### *TEMMI/MCF<sup>3</sup>*

This commercial program *TEMMI/MCF<sup>3</sup>* (Ellis & Mathews 2001) is used to perform thermal analysis for non-residential buildings. This program intends to design building envelope with the minimum thermal load. This program uses an electric analogy model (three-node) for performing the thermal analysis. The outputs include thermal load and indoor air temperature. To provide feedback to architects, the program performs an automatic comparison among envelope design alternatives on the basis of the thermal load.

#### *FACES (Forecasts of Air-Conditioning System's Energy, Environment, and Economical Performance by Simulation)*

*FACES* (Sakurai et al. 2007) is a simplified simulation program for choosing a suitable heat source system. The program couples the dynamic thermal load calculation and the HVAC system simulation. Automatic design algorithms of the building model and the HVAC system are introduced into *FACES*. The program is equipped with five building models and thirteen heat source systems for selection. The outputs are the peak load, the annual thermal load, the amount of energy consumption, the amount of

carbon emissions and the cost.

### *BuildingCalc*

*BuildingCalc* (Nielsen 2005) was developed to estimate the thermal load and the indoor environment for non-residential buildings. The program is based on *WinSim*. Thus, the model and calculation objects are the same as those of *WinSim*. The solar gains through the windows are thoroughly described. Beyond the thermal load, the program can also examine the effects of shading, venting and mechanical ventilation. The program exports the thermal load, the indoor air temperature, the hours of overheating. It can also export the value of Predicted Percentage of Dissatisfied (PPD) and Predicted Mean Vote (PMV).

### *CoolVent*

*CoolVent* (M-A. Menchaca-B 2008) was developed to evaluate the performance of natural ventilation. A multi-zone coupled thermal and airflow model is used to predict the zone temperature and the direction, the temperature and the rate of airflow. The program can perform both transient (24-hour period) and steady calculations. Architects can understand how some design parameters affect the internal temperature and airflow and confirm the measurable effects from the design of natural ventilation.

### *DPV (Design Performance Viewer)*

*DPV* (Schlueter & Thesseling 2009) was combined with the BIM software (Revit from AUTODESK) to access the geometry inputs. *DPV* mainly focuses on the heating demand of buildings. A mathematical model was used to perform energy and exergy analysis. The concept of exergy is defined as the potential of an energy source dispersing from heat generation to emission into the room. The analysis results of *DPV* are the energy balance and exergy balance of selected heat chain. *DPV* can assist architects in making a balance among building form, building material and technical systems

in the early design stages.

### *EcoDesigner*

GRAPHISOFT (2011) developed *EcoDesigner* as an add-on application operating inside of ArchiCAD. Multiple thermal models can be automatically generated in the design environment. *EcoDesigner* can evaluate key design decisions, such as materials, glazing and ventilation. The output of *EcoDesigner* are the yearly energy consumption, the carbon emissions and the monthly energy balance.

## **1.5.2 The necessary inputs and their organization approaches**

The necessary input data of the ten simple tools and whether these necessary input data can be easily acquired or not are discussed in this section. Table 1.3 presents the necessary inputs collected from the ten simple tools. Although, FACES, DPV and EcoDesigner can also consider the HVAC system to further calculate the specific performance of buildings. For the sake of unification, the use of the thermal load as the objective function is focused on. Thus, only the inputs related to the thermal load analysis are listed for these three tools in table 1.3. The collected necessary inputs can be divided into three large categories: weather data, building geometry data and building properties (BP) data. BP data are defined as the non-geometrical inputs required by energy models (Cerezo et al. 2014).

Firstly, the measure which can assist these necessary input data filling is indicated. Both simple analysis programs and BIM relevant programs use approaches based on the hourly climate data to represent the standardized annual climate. Thus, users only need to know the location of their project to acquire the climate data. ERED is the only design index tool requiring simple climate inputs. These required inputs can be easily obtained from the “epw” climate file format that is made freely available to the public by the DOE (Crawley et al. 1999).

Table 1.3. Necessary input data of ten simple tools.

		Design index			Simple analysis program					BIM relevant program	
		C <sub>f</sub>	PAL*	ERED	WinSim	TEMMI/MCI <sup>3</sup>	FACES	BuildingCalc	CoolVent	DPV	EcoDesigner
<b>Weather data</b>	location (weather data file)				○	○	○	○	○	○	○
	outdoor temp.			○							
	wind speed							○ <sup>2)</sup>			
	wind direction							○ <sup>2)</sup>			
	solar radiation			○							
<b>Building geometry data</b>	orientation		○	○	○	○	○	○	○	○	○
	volume	○								○	○
	number of floors		○			○	○	○	○		○
	floor dimensions		○			○	○	○	○		○
	interior wall length					○					
	floor areas		○	○	○	○	○	○		○	○
	exterior wall areas	○	○	○	○	○		○		○	○
	internal wall areas				○			○			○
	roof areas	○		○				○			○
	ground floor areas	○								○	○
	window dimensions		○	○	○			○	○		○
<b>Building properties data</b>	<b>General data</b>	artium dimensions						○			○
		appliance		○			○		○		○
		terrain information							○		○
	<b>Construction data</b>	surrounding building				○			○		○
		exterior wall properties		○	○	○	○	○	○	○	○
		roof properties			○	○	○	○	○	○	○
		floor properties					○	○	○	○	○
		interior wall properties					○	○	○	○	○
		thermal capacity of construction			○	○			○		
		glazing properties		○	○	○	○	○	○	○	○
		frame properties							○		○
SHGC			○	○	○			○		○	
SHGC <sub>WS</sub> <sup>1)</sup>			○								
<b>Internal load data</b>	exterior wall /roof color					○					
	window-to-wall ratio(WWR)					○	○		○	○	
	occupation density					○	○		○	○	
	equipment density					○	○		○	○	
	lighting density					○	○		○	○	
	total internal load							○			
	occupation schedule						○		○	○	
	equipment schedule							○		○	
	lighting schedule							○		○	
<b>Conditioning data</b>	heating set points			○			○		○	○	
	cooling set points			○			○			○	
	heating season			○			○				
	cooling season			○			○				
	overtemp. limit				○						
	initial building temp.							○			
	artificial lighting type								○		
	infiltration rate						○			○	
	blind		○				○				
	window opening seting temp.							○			
	window opening parameters							○		○	
	ventilation type							○		○	
	mechanical ventilation rates						○	○		○	
natural ventilation rates									○		
shading device	○			○	○		○			○	

1):solar heat gain coefficient of the windows with the shading device on

2):user need to define this value when performing a steady caculation

Regarding geometry data, a simple method with the capacity of converting 2D building models to the representative “shoebox” thermal models has been described (Dogan & Reinhart 2013). In addition,

the “simulation domain model” is able to exchange data between the 3D BIM software and the simulation domain and makes it possible to directly generate building information to reduce the efforts required to handle geometry inputs (Donnell et al. 2011). The huge progress of typical meteorological years, the BIM technique, and the data converting algorithms extensively simplify the setup of weather and geometry input data. For geometry data excluding the window dimensions and the atrium dimensions, they can be determined on the basic building information from client demand and construction planning. Therefore, the building shape is usually discussed in the early design stages with the uncertainties of window configuration and atrium arrangement which is designed for natural ventilation.

BP data can be further divided into general data, construction data, internal load data and conditioning data according to the previous study. General data represent the building application and building site information, including terrain and surrounding building. A majority of construction data are used to describe the building material properties, which are specified as the properties of opaque envelope and glazing. The rest of the construction data are used to describe the area of the openings which is expressed as the window-to-wall ratio (WWR). Internal load data are composed of the internal heat gain density and their corresponding schedules. Conditioning data are composed of two groups. One group comprises the indoor environment controlling data to maintain the comfortable level of occupants. The other group comprises the passive design strategies, such as natural ventilation and shading devices.

General data can be completely obtained from the client demand, even during the very early design stages. Besides general data, a part of internal load data and indoor environment controlling data within the conditioning data also depend on the client demand. The establishment of remnant BP data can be greatly simplified by databased, such as BP templates (Cerezo et al. 2014). The BP templates proposed for building performance simulation are defined as a comprehensive database of the thermal zone

attribution data. The utilization of BP templates can greatly reduce the time consumption and the risk of error in inputs filling. The predefined data in BP templates mainly originate from the reference design guideline and design experience. Therefore, building material properties data in construction data and the remnant indoor environment controlling data in conditioning data can be precisely obtained through the BP templates. It is explained that such data in BP templates are mainly from the design guideline. All of the BP data mentioned above can be acquired from reliable sources, as shown in Figure 1.7.

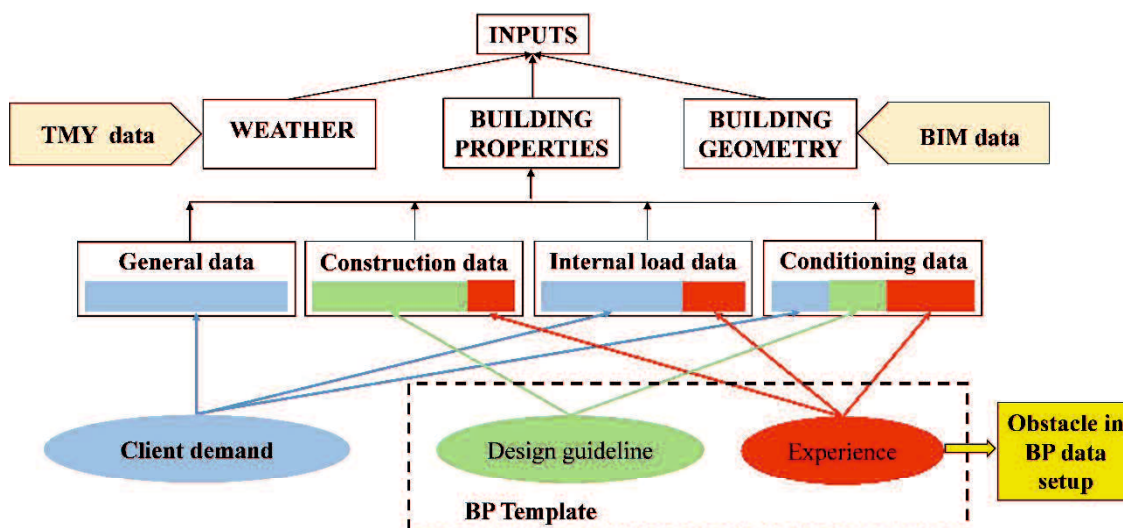


Figure 1.7. Reliable sources of BP data.

Based on the discussion results above, the data without reliable sources are clarified. They are the window geometry data and atrium dimensions data in building geometry data, WWR belonging to construction data, and shading device data and natural ventilation settings belonging to conditioning data, as shown in Table 1.4 (the data in the red frames). The lack of measure to efficiently and rapidly establish those data is recognized as the obstacle in performing DPM using the simple tools. Although, these input data are collected from only ten simple tools. Natural ventilation, WWR, daylight



utilization, Photovoltaics are indicated as the necessary input data for early analysis by Grinberg (M Grinberg 2013). In addition, the target percentage glazing, shade depth, target percentage skylight and conceptual construction-mass glazing were reported to be very sensitive to the predicted results and should be carefully given in the early design stages. Such parameters are called energy setting parameters (Lin & Gerber 2014). Energy setting parameters cannot be solely determined by uniform standards or design guidelines. The issues involved with energy setting parameters are highlighted by the example of setting up the WWR. The ANSI/ASHRAE/IESNAI Standard 90.1-2010 recommends that the maximum value of WWR should be 40%. According to Japan's Building Standards Act, the window area should be 1/7 of the floor area (建築基準法解説抜粋). However, the analysis results of case studies indicated that the optimal WWR was greatly influenced by the building design conditions, such as the building scale, location, and operation mode (daylighting and natural ventilation). For a building with a relatively larger floor area, the largest WWR was found to be the best solution (Hiyama 2014). This result contradicts the suggested value by ASHARE design guideline and Japan's Building Standards Act. In addition, natural ventilation does not only impact building performance but also the discussion of building shape. It is urgent to be integrated into the modeling in an early time if a ventilation shaft is necessary. According to the reference book with respect to natural ventilation design which was published by Architectural Institute of Japan, the target of air change rate is suggested as 4ac/h for controlling the indoor temperature (実務者のための自然換気設計ハンドブック). However, the reference book also mentioned that this target air change amount of natural ventilation significantly impacted by the internal gains of the building and the thermal properties of the envelope. In addition, the climate condition of the project is also indicated as influence factor in previous studies. Therefore, it is difficult to define a design standard for natural ventilation design. Consequently, window configuration (considering the daylight utilization) and natural ventilation are selected as the support objects of this thesis based on the previous studies.

Table 1.4. Necessary Input data without reliable source.

<b>Building geometry data</b>		orientation	<p>Building geometry information  <b>Source: Client Demand</b></p>
		volume	
		number of floors	
		floor dimensions	
		interior wall length	
		floor areas	
		exterior wall areas	
		internal wall areas	
		roof areas	
		ground floor areas	
		window dimensions	Window configuration
		artium dimensions	Natural ventilation
<b>Building properties data</b>	<b>General data</b>	appliaction	<p>Building application, site information  <b>Source: Client Demad</b></p>
		terrain information	
		surrounding building	
	<b>Construction data</b>	exterior wall properties	<p>Properties of building material  <b>Source: Design guideline</b></p>
		roof properties	
		floor properties	
		interior wall properties	
		thermal capacity of construction	
		glazing properties	
		frame properties	
		SHGC	
		SHGC <sub>ws</sub> <sup>1)</sup>	
	exterior wall /roof color		
		window-to-wall ratio(WWR)	Window configuration
	<b>Internal load data</b>	occupation density	<p>Internal gain density  <b>Source: Design Guideline</b></p>
		equipment density	
lighting density			
total internal load		<p>Internal gain schedule  <b>Source: Client Demand</b></p>	
occupation schedule			
equipment schedule			
	lighting schedule		
<b>Conditioning data</b>	heating set points	<p>Indoor environment controlling  <b>Source: Design guideline</b>  <b>Client Demand</b></p>	
	cooling set points		
	heating season		
	cooling season		
	overtemp. limit		
	initial building temp.		
	artificial lighting type		
	infiltration rate		
	blind		
			window opening seting temp.
	window opening parameters		
	ventilation type		
	mechanical ventilation rates		
	natural ventilation rates		
	shading device	Shading device	

## References

- Al-Homoud, M.S., 1997. Optimum Thermal Design of Air-Conditioned Residential Buildings. *Building and Environment*, 32(3), pp.203–210.
- Attia, S. et al., 2012. Simulation-based decision support tool for early stages of zero-energy building design. *Energy and Buildings*, 49, pp.2–15.
- Attia, S. & Herde, A. De, 2011. Early design simulation tools for net zero energy buildings: a comparison of ten tools. In: *Proceedings of Building Simulation 2011: 12th Conference of International Building Performance Simulation Association, Sydney, 14-16 November*, pp.94–101.
- Bazjanac, V. et al., 2011. An assessment of the use of building energy performance simulation in early design. In: *Proceedings of Building Simulation 2011: 12th Conference of International Building Performance Simulation Association, Sydney, 14-16 November*, pp. 1579–1585.
- Benni, S. et al., 2016. Efficacy of greenhouse natural ventilation: Environmental monitoring and CFD simulations of a study case. *Energy and Buildings*, 125, pp.276–286.
- CASBEE: Comprehensive Assessment System for Built Environment Efficiency [on line]  
<http://www.ibec.or.jp/CASBEE/index.htm> [accessed 06. 17].
- Cerezo, C., Dogan, T. & Reinhart, C., 2014. Towards standardized building properties template files for early design energy model generation. In: *2014 ASHRAE/IBPSA-USA: Building Simulation Conference, Atlanta, GA, September 10-12, 2014*, pp. 25–32.
- Crawley, D.B. et al., 2008. Contrasting the capabilities of building energy performance simulation programs. *Building and Environment*, 43(4), pp.661–673.
- Crawley, D.B., Hand, J., & Lawrie, L.K., 1999. Improving the Weather Information Available To Simulation Programs. *Proceeding of BS 1999, Kyoto, Japan*, pp.529–536.
- Depecker, P. et al., 2001. Design of buildings shape and energetic consumption.

- Building and Environment*, 36(5), pp.627–635.
- Dogan, T. & Reinhart, C., 2013. AUTOMATED CONVERSION OF ARCHITECTURAL MASSING MODELS INTO THERMAL “SHOEBOX” MODELS. In *Proceedings of BS2013: 13th Conference of International Building Performance Simulation Association, Chambéry, France, August 26-28*. pp. 3745–3752.
- Donnell, J.O. et al., 2011. SIMMODEL : A DOMAIN DATA MODEL FOR WHOLE BUILDING ENERGY SIMULATION. In *Proceedings of Building Simulation2011: 12th Conference of International Building Performance Simulation Association, Sydney, 14-16 November*. pp. 382–389.
- Ellis, M.W. & Mathews, E.H., 2001. A new simplified thermal design tool for architects. *Building and Environment*, 36, pp.1009–1021.
- Granadeiro, V., Duarte, J.P., et al., 2013. Building envelope shape design in early stages of the design process: Integrating architectural design systems and energy simulation. *Automation in Construction*, 32, pp.196–209.
- Granadeiro, V., Correia, J.R., et al., 2013. Envelope-related energy demand: A design indicator of energy performance for residential buildings in early design stages. *Energy and Buildings*, 61, pp.215–223.
- GRAPHISOFT. 2011. GRAPHISOFT EcoDesigner User Guide.
- Greenhouse Gas Inventory Office of Japan, [Online].  
Available:<http://www-gio.nies.go.jp/aboutghg/nir/nir-j.html> [accessed 02. 17].
- Hiyama, K. et al., 2014. A new method for reusing building information models of past projects to optimize the default configuration for performance simulations. *Energy and Buildings*, 73, pp.83–91.
- Hiyama, K., 2014. Assigning Robust Default Values in Building Performance Simulation Software for

- Improved Decision-Making in the Initial Stages of Building Design. *The Scientific World Journal*.
- Hong, T., Chou, S., & Bong, T., 2000. Building simulation: an overview of developments and information sources. *Building and Environment*, 35(4), pp.347–361.
- Hopfe, C.J., Augenbroe, G.L.M. & Hensen, J.L.M., 2013. Multi-criteria decision making under uncertainty in building performance assessment. *Building and Environment*, 69, pp.81–90.
- Hygh, J.S. et al., 2012. Multivariate regression as an energy assessment tool in early building design. *Building and Environment*, 57, pp.165–175.
- IPCC, 2014. Intergovernmental panel on climate change, 2014, Synthesis Report. International Energy Agency. India Energy Outlook 2015.
- Ji, Y., Lomas, K.J. & Cook, M.J., 2009. Hybrid ventilation for low energy building design in south China. *Building and Environment*, 44(11), pp.2245–2255.
- Kim, H., Stumpf, A. & Kim, W., 2011. Analysis of an energy efficient building design through data mining approach. *Automation in Construction*, 20(1), pp.37–43.
- Levine, M., D. Ürge-Vorsatz, K. Blok, L. Geng, D. Harvey, S. Lang, G. Levermore, A. Mongameli Mehlwana, S. Mirasgedis, A. Novikova, J. Rilling, and H. Yoshino, 2007: Residential and commercial buildings. In: *Climate Change 2007: Mitigation. Contribution of Working Group III to the Fourth Assessment Report of the Intergovernmental Panel on Climate Change* [Metz, B., O.R. Davidson, P.R. Bosch, R. Dave and L.A. Meyer]. Cambridge University Press, Cambridge, United Kingdom and New York, NY, USA, pp. 387-446.
- Lin, S.-H.E. & Gerber, D.J., 2014. Designing-in performance: A framework for evolutionary energy performance feedback in early stage design. *Automation in Construction*, 38, pp.59–73.
- Liu, F., A.S. Meyer, and J.F. Hogan, 2010: Mainstreaming Building Energy Efficiency Codes in Developing Countries: Global Experiences and Lessons from Early Adopters. *World Bank*

- Working Paper* No. 204. The World Bank, Washington, D.C.
- Long, N., Fleming, K. & Brackney, L., 2011. An object-oriented database for managing building modeling components and metadata. *In Proceedings of Building Simulation 2011 Sydney, Australia November 14-16, 2011*, pp.2356–2362.
- Lynn, G., & Bellenger, 2010. Modeling a sustainable world. *ASHRAE Journal*, vol. 52, no. 8, pp. 18-22
- M-A. Menchaca-B, L.G., 2008. Coolvent : a multizone airflow and thermal analysis simulator for natural ventilation in buildings. *In SimBuild 2008, Berkeley, California, USA, 2008*. pp. 132–139.
- M Grinberg, A.R., 2013. Architecture & energy in practice:implementing an information sharing workflow. *In Proceedings of BS 2013: 13th Conference of International Building Performance Simulation Association, Chambéry, France, August 26-28*. pp. 121–128.
- Ministry of Land, Infrastructure, Transport and Tourism, Japan. 2013. Energy Standard: Manual of Program for Building Envelop Performance in Buildings. No.150
- National Renewable Energy Laboratory, Building Component Library, 2015. [Online]. Available: <https://bcl.nrel.gov/> [accessed 02. 17].
- Nielsen, R.T., 2005. Simple tool to evaluate energy demand and indoor environment in the early stages of building design. *Solar Energy*, 78(1), pp.73–83.
- Østergård, T., Jensen, R.L. & Maagaard, S.E., 2016. Building simulations supporting decision making in early design - A review. *Renewable and Sustainable Energy Reviews*, 61, pp.187–201.
- Ourghi, R., Al-Anzi, A. & Krarti, M., 2007. A simplified analysis method to predict the impact of shape on annual energy use for office buildings. *Energy Conversion and Management*, 48(1), pp.300–305.
- Sakurai, F. et al., 2007. FACES ( FORECASTS OF AIR-CONDITIONING SYSTEM ' S ENERGY ,

- ENVIRONMENTAL , AND ECONOMICAL PERFORMANCE BY SIMULATION ). In *Proceedings of Building Simulation 2007 Tokyo, Japan*. pp. 1661–1668.
- Samuelson, H. et al., 2016. Parametric energy simulation in early design: High-rise residential buildings in urban contexts. *Building and Environment*, 101, pp.19–31.
- Schlueter, A. & Thesseling, F., 2009. Building information model based energy/exergy performance assessment in early design stages. *Automation in Construction*, 18(2), pp.153–163.
- Schultz, J.M. & Svendsen, S., 1998. WinSim: A simple simulation program for evaluating the influence of windows on heating demand and risk of overheating. *Solar Energy*, 63(4), pp.251–258.
- Singh, R., Lazarus, I.J. & Kishore, V.V.N., 2015. Effect of internal woven roller shade and glazing on the energy and daylighting performances of an office building in the cold climate of Shillong. *Applied Energy*, 159, pp.317–333.
- The American Institute of Architects, 2012. An Architect’s Guide to Integrating Energy Modeling In The Design Process. Process. p. 8.
- Tong, Z., Chen, Y. & Malkawi, A., 2017. Estimating natural ventilation potential for high-rise buildings considering boundary layer meteorology. *Applied Energy*, 193, pp.276–286.
- U.S. Energy Information Administration, [Online].  
Available:<http://www.eia.gov/totalenergy/data/browser/?tbl=T02.01#/?f=A&start=1949&end=2015&charted=3-6-9-12> [accessed 02. 17].
- U.S. Energy Information Administration, [Online].  
Available: <http://www.eia.gov/environment/emissions/carbon/> [accessed 02. 17].
- Viebahn, P. et al., 2013. Annual Energy Outlook 2012. Energy Policy.
- Wen, L. & Hiyama, K., 2016. A Review: Simple Tools for Evaluating the Energy Performance in Early Design Stages. *Procedia Engineering*, 146, pp.32–39.

新成長戦略～「元気な日本」復活のシナリオ～（2010年6月18日 閣議決定）

建築基準法解説抜粋 <http://www.iny.jp/regulation/cnstreg.html> [accessed 06.17]

実務者のための自然換気設計ハンドブック，日本建築学会編，技報堂出版，p.37, (2013).



## 2.

# **A Method for Creating Recommended Window-to-Wall Ratios (WWR) Maps to Provide Information on Appropriate Default WWR Values for Design Performance Modeling**

To support the appropriate default value assignment in design performance modeling (DPM), which is defined as energy/performance simulations in the concept and schematic stages of the design process, a methodology for creating maps of the recommended window-to-wall ratio (WWR) is proposed using integrated simulations and optimizations. A case study is conducted to create maps of recommended WWR in Japan. The overall distribution of optimal WWR under varying design conditions exhibits three different patterns: (i) the smaller the WWR is, the lower the CO<sub>2</sub> emissions are; (ii) an appropriate WWR value exists (between 30-50 %) to minimize the CO<sub>2</sub> emissions; and (iii) the larger the WWR is, the lower the CO<sub>2</sub> emissions are. Six design conditions of lighting power density, climate, window orientation, internal gains, building scale and glazing type are examined in this investigation. The results of the quantitative evaluation indicate that the lighting power density, climate, window orientation, and glazing type significantly impact the optimal WWR configuration. Therefore, the optimization results of 10 representative locations in four main orientations with two lighting power densities (10 W/m<sup>2</sup> and 5 W/m<sup>2</sup>) and 14 types of glazing are processed according to the investigated optimal WWR distribution patterns to generate the recommended WWR maps in Japan. The maps provide architects with information to determine the setting direction of default WWR values for building performance. For example, a larger WWR is recommended for buildings in zones 6-8 of the

Japanese climate regions for the current lighting load ( $10 \text{ W/m}^2$ ), except for an eastern façade. However, a moderate or a smaller WWR default value should be carefully assigned according to the window orientation in zones 4-8 when a future lighting power density of  $5 \text{ W/m}^2$  is considered.

## 2.1 General statement

Building window area, expressed as the window-to-wall ratio (WWR), is part of the required input data for discussing the building shape and sketch in the very beginning of the design process (M Grinberg 2013) (Cerezo et al. 2014); the WWR influences the daylighting and thermal load performance. Thus, WWR is regarded as one of the most influential factors that affects the results of energy/performance simulations (Pino et al. 2012) (Shen & Tzempelikos 2013) (Grynning et al. 2013). In actual design practice, WWR greatly depends on the design philosophy of architects and the demands from clients because energy modelers and experts are not yet involved in the early design stage. A glass curtain wall creates an aesthetic building appearance and provides a good views for the occupancy; therefore, it has gained a worldwide popularity in office building design (Wang et al. 2017). However, whether a larger window area is beneficial to building performance is still debatable (Tian et al. 2010). As mentioned in the Introduction Chapter, DPM with improper input data can produce misleading information for design decisions making. These unreliable design decisions further impact the efficiency of the building design and even the final performance of the building. Thus, to improve the accuracy of DPM results and avoid questionable design decisions, the default value assignment of WWR in DPM is focused on in this Chapter.

The design optimization criteria for WWR including energy consumption and visual aspects were pointed out by Ochoa (Ochoa et al. 2012). The meaning of the optimal solution for different projects varies due to the complexity of building design. A calculation method of the recommended maximum

WWR based on the design variables of envelop thermal conductivity and ambient temperature amplitude was proposed by Ma (Ma et al. 2015). The research object of maximum WWR in that study is useful for building design which is characterized by multi-objective optimization. However, the proposed method was confined within the thermal autonomous model. In addition, a flexible measure using maps creation was developed by Arinami (Arinami et al 2013) to provide the information. This visualization measure is easy to comprehend and suitable to represent the design parameters which depend on the climate data.

In these context, a methodology for creating maps of recommended WWR is described in this chapter to support the assignment of default WWR value in DPM. This methodology includes integrated thermal and daylighting simulations and optimizations. The proposed maps provide visual information of the recommended WWR under specific design conditions based on building performance.

It is necessary to highlight that this study does not aim to suggest an exact optimal default value of WWR for architects but to instead guide them in determining a small, moderate, or large default WWR value. The reasons are summarized as follow: (1) it is difficult to provide a global optimal WWR because that the actual building design is an optimization process under multi-objectives; (2) every building is unique and different factors are usually interacted in this unique design process. It is very hard to include all affecting factors into the investigation. Thus, this study shows the recommended setting direction of WWR which is based on the correlation between WWR and building performance (CO<sub>2</sub> emissions) rather than the exact WWR. Architects can select their own optimal solutions considering the multiple objectives of building performance, design preferences, and client demands. In addition, a case study is conducted to create maps of recommended WWR in Japan using a typical Japanese office building.

## **2.2 Methodology for creating recommended WWR maps**

The methodology for creating maps of recommended WWR proposed in this study includes two main procedures. First, integrated thermal and daylighting simulations are performed to investigate the possible distribution of optimal WWR under different design conditions (Wen & Hiyama 2016). The distribution of optimal WWR in our study is defined as the varying trend of WWR in the improvement of the building performance (reduction in the CO<sub>2</sub> emissions). Furthermore, critical design conditions that significantly impact the optimal WWR configuration (exact optimal WWR) are discussed through quantitative evaluation, which is conducted by examining the variation in the objective function when the determined optimal WWR is adopted in cases with variable design conditions. Design conditions associated with building geometry and primary application are considered in the integrated simulations. The six design conditions investigated are lighting power density, climate, window orientation, internal gains, building scale, and glass type. The strong impacts of climate and window orientation on the optimal window design have been noted in several previous studies (Persson et al. 2006) (Lee et al. 2013). Building scale is included because the geometry factor is correlated with daylighting performance (Hiyama 2014) (Susorova et al. 2013). For a building with a daylight-linked lighting control system, a principal contradiction in window area design is to balance daylight use from a larger window area and the increasing thermal load. The weight of lighting and cooling energy use is an influential factor in addressing this contradiction. Therefore, lighting power density and internal gains that would impact the magnitude of lighting and cooling energy demand are also examined in this study. Various glass types are currently available, such as double, three-layers, and tinted glazing, due to the development of glazing technology. Glazing characterized by thermal and optical properties significantly impacts the heating/cooling and lighting energy consumption of buildings (Persson et al. 2006) (Lee et al. 2013) (Fernandes et al. 2015). Thus, glazing type is also selected as a varying design condition to investigate the possible distribution of optimal WWR.

Second, optimization calculations are implemented to determine the best solutions under the critical design conditions. It significantly impacts the optimal WWR configuration and determined by quantitative evaluation. The optimization results are processed according to the investigated patterns of optimal WWR distribution in the first step to generate the recommended WWR maps. The recommended WWR of a new project can be obtained from the maps by examining the new project's features associated with those critical design conditions. The methodology mentioned above is summarized in the flow chart as shown in Figure 2.1.

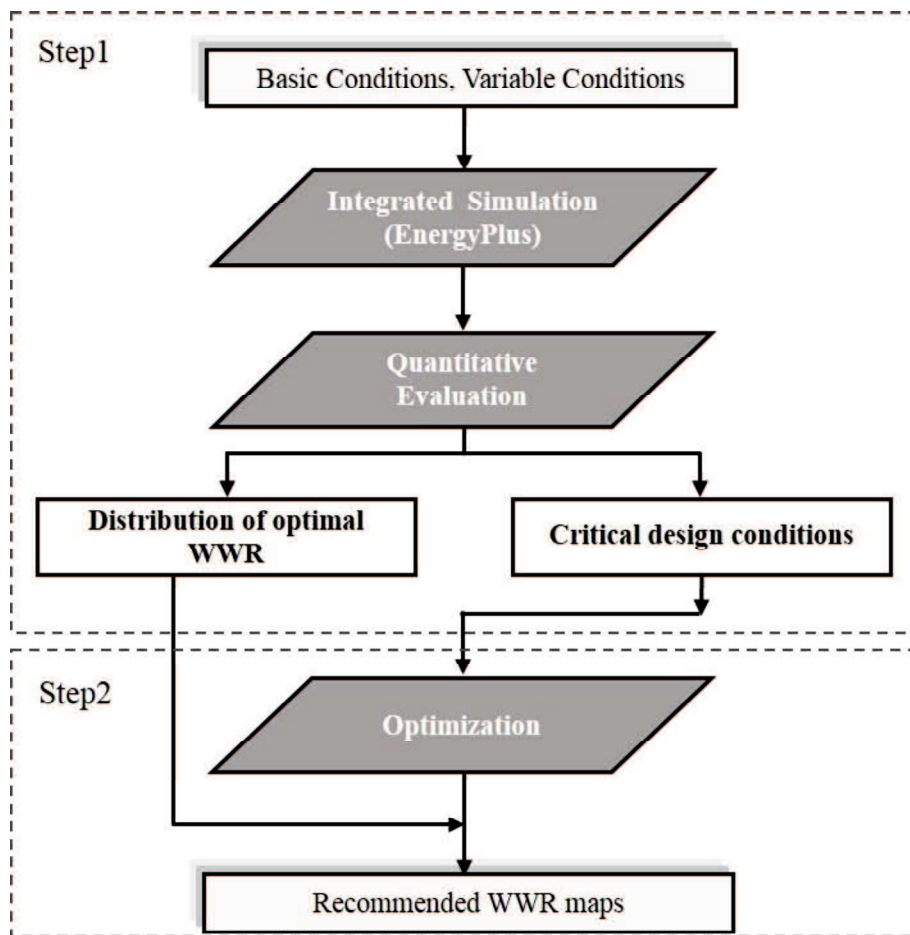


Figure 2.1. Flow chart of recommended WWR map creation.

All the integrated simulations and optimizations are performed using EnergyPlus software (Crawley et al. 2001). The daylighting analysis in this tool has been validated by comparing the results calculated by EnergyPlus to those from other software: Daysim, Radiance, and TropLux (Ramos & Ghisi 2010). EnergyPlus has been widely adopted for assessing the effect of window configurations on the thermal and daylighting performance of a building (Ochoa et al. 2012) (Kim et al. 2014) (Goia 2016).

## **2.3 Case study**

As a case study, the recommended WWR maps in Japan are created using the proposed method described above.

### **2.3.1 Distribution of optimal WWR under different design conditions**

#### **2.3.1.1 Basic simulation conditions**

The scheme of integrated simulation is described in this section. An office building based on a typical Japanese office model for validations of energy simulation software (Takizawa 1984) is created for the integrated simulations. Figures 2.2 and 2.3 shows the southwest corner's external appearance and plan view of the analyzed building modeled in the simulation software. It is a five-story office building designed with an open office concept. In a typical floor, a central core holds the stairs and the elevator lobby and connects two identical open office zones (zone 1 and zone 2) with a width-to-depth ratio of 2:1. The basic module of the floor plan is 3.6 m × 3.6 m. In order to investigate the impact of window orientation, windows are assumed to be only installed in the main façade (width facade) in each office zone (see figure 2.2). It means that the windows of the building could face north and south, or east and west. Tables 2.1 list the thermal properties of the building envelope. Table 2.2 shows the settings of the heating, ventilation, and air conditioning (HVAC) system. These corresponding

conditions mainly originate from the definition of the typical office model mentioned above. Some modifications are made to satisfy the current insulation specification. The simulation results based on a typical building model and representative operation conditions can provide information about the average performance of different window area.

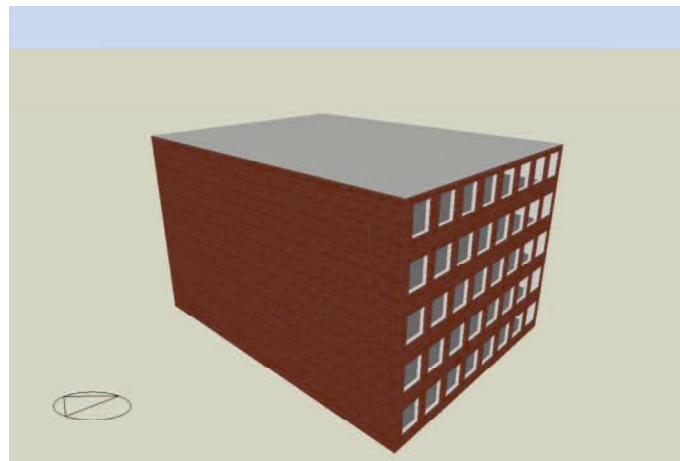


Figure 2.2. 3D model of the building model.

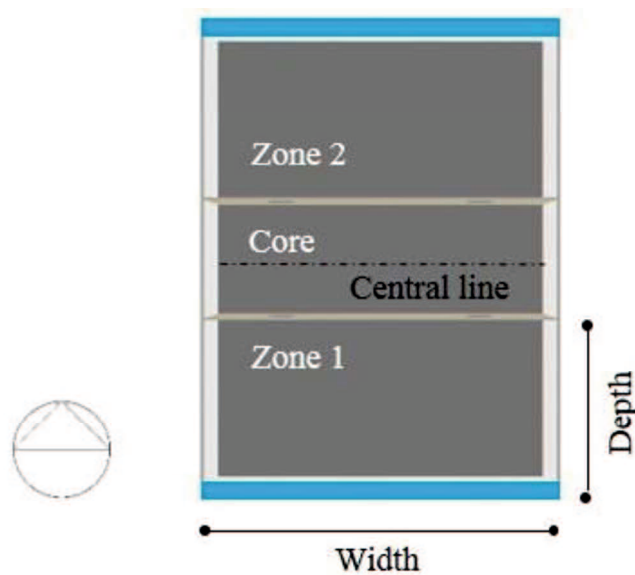


Figure 2.3. Plan view of the building model.

In order to avoid the occurrence of glare and maintain the visual comfort of occupants, internal blind with high reflectivity slats is assumed to be installed in the simulated building. Solar control with a set-point of  $120\text{W/m}^2$  which is considered as the solar radiation threshold of a sun day is selected to control the on/off mode of the blind.

A daylight-linked lighting control system is used in the simulations to consider the conservation of artificial lighting energy due to daylight. On/off mode and the continuous dimming mode are two common manner adopted in simulation (Galasiu et al. 2004) (Kim & Kim 2007). Despite the presence of a basic input power and its corresponding lighting output even though that the illuminance level exceeds the required level, a continuous dimming control mode is selected to prevent disturbing the occupants by frequently switching the lighting on and off in on/off control system (Alrubaih et al. 2013). Figure 2.4 shows the linear relation between lighting output and input power of the adopted continuous dimming control system. A work plane assumed to be a surface 0.8 m above the floor is predefined for daylighting evaluation. The target illuminance required on this work plane is set to 400 lx in the office zones (JIS Z 9110). The output level of the artificial lighting can be adjusted according to the daylight illuminance measured by the daylight sensors to confirm that this target illuminance is met. A maximum of two daylight sensors is allowed in an individual zone by the EnergyPlus software. Thus, the two open office zones are all assumed to be divided into a perimeter zone and an interior zone by a boundary line that is 4.6 m (States 2012) away from the main façade, as shown in Figure 2.5. In each zone, the first daylight sensor is placed at the assumed boundary line between the perimeter zone and the interior zone; the second one is located at the center of the interior zone. Furthermore, in the central core, the target illuminance is set to 40 lx, and the cooling/heating system is constantly off. The mechanical ventilation in central core maintains the minimum air change rate level of 0.5 ac/h. In the simulations for this study, the coefficient of performance (COP) for the cooling system is 3, and the COP for the heating system is 2, which are based on the annual performance evaluation results for



a multi-split variable refrigerant volume (VRV) air-conditioning system in an actual office building of Japan from a previous study. Multi-split VRV systems are widely used in the commercial buildings of Japan due to their benefits in terms of convenience and energy efficiency. Therefore, this study selects the realistic COP values of a representative multi-split VRV air-conditioning system as the input parameters of simulations.

Table 2.1. Thermal properties of the construction elements (layers are listed from outside to inside).

External wall	U-value: 0.55 W/m <sup>2</sup> K  Tile: 8 mm, Mortar: 20 mm, Concrete: 150 mm, Expanded Polystyrene: 50 mm,  Air Gap, Gypsum Plasterboard: 12 mm
Roof	U-value: 0.46 W/m <sup>2</sup> K  Concrete (Lightweight): 60 mm, Expanded Polystyrene: 50 mm, Asphalt: 10 mm,  Concrete: 150 mm, Air Gap, Plasterboard: 9 mm, Fiberboard: 12 mm
Internal floor	U-value: 1.13 W/m <sup>2</sup> K  Rock Wool Board: 12 mm, Plasterboard: 9 mm, Air Gap, Concrete: 150 mm,  Plastic Tile: 3 mm
Internal partition	U-value: 2.43 W/m <sup>2</sup> K  Mortar: 20 mm, Concrete: 120 mm, Mortar: 20 mm
Window	Low-E Double-Glazing (6 mm-13 mm-6 mm),  U-value: 1.8 W/m <sup>2</sup> K, SHGC: 0.56, VT: 0.7
Window shading	Blinds with high reflectivity slats (Position: inside),  Solar control, Set-point: 120 W/m <sup>2</sup>  Schedule (Weekdays): off-9:00-on-18:00-off

Table 2.2. HVAC system settings.

Mechanical ventilation	7 l/s-person (minimum ventilation rate: 0.5 ac/h), Schedule (Weekdays): off-9:00-on-18:00-off
Cooling	Electricity from grid (carbon emissions factor: 0.685 kgCO <sub>2</sub> /KWh), Cooling system COP: 3*, Set-point temperature: 28 °C. Schedule (Weekdays): off-8:00-on-18:00-off
Heating	Electricity from grid (carbon emissions factor: 0.685 kgCO <sub>2</sub> /KWh), Heating system COP: 2*, Set-point temperature: 20 °C, Schedule (Weekdays): off-8:00-on-18:00-off

\* These values refer to the annual evaluation results of a multi-split type (VRV) air conditioning system (M. Hiraoka, S. Hiromoto, H. Komoda, S. Tabuchi, S. Tanabe, T. kai, S. Hashimoto, A 2011).

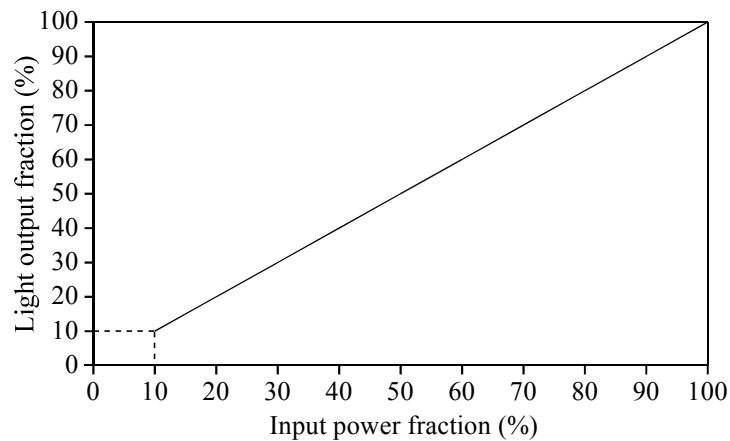


Figure 2.4. Correlation between lighting output and input power of adopted continuous dimming control system.

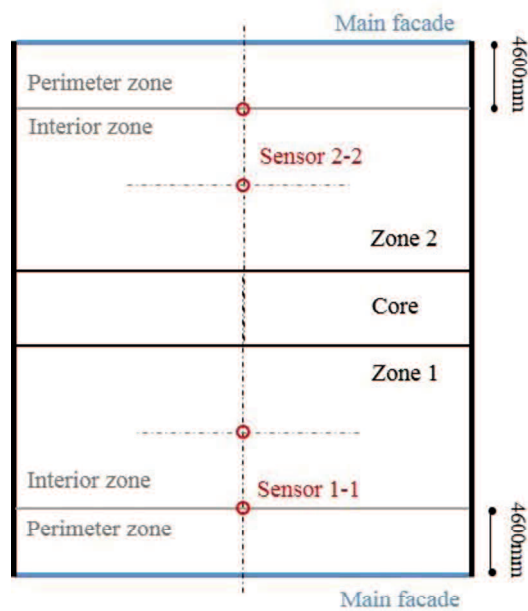


Figure 2.5. Locations of the daylight sensors in zones 1 and 2.

### 2.3.1.2 Variable design conditions

The six design conditions investigated are lighting power density, climate, window orientation, internal gains, building scale, and glazing type. The modifications on these six design conditions are summarized in Table 2.3. The specific explanation of these modifications are described in the follow paragraph.

Two lighting power density values are used in the simulations. The value of  $10 \text{ W/m}^2$  represents the level realized by highly efficiency lighting systems in new Japanese office buildings. Lighting energy use can be reduced even further in the future due to the rapid development of various energy efficient luminaires (Wang & Tan 2013) and daylighting control systems (Li et al. 2010) (Li et al. 2014). Thus, a value of  $5 \text{ W/m}^2$  is assumed for a future building. The lighting power densities of  $10 \text{ W/m}^2$  and  $5 \text{ W/m}^2$  are defined as the current and future lighting conditions in this Chapter, respectively.

Table 2.3. Description of design variables.

Lighting power density	10 W/m <sup>2</sup> (2.5 W/m <sup>2</sup> -100 lx), 5 W/m <sup>2</sup> (1.25 W/m <sup>2</sup> -100 lx)
Climate conditions	Sapporo, Tokyo, Naha
Window orientation	North and South, East and West
Internal gain	<p>Low internal gain: occupancy density of 0.1 W/m<sup>2</sup>, equipment density of 10 W/m<sup>2</sup></p> <p>Medium internal gain: occupancy density of 0.2 W/m<sup>2</sup>, equipment density of 20 W/m<sup>2</sup></p> <p>High internal gain: occupancy density of 0.4 W/m<sup>2</sup>, equipment density of 40 W/m<sup>2</sup></p>
Building scale	<p>Small-scale: space depth of 10.8 m, floor area of 622 m<sup>2</sup></p> <p>Large-scale: space depth of 18 m, floor area of 1555 m<sup>2</sup></p> <p>Space depth: distance between the external windows and the internal partition in each zone</p>
Glazing type	<p>Double Low-E Glazing (6 mm-13 mm-6 mm)</p> <p>Double Clear Glazing (6 mm-13 mm-6 mm)</p> <p>Double Ref-A-H Clear Glazing (6 mm-13 mm-6 mm)</p>

The Expanded AMeDAS Weather Data from Sapporo (43.03 N, 141.20 E), Tokyo (35.41 N, 139.46 E) and Naha (26.12 N, 127.41 E) are used in the simulations to determine the impact of climate (the locations of these three cities are shown in Figure 2.6). According to the Koppen-Geiger climate classification, Sapporo is in the Dfb climate region, while Tokyo and Naha are located in the Cfa climate region (Kottek et al. 2006). However, Naha has a relatively higher external temperature and global solar radiation than Tokyo, as shown in Table 2.4.



Figure 2.6. Three cities (Sapporo, Tokyo, and Naha) selected for simulation.

Table 2.4. Climate characteristic of three cities (Sapporo, Tokyo, and Naha).

Cities	Mean external temperature			Mean global solar radiation		
	(°C)			(Wh/m <sup>2</sup> )		
	Year	Jan	Aug	Year	Jan	Aug
Sapporo	8.8	-3.3	21.1	135.4	68.8	165.3
Tokyo	16.6	6.3	27.0	142.7	106.9	170.6
Naha	23.3	18.0	29.0	163.9	97.9	233.1

The third floor, which is located at the middle of the building, is selected as the analysis object. The reasons can be summarized as flow: (1) the study object of sensitivity analysis should be as simple as possible to avoid additional impact caused by the other factors in exception of the investigated

variables. The rooms located at the top and bottom floors with relatively complex conditions, i.e., a larger heat conduction, should be abandoned in the selection of study object (Susorova et al. 2013). (2) the simulated performance of a typical floor or room is considered to be approximately equal to the average level of the whole building. Thus, it becomes a common practice that one floor or one cell from the whole building is selected as study object in recent studies (Pino et al. 2012) (Hiyama & Wen 2015). (3) to perform a sensitivity analysis, a larger number of simulations is commonly required. Therefore, reduction of time consumption for dynamic simulation through the selection of one floor from the whole building is also considered as a reason.

The selected third floor can be equally divided into two parts by its central line parallel to the main façade (see figure 2.3); the simulation results are processed separately in each part. Therefore, due to the symmetry, the four main window orientations can be evaluated with just two building orientations: the main façade facing south-north and the main façade facing east-west.

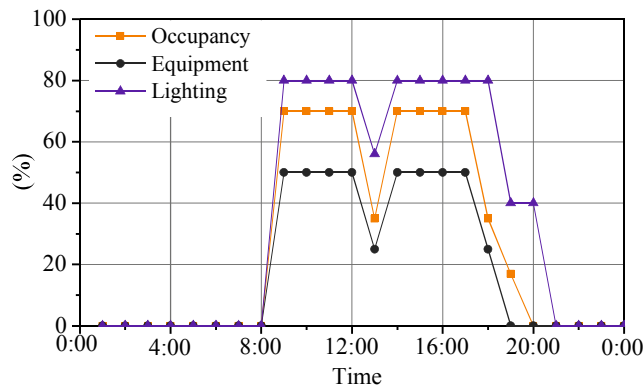


Figure 2.7. Activity schedules for a weekday

The internal gains in this study are regarded as the combination of heat gains from the occupancy and equipment; low, medium, and high levels of internal gains are considered in the simulations. The occupancy and equipment densities of 0.2 people/m<sup>2</sup> and 20 W/m<sup>2</sup>, respectively, in accordance with

the levels of a typical Japanese office building, are the medium internal gains. For the low and high levels of internal gains, the occupancy and equipment density values are 0.5 and 2 times those values for the medium internal gains, respectively. The schedule of activities in a weekday are shown in figure 2.7.

The fifth design condition investigated is the building scale. Specifically, the distance between the main façade and the internal partition in each office zone is used to characterize building scale; this parameter is called the space depth (see figure 2.8). Small-scale and large-scale building models are simulated to examine the effect of building scale. The small-scale model has a space depth of 10.8 m and an area of 233 m<sup>2</sup> for a single office zone. In contrast, the large-scale model has a space depth of 18 m and an area of 648 m<sup>2</sup> for a single office zone. The floor areas of the two models are 622 m<sup>2</sup> and 1555 m<sup>2</sup>, respectively.

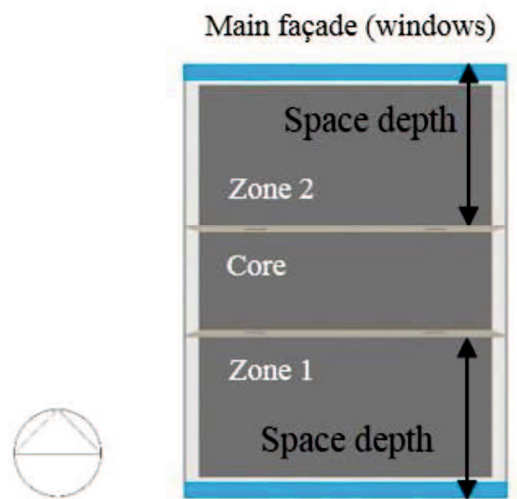


Figure 2.8. Space depth of the building.

The last design condition investigated is the glazing type. Three representative glazing types are selected for simulation (1) Double Low-E (low emissivity metallic coating to increase thermal

reflectance) Glazing 6 mm-13 mm-6 mm (U-value: 1.8 W/m<sup>2</sup> K, SHGC: 0.56, VT: 0.7); (2) Double Clear (no impurities) Glazing 6 mm-13 mm-6 mm (U-value: 2.7 W/m<sup>2</sup> K, SHGC: 0.70, VT: 0.78); (3) Double Ref-A-H (stainless steel high transmittance coating to increase solar reflection) Glazing 6 mm-13 mm-6 mm (U-value: 2.5 W/m<sup>2</sup> K, SHGC: 0.22, VT: 0.18).

A total number of 216 simulation cases are created through combining the above modifications for the six design conditions (lighting power density (2) × climate (3) × building orientation (2) × internal gains (3) × building scale (2) × glazing type (3)=216). For each simulation case, WWR varies from 10 % to 70 % at intervals of 10 %, as shown in figure 2.9. The preferred window height is 2 m; when the desired window area cannot be provided by increasing window width, the window height is adjusted to reach the target WWR. Consequently, 1512 (216×7) times of calculation are implemented to fully understand the influence of the six design conditions on the distribution of optimal WWR. The simulation results are evaluated in terms of the annual total CO<sub>2</sub> emissions  $Q_{TOT}$ , expressed by Eq. 2-1. The optimal WWR is determined by the minimum value of  $Q_{TOT}$ .

$$Q_{TOT} = Q_C + Q_H + Q_L \text{ (kg)} \quad (2-1)$$

where  $Q_C$  and  $Q_H$  are the CO<sub>2</sub> emissions corresponding to the electricity use of cooling and heating, respectively, and  $Q_L$  is the CO<sub>2</sub> emission caused by the lighting consumption. The CO<sub>2</sub> emissions from these three resources are considered to be closely correlated with the optimal window area (Goia et al. 2013).



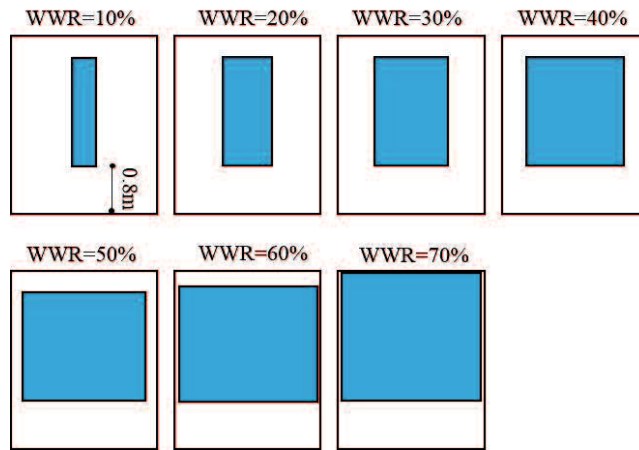


Figure 2.9. Variations in the window-to-wall Ratio (WWR).

### 2.3.1.3 Investigation results

In this study, the influences of six design conditions on the distribution of optimal WWR are investigated. In order to help us to well and concisely understand the investigated results, the results obtained from Double Low-E glazing (well insulated) which is widely adopted in current design practice is described and explained in detail here.

#### *Results under the current lighting condition (lighting power density of 10 W/m<sup>2</sup>)*

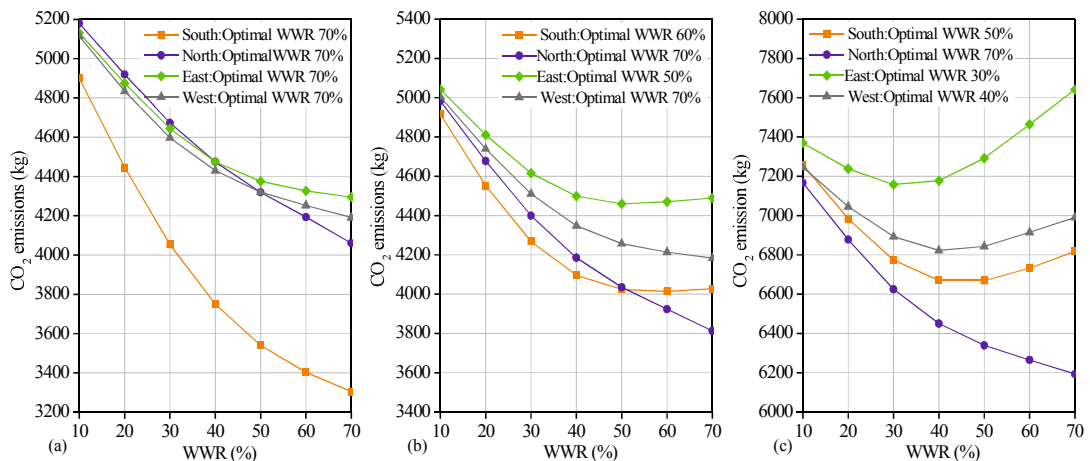


Figure 2. 10. Distribution of optimal WWR for three cities and four main orientations of a small-scale building with medium internal gains: (a) Sapporo; (b) Tokyo; (c) Naha.

Figures 2.10 (a), (b) and (c) show the relationship between the CO<sub>2</sub> emissions and the WWR of Sapporo, Tokyo, and Naha in the small-scale simulation building with medium internal gains. The CO<sub>2</sub> emissions monotonically decrease with increasing WWR in Sapporo regardless of window orientation, as shown in Figure 2.10 (a). Similar decreasing tendencies of CO<sub>2</sub> emissions with increasing window area are also shown for the north- and west-facing orientations of Tokyo in Figure 2.10 (b). However, the CO<sub>2</sub> emissions for the south- and east-facing orientations significantly decrease with increasing WWR and subsequently exhibit a very slight increasing tendency after the WWR exceeds a certain value. For Tokyo, the optimal WWR values are 60 % and 50 % for the south- and east-facing orientations, respectively. However, the increase in CO<sub>2</sub> emissions is minimal (less than 1 %) when the WWR exceeds the optimal value for these two orientations. Thus, the maximum WWR is still suitable for the south- and east-facing orientations in Tokyo when large window areas are preferred. The exact value of the optimal WWR under specific design conditions is given in the label of figures. Geographic location is an influential factor governing climate conditions. The latitudes varying from Sapporo to Tokyo cover almost all the possible ranges in the main island of Japan. It is inferred that the influence of climate conditions on the distribution of optimal WWR is negligible in the majority of main island Japan. Moreover, a larger window area is advantageous irrespective of window orientation.

Different variable tendencies of total CO<sub>2</sub> emissions with increasing WWR are shown for Naha, where global solar radiation and external temperature are relatively high, as shown in Figure 2.10 (c). Due to the high cooling demand in Naha, total CO<sub>2</sub> emissions are remarkably higher than those of the other two cities for all four orientations. Furthermore, obvious inflection points corresponding to the minimum total CO<sub>2</sub> emissions can be observed for south-, east-, and west-facing orientations. The inflection points on the CO<sub>2</sub> emissions and WWR curves differ for these three orientations; generally, they fall within 30 % to 50 %. However, there is no inflection point for the north-facing orientation.

Figures 2. 11 and 2.12 show the individual effects of WWR on the CO<sub>2</sub> emissions corresponding to cooling, heating, and lighting energy use for four orientations in Sapporo and Tokyo to understand the continually decreasing tendency of total CO<sub>2</sub> emissions with increasing WWR in Figures 2.10 (a) and (b). The CO<sub>2</sub> emissions from lighting energy consumption are well known to decrease with increasing WWR due to the greater daylight penetration. Conversely, cooling CO<sub>2</sub> emissions tend to increase with increasing WWR due to the higher solar gain and thermal transmission through the windows, as indicated in Figures 2. 11 and 2.12. The CO<sub>2</sub> emissions associated with heating energy use comprise a large proportion of the total value for all four orientations in Sapporo due to this city's cold climate, as shown in Figure 2. 11. However, the decreasing tendency of heating CO<sub>2</sub> emissions with increasing WWR is observed for only the south-facing orientation. No remarkable benefit from passive solar heating can be obtained from increasing the window area for the other three orientations. This trend also explains why the curve of total CO<sub>2</sub> emissions and WWR for the south-facing orientation is sharper than those for the other orientations in Sapporo shown in Figure 2.10 (a). The total CO<sub>2</sub> emissions in Tokyo are mainly from the cooling and lighting energy use, as shown in Figure 2. 12. Almost no heating energy is required due to the high solar and internal gains. The decrease in lighting demand is always greater than or approximately equal to the increase in cooling demand caused by increasing the window area. Thus, the maximum WWR shows optimal performance for Sapporo and Tokyo.

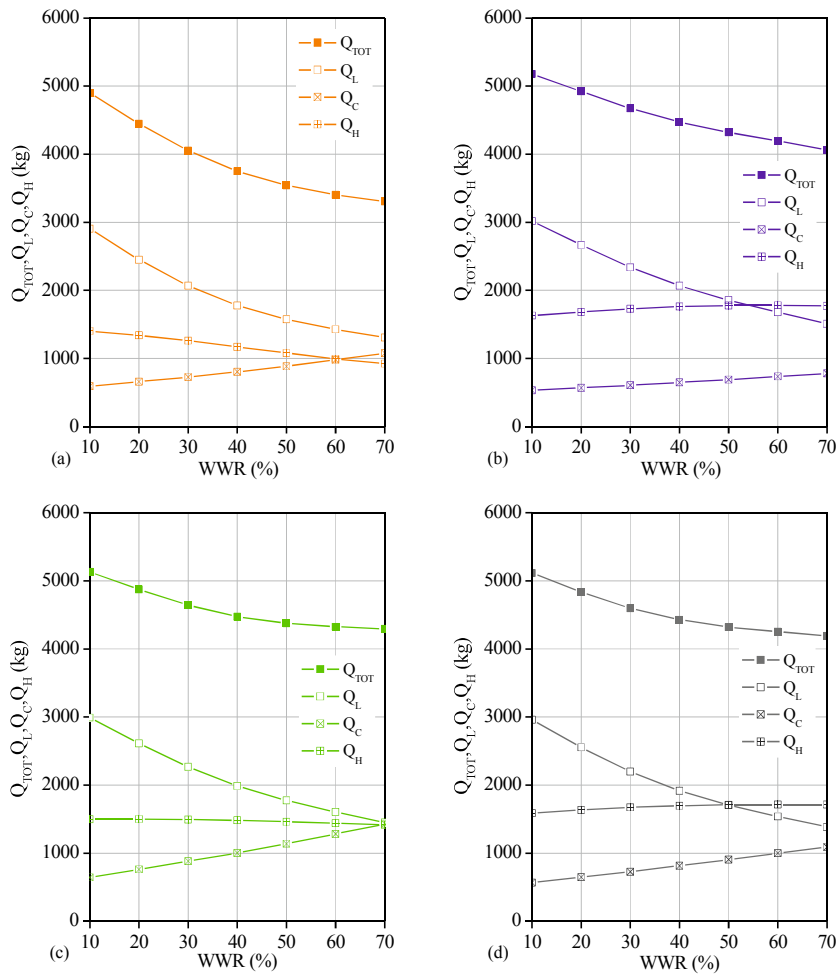


Figure 2. 11. The effects of WWR on the CO<sub>2</sub> emissions corresponding to cooling, heating, and lighting energy use for four orientations in a small-scale building with medium internal gains in

Sapporo: (a) South; (b) North; (c) East; (d) West.

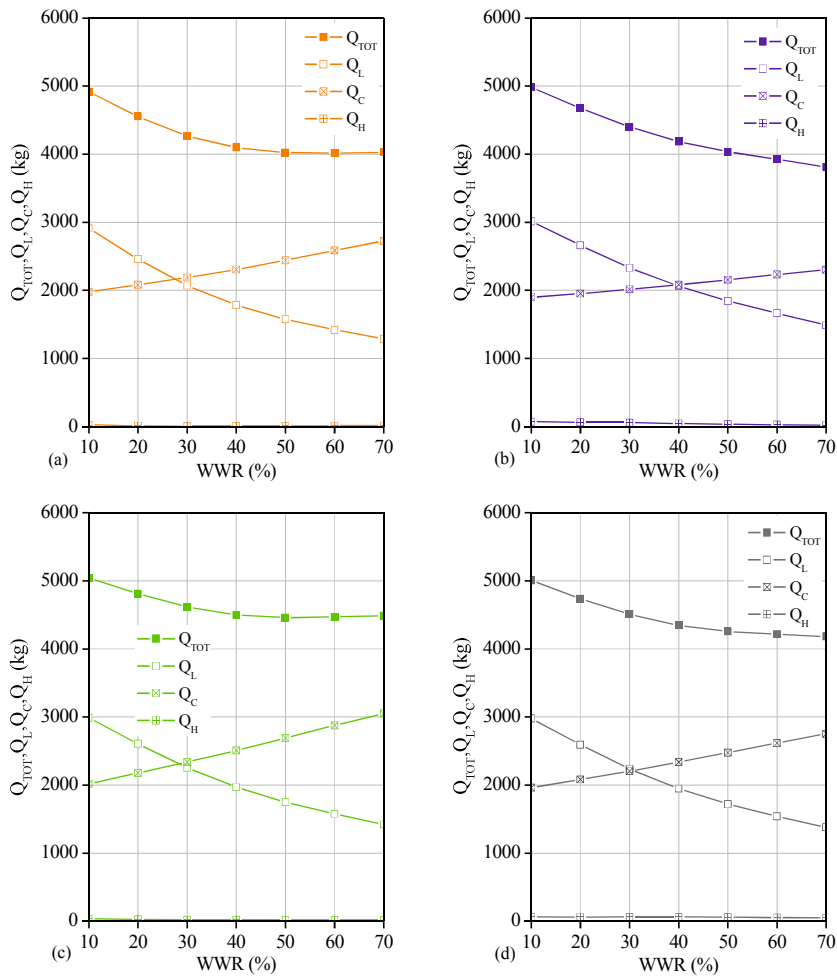


Figure 2.12. The effects of WWR on the CO<sub>2</sub> emissions corresponding to cooling, heating, and lighting energy use for four orientations in a small-scale building with medium internal gains in Tokyo: (a) South; (b) North; (c) East; (d) West.

Figure 2.13 presents the individual influences of WWR on the CO<sub>2</sub> emissions with regard to cooling, heating, and lighting energy use for four window orientations in Naha. There is completely no heating demand in Naha; the simulation results obtained from the representative Japanese climate of Sapporo, Tokyo, and Naha highlight that heating energy use is not a principal factor for determining the optimal window area for office buildings in Japan. Moreover, the slopes of the curves representing the increase in cooling CO<sub>2</sub> emissions with increasing WWR in Naha are greater than those in Sapporo and Tokyo.

Thus, using daylight to decrease the total CO<sub>2</sub> emissions occurs only at a smaller WWR. After WWR exceeds the inflection point, total CO<sub>2</sub> emissions begin to increase because the increase in the cooling demand becomes larger than the decrease in the lighting demand.

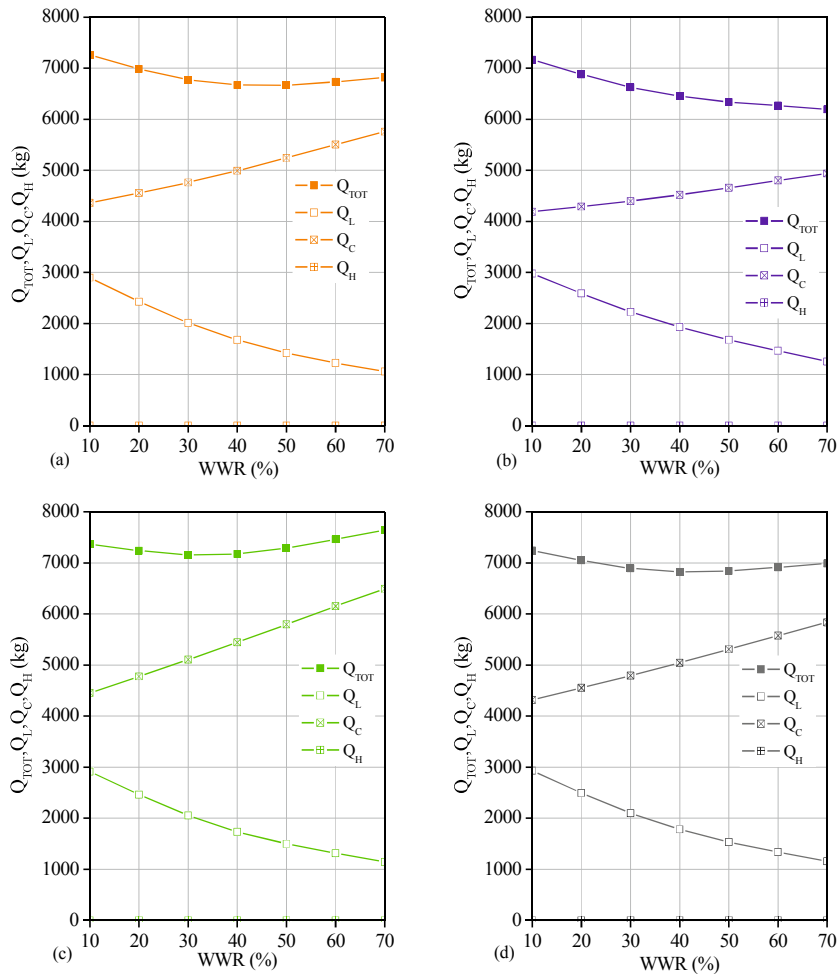


Figure 2.13. The effects of WWR on the CO<sub>2</sub> emissions corresponding to cooling, heating, and lighting energy use for four orientations in a small-scale building with medium internal gains in Naha: (a) South; (b) North; (c) East; (d) West.

Figure 2.14 shows the plot of CO<sub>2</sub> emissions against WWR at low, medium, and high internal gains for an east-facing orientation of the small-scale building in three cities. The total CO<sub>2</sub> emissions

markedly increase as the internal gains increase from low to high. The results indicate that the optimal WWR values for different levels of internal gains differ by no more than 10 % in Tokyo and Naha and show almost no difference in Sapporo. The maximum WWR is always the best solution for Sapporo regardless of the internal gains, as shown in Figure 2.14 (a). For Tokyo, a similar variable tendency of CO<sub>2</sub> emissions with increasing WWR is also shown in Figure 2.14 (b). This tendency is characterized by the negligible constraint of building performance on window area design (around 1 %) when WWR exceeds a relatively large optimal value. Figure 2.14 (c) shows distinct inflection points within 30 to 50 % in Naha for low, medium, and high internal gains. For the other three orientations (south, north, and west), the internal gains have minimal influence on the distribution of optimal WWR and even the exact optimal WWR value as shown in Figures 2.15-2.17.

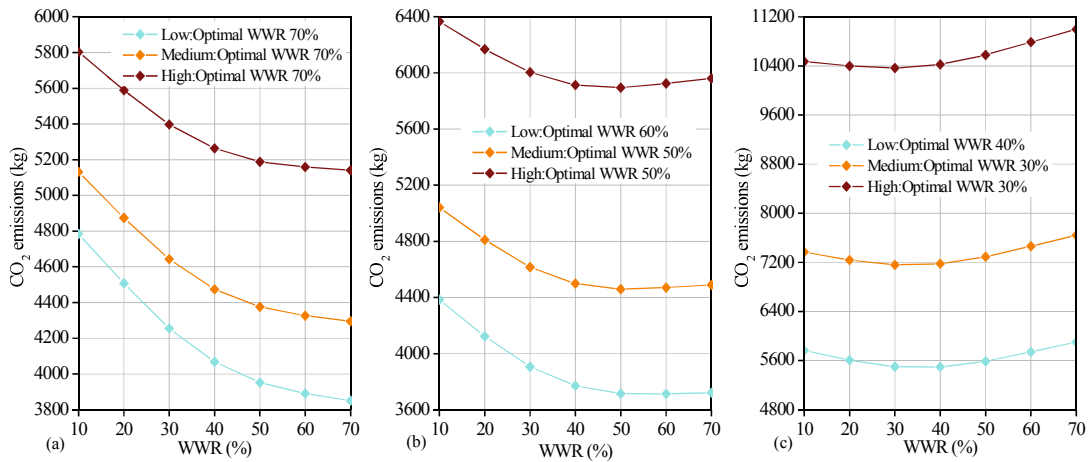


Figure 2.14. Distribution of optimal WWR for three cities at low, medium, and high internal gains for an east-facing orientation in a small-scale building: (a) Sapporo; (b) Tokyo; (c) Naha.

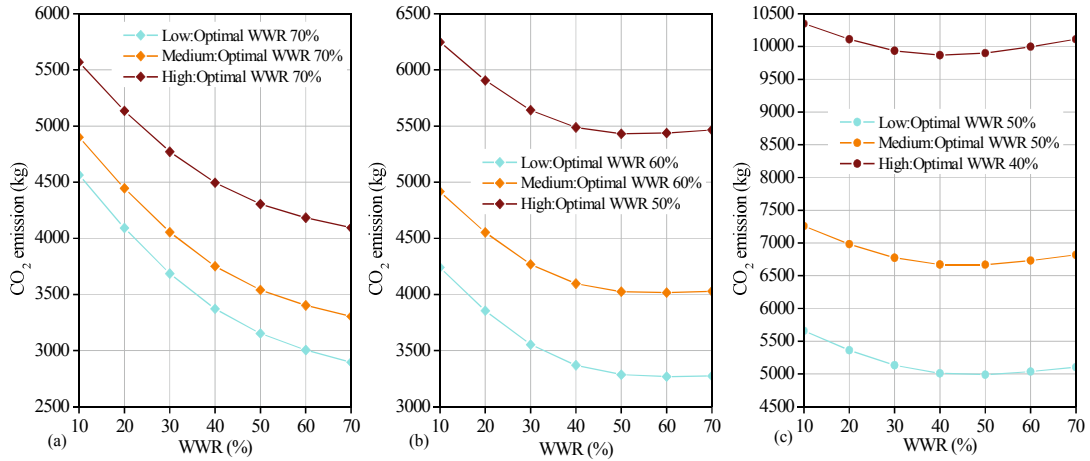


Figure 2.15. Distribution of optimal WWR for three cities at low, medium, and high internal gains

for a south-facing orientation in a small-scale building: (a) Sapporo; (b) Tokyo; (c) Naha

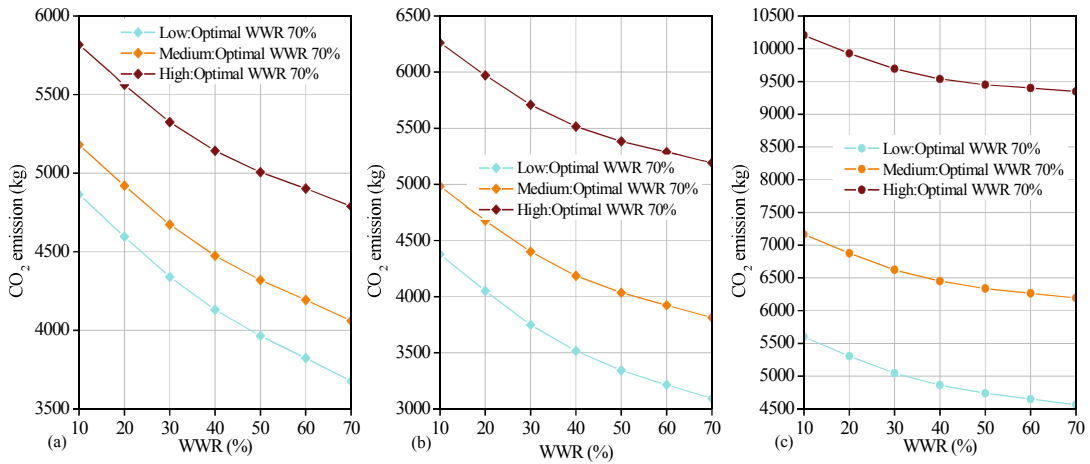


Figure 2.16. Distribution of optimal WWR for three cities at low, medium, and high internal gains

for a north-facing orientation in a small-scale building: (a) Sapporo; (b) Tokyo; (c) Naha.



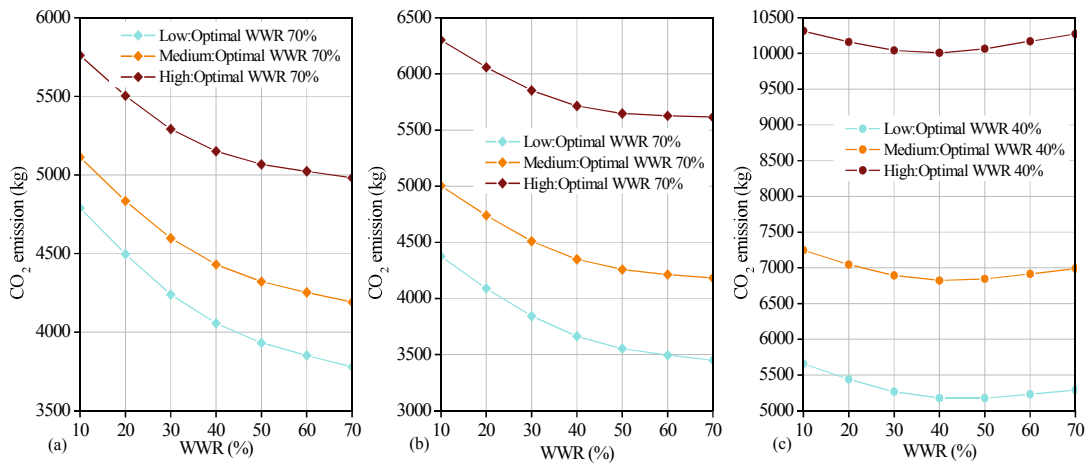


Figure 2.17. Distribution of optimal WWR for three cities at low, medium, and high internal gains for a west-facing orientation in a small-scale building: (a) Sapporo; (b) Tokyo; (c) Naha.

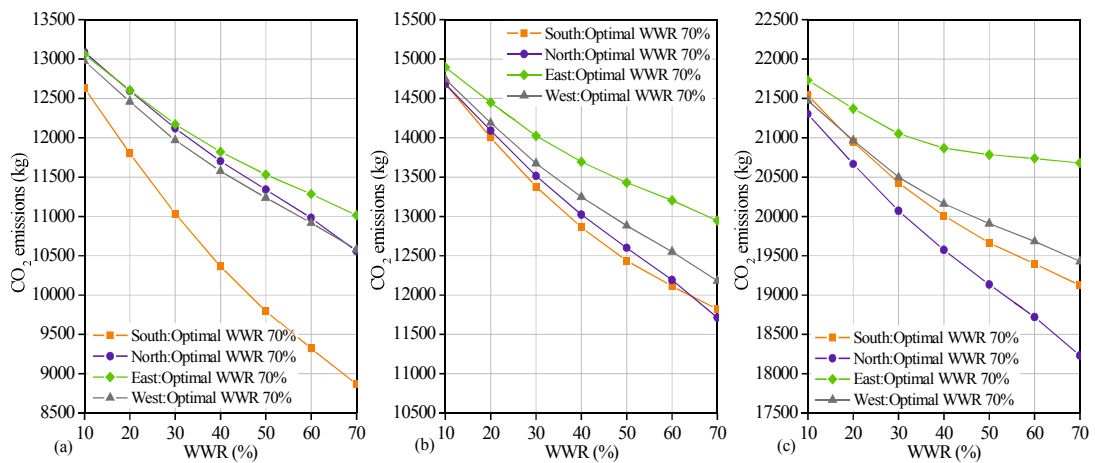


Figure 2.18. Distribution of optimal WWR for three cities and four main orientations for a large-scale building with medium internal gains: (a) Sapporo; (b) Tokyo; (c) Naha.

Figures 2.18 (a), (b), and (c) show the relationship between the CO<sub>2</sub> emissions and the WWR of Sapporo, Tokyo and Naha in the large-scale simulation model with medium internal gains. Figures 2.10 and 2.18 can be compared to examine the effect of building scale on the distribution of optimal WWR. The curves expressing the decrease tendency of CO<sub>2</sub> emissions with increasing WWR become sharper in Sapporo and Tokyo when the building scale is enlarged. Furthermore, the inflection points

on the CO<sub>2</sub> emissions and WWR curves disappear for the south-, west-, and east- facing orientations of Naha. The largest possible window area is the best solution for all of the cases shown in Figure 2.18.

Both the distribution of optimal WWR and the exact value of optimal WWR are less dependent on the level of internal gains in the large-scale building except for the eastern exposure in Naha. Figure 2.19 plots CO<sub>2</sub> emissions against WWR at low, medium, and high internal gains for an eastern facade of the large-scale building in three cities. For high internal gains condition in Naha, the increase in total CO<sub>2</sub> emissions is only approximately 1 % when WWR varies from the optimal value of 50 % to the maximum value of 70 %. It is distinctive that the impacts of climate, window orientation, and internal gains on the distribution of optimal WWR are less important at a larger building scale. The increase in optimal window area occurs because a zone with a deeper space depth has a greater potential for daylighting to reach the working plane (Hiyama 2014). Simultaneously, the cooling load per unit floor area caused by solar and thermal gains due to increasing window area decreases in a building with a deeper space depth (Ghisi & Tinker 2005). This advantage of a larger window area can always be expected even under the conditions of high solar radiation and internal gains. In addition, Figure 2.20-2.22 show the relationship between CO<sub>2</sub> emissions and WWR at low, medium, and high internal gains for southern, northern, and western facade of the large-scale building in three cities as a reference.

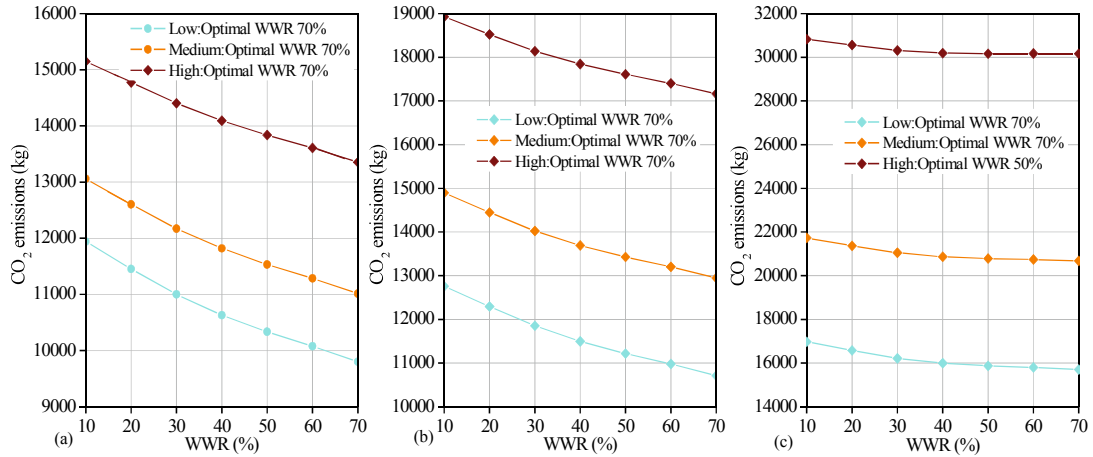


Figure 2.19. Distribution of optimal WWR for three cities at low, medium, and high internal gains

for an east-facing orientation in a large-scale building: (a) Sapporo; (b) Tokyo; (c) Naha.

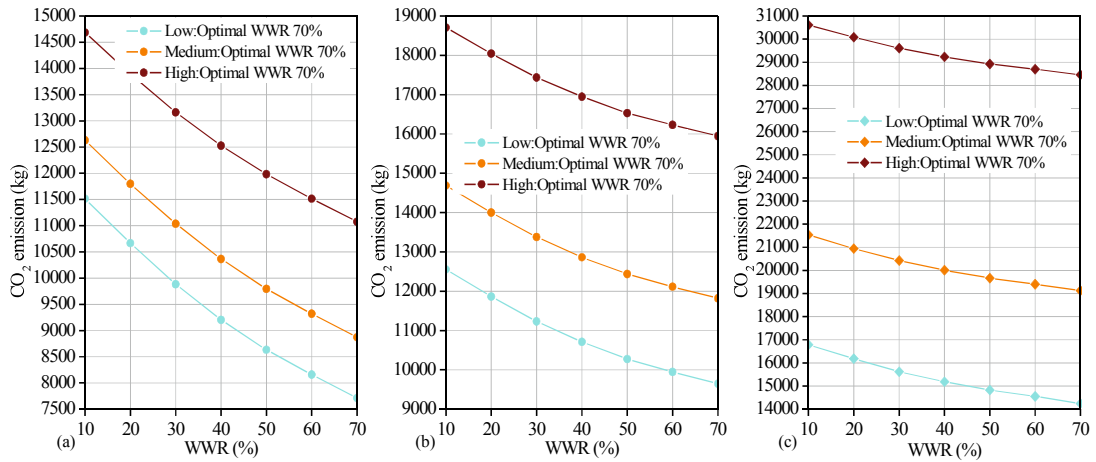


Figure 2.20. Distribution of optimal WWR for three cities at low, medium, and high internal gains

for a south-facing orientation in a large-scale building: (a) Sapporo; (b) Tokyo; (c) Naha.

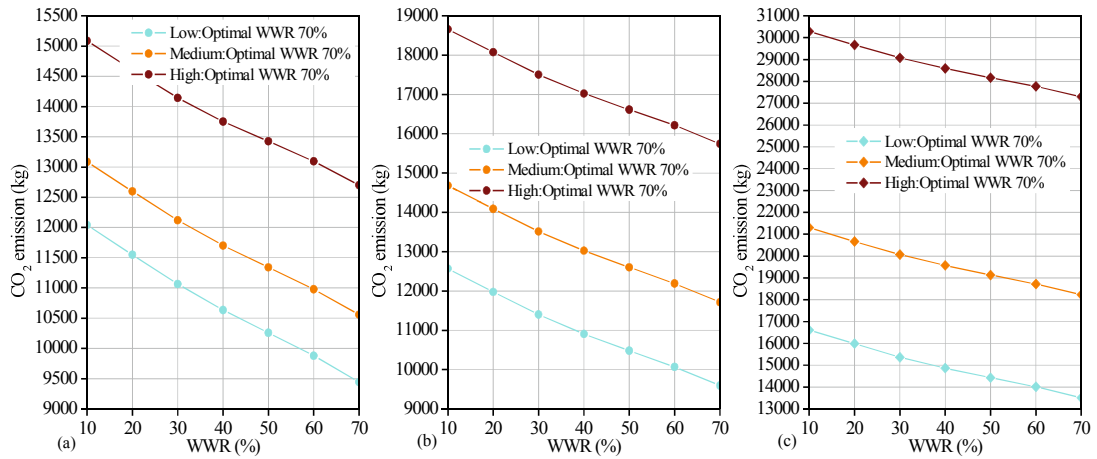


Figure 2.21. Distribution of optimal WWR for three cities at low, medium, and high internal gains

for a north-facing orientation in a large-scale building: (a) Sapporo; (b) Tokyo; (c) Naha.

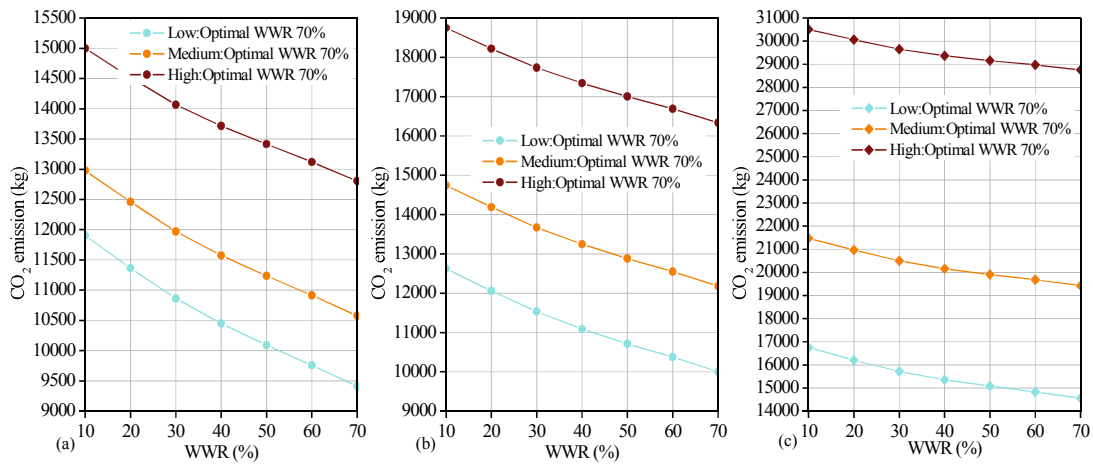


Figure 2.22. Distribution of optimal WWR for three cities at low, medium, and high internal gains

for a west-facing orientation in a large-scale building: (a) Sapporo; (b) Tokyo; (c) Naha.

**Results under the future lighting condition (lighting power density of  $5 \text{ W/m}^2$ )**

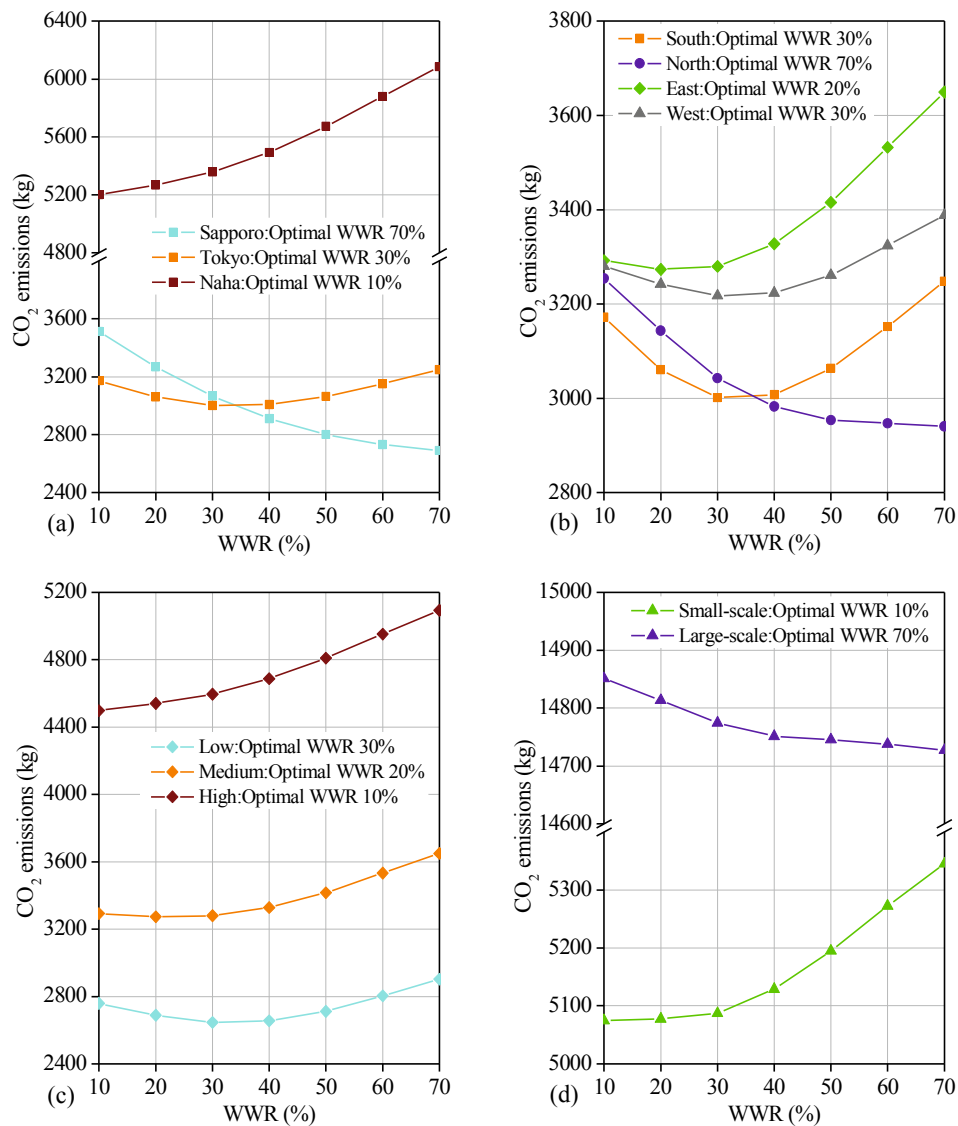


Figure 2.23 Representative simulation results for the lighting power density of  $5 \text{ W/m}^2$

- (a) Distribution of optimal WWR for three cities for a south-facing orientation in a small-scale building with medium internal gains;
- (b) Distribution of optimal WWR in four main orientations for a small-scale building with medium internal gains located in Tokyo;
- (c) Distribution of optimal WWR at low, medium, and high internal gains for an east-facing orientation in a small-scale building located in Tokyo;
- (d) Distribution of optimal WWR for small- and large-scale buildings for a north-facing orientation with medium internal gains located in Naha

For conciseness, the most representative simulation results under the lighting power density of 5 W/m<sup>2</sup> are displayed in Figure 2.23 to explain the possible distribution of optimal WWR. The simulation results for other cases are shown in appendix A. Figure 2.23 (a) shows the optimal WWR distribution for Sapporo, Tokyo, and Naha using the simulation case of a southern facade in the small-scale building with medium internal gains. For the three cities, three different tendencies of CO<sub>2</sub> emissions with increasing WWR can be observed. CO<sub>2</sub> emissions monotonically decrease with increasing WWR in Sapporo. An inflection point of 30 % (in the range of 30-50 %) is shown in Tokyo. However, the CO<sub>2</sub> emissions in Naha constantly increase with increasing WWR. Figure 2.23 (b) presents the impact of window orientation on the distribution of optimal WWR when the design conditions of a small-scale building model, medium internal gains, and weather data from Tokyo are selected. In the northern facade, the CO<sub>2</sub> emissions continually decrease as the window area increases. In both the south- and west-facing orientations, remarkable inflection points are shown at 30 % (in the range of 30-50 %). Furthermore, an inflection point is observed at 20 % in the east-facing orientation; however, the decrease in CO<sub>2</sub> emissions prior to WWR attaining this inflection point is unclear. Conversely, the increasing tendency of CO<sub>2</sub> emissions is predominant when the WWR exceeds 20 %. Figure 2.23 (c) reveals the effect of internal gains on the optimal WWR distribution in the case characterized by an eastern façade in the small-scale building located in Tokyo. The exact value of the optimal WWR still tends to decrease by 10 % when the internal gains increase. Furthermore, the distribution of optimal WWR is slightly influenced by internal gains. At a low level of internal gains, an inflection point of 30 % (in the range of 30-50 %) is observed. The continuously increasing tendency of CO<sub>2</sub> emissions with increasing window area becomes significant when the internal gains increase to the medium and high levels. Under the current lighting condition, the maximum WWR is the best solution for all of the large-scale building cases. However, only some cases display an obvious increase in the optimal WWR value under the future lighting condition. The relatively obvious change

in the optimal WWR distribution due to the variation in building scale is shown in Figure 2.23 (d) for a north-facing orientation, medium internal gains, and weather data from Naha. The CO<sub>2</sub> emissions of the small-scale building continually increase with increasing WWR. This increasing tendency intensifies when the WWR value exceeds 30 %. However, the relationship between CO<sub>2</sub> emissions and WWR of the large-scale building is opposite that of the small-scale building. The larger the WWR is, the lower the CO<sub>2</sub> emissions are.

#### **2.3.1.4. Discussion**

Based on the simulated results of well insulated Double Low-E glazing, some meaningful result are obtained. First, the possible distribution of optimal WWR under different design conditions can be summarized by three major patterns: (i) the smaller the WWR is, the lower the CO<sub>2</sub> emissions are; (ii) an appropriate WWR value exists (in the range of 30-50 %) to minimize the CO<sub>2</sub> emission; and (iii) the larger the WWR is, the lower the CO<sub>2</sub> emissions are. In a few cases, an inflection point is observed at 20 % or 60 %. However, compared to the dominantly increasing tendency of CO<sub>2</sub> emissions, the decrease in CO<sub>2</sub> emissions prior to the inflection point of 20 % is minimal (less than 1 %). Similarly, the decreasing tendency of CO<sub>2</sub> emissions with increasing WWR is more representative for cases with an inflection point of 60 %. Therefore, it is reasonable to classify the optimal WWR distribution of cases with an inflection point of 20 % as pattern (i), whereas the optimal WWR distribution of cases with an inflection point of 60 % as pattern (iii). Although, the three optimal WWR distribution patterns are obtained from the simulation results of Double Low-E glazing (6mm-13mm-6mm). There is no additional optimal WWR distribution besides these three patterns when the Double Clear glazing (6mm-13mm-6mm) and Double Ref-A-H (6mm-13mm-6mm) glazing are simulated. The simulation results of Double Clear glazing and Double Ref-A-H glazing are not illustrated here. However, these results can be found in Appendix B and C, respectively.

Second, from the simulation results obtained from Double Low-E glazing, the five design conditions of climate, window orientation, lighting power density, internal gains, and building scale all show different degrees of influence on the optimal WWR distribution and exact optimal WWR value. Specifically, the lighting power density, climate, window orientation, and building scale impact both the exact optimal WWR value and the distribution of the optimal WWR. The slight impact of the internal gains on the optimal WWR distribution can be observed under the future lighting condition. In addition, the optimal WWR value changes only 10 % when the internal gains increase to a higher level.

In order to quantitatively estimate the impact of each design condition on the optimal WWR configuration, evaluation and discussion are performance in the section. Design conditions with minimal effect are considered to minimize the variation in objective function when the design conditions are changed (Pino et al. 2012). Therefore, the evaluation is conducted by examining the variation in objective function (CO<sub>2</sub> emissions in this study) when the determined optimal WWR values under predefined design conditions are assigned to the cases with variable design conditions.

Firstly, the impacts of internal gains and building scale on the optimal WWR configuration are evaluated. In the evaluation, using Eq. (2-2) the robustness of the optimal WWR values obtained from medium internal gains and small-scale building are examined for varying internal gains (i.e., low and high levels) and building scale (i.e., large-scale) condition, respectively.

$$\Delta Q_{TOT} = \frac{Q_{TOT}(WWR_{REF}) - Q_{TOT}(WWR_{OPTI})}{Q_{TOT}(WWR_{OPTI})} \times 100\% \quad (2-2)$$

where  $Q_{TOT}(WWR_{REF})$  is the total CO<sub>2</sub> emissions for the reference default values (non-optimal), which corresponds to medium internal gains for evaluation the effect of internal gains, and a small-scale



building for evaluation the effect of building scale,  $Q_{TOT}(WWR_{OPTI})$  is the total CO<sub>2</sub> emissions at the optimal default values, and  $\Delta$  indicates the incremental value.

Table 2.5 lists the maximum  $\Delta Q_{TOT}$  calculated using Eq. (2) under the current and future lighting conditions when the Double Low-E glazing is adopted. The maximum increase in CO<sub>2</sub> emissions is 3.8 % when the reference default value obtained from the small-scale building is assigned to the large-scale building under the current lighting load. For the future lighting load, the maximum increase in total CO<sub>2</sub> emissions due to replacing the optimal WWR values with the reference default values are all within 2 %. The increase in the objective function of within 5 % produced by adopting a non-optimal value is believed to have a less critical influence, and the inclusion of such a tiny error in the building design process is acceptable (Goia 2016). Thus, the optimal results determined for medium internal gains and a small-scale building are sufficiently robust for a building with variable internal gains and building scale conditions. Although, the evaluation is illustrated using the case study with Double low-E glazing. These indistinctive impacts of internal gains and building scale on optimal WWR configuration can also be verified by cases with Double Clear glazing and Double Ref-A-H glazing, as shown in Tables 2.6 and 2.7. The maximum increase in CO<sub>2</sub> emissions is 4.7 % when the optimal WWR value of a small-scale building is assigned to a large-scale building under the current lighting condition with the Double Clear glazing in Table 2.6. It is distinctive that the increase in the objective function of CO<sub>2</sub> emissions due to the adoption of reference default WWR values from medium internal gains and small scale building are all less than the threshold of 5 %. Thus, the internal gains and building scale conditions can be simplified as the medium level and small scale in the discussion of default WWR value during the early design stages.

Table 2.5. Maximum increase in total CO<sub>2</sub> emissions obtained by replacing the optimal default value with the reference default value (Glazing type: Double Low-E glazing 6mm-13mm-6mm).

	Medium internal gains	Small-scale building
Current lighting condition	0.3 %	3.8 %
Future lighting condition	1.6 %	1.8 %

Table 2.6. Maximum increase in total CO<sub>2</sub> emissions obtained by replacing the optimal default value with the reference default value (Glazing type: Double Clear glazing 6mm-13mm-6mm).

	Medium internal gains	Small-scale building
Current lighting condition	0.3 %	4.7 %
Future lighting condition	1.7 %	2.6 %

Table 2. 7. Maximum increase in total CO<sub>2</sub> emissions obtained by replacing the optimal default value with the reference default value (Glazing type: Double Ref-A-H glazing 6mm-13mm-6mm).

	Medium internal gains	Small-scale building
Current lighting condition	0	0 %
Future lighting condition	0.6 %	3.4 %

It is difficult to find a reference condition for lighting power density, climate, and window orientation. Therefore, to evaluate the influence of lighting power density, climate, and window orientation on the optimal WWR configuration, the  $Q_{TOT}(WWR_{REF})$  in Eq. (2-2) is replaced by the total CO<sub>2</sub> emissions determined at an arbitrary non-optimal WWR value as shown in Eq. (2-3).

$$\Delta Q_{TOT} = \frac{Q_{TOT}(WWR_{NON-OPTI}) - Q_{TOT}(WWR_{OPTI})}{Q_{TOT}(WWR_{OPTI})} \times 100\% \quad (2-3)$$

where  $Q_{TOT}(WWR_{NON-OPTI})$  is the total CO<sub>2</sub> emissions obtained from an arbitrary non-optimal WWR value.

It can be illustrated using the simulation results in figure 2.23. As an example, figure 2.23 (a) shows that the optimal WWR value of Sapporo (70 %) is one of non-optimal WWR for Naha. Table 2.8 lists the maximum  $\Delta Q_{TOT}$  when the worst WWR is adopted to replace the optimal one for cases with the Double Low-E glazing. It is observed that these values are all beyond the acceptable level of 5 %. The maximum increase in objective function of CO<sub>2</sub> emissions even reaches up to 29 % when the climate impact is neglected. The lighting power density, climate, and window orientation are therefore the critical design conditions that strongly impact the optimal WWR configuration. It is necessary to consider the difference regarding these conditions when the appropriate WWR value for a new project during the early design stages is determined. Furthermore, it is found that the climate and window orientation have increasingly significant impacts as the lighting efficiency considerably improves in the future based on these results shown in Table 2. 7.

As mentioned above, reusing BIM data of optimal design in the past can make the simulation in the early design stages more efficient (Hiyama et al. 2014). The challenge in the adoption of this method is to estimate the similarities between a new project and a past optimal design. Based on the evaluation results in this section, these critical conditions of lighting power density, climate, and window orientation could also be helpful in determining the similarity between a new project and the previous optimal projects.

Table 2.8. Maximum increase in total CO<sub>2</sub> emissions obtained by replacing the optimal default value with a non-optimal value (Double Low-E glazing).

	Climate	Window orientation
Current lighting condition	6.8 %	6.8 %
Future lighting condition	29.0 %	11.5 %

### 2.3.2 Recommended WWR maps based on optimization results

In this section, maps of recommended WWR in Japan are created to show the climate suitability of the suggested WWR options proposed in this study. According to the results of quantitative evaluation, the optimization calculations of 10 locations with south-, north-, east-, and west-facing orientations are performed for lighting power densities of 10 W/m<sup>2</sup> and 5 W/m<sup>2</sup> to determine the best solutions for current and future lighting conditions, respectively. The optimization results are processed according to the investigated patterns of optimal WWR distribution 2.3.1 to generate the recommended WWR maps.

#### 2.3.2.1 Optimization scheme

The small-scale building model and the medium internal gains conditions are fixed in the optimizations because that their optimal WWR are verified sufficiently robust for buildings with variable building scales and internal gains. The analyzed third floor is divided by a virtual partition that is assumed to be adiabatic along the central line, and only half of this floor is considered for the results (plan view in figure 2.3). The conditions used in the optimizations are identical to those of the integrated simulations described in section 2.3.1.1. Ten locations are selected according to the Japanese climate regions that divides Japan into 8 numbered zones (Takamoto 2000). Three locations

are selected from zone 6 due to the relatively complex climate in this zone. For the other zones (1-5, 7-8), only one representative location is selected to generate the recommended WWR maps. Furthermore, the 10 locations denoted on the maps are all prefectural capitals. Table 2. 9 lists the basic information for these 10 locations selected. The objective function is the minimization of CO<sub>2</sub> emissions.

Table 2. 9. Basic information of the ten selected locations.

No.	Selected locations	Prefecture	Region in Japan	Mean external temperature (°C)			Mean global solar radiation (Wh/m <sup>2</sup> )		
				Year	Jan	Aug	Year	Jan	Aug
				1	Asahikawa	Hokkaido	1 (Dfb)	6.8	-7.1
2	Sapporo	Hokkaido	2 (Dfa)	8.8	-3.3	21.1	135.4	68.8	165.3
3	Morioka	Iwate	3 (Dfa)	10.5	-1.5	23.0	133.1	82.6	163.5
4	Niigata	Niigata	4 (Dfa)	14.0	3.1	26.2	142.5	62.8	204.2
5	Maebashi	Gunma	5 (Cfa)	14.9	3.8	26.2	152.5	108.4	195.4
6	Tokyo	Tokyo	6 (Cfa)	16.6	6.3	27.0	142.7	106.9	170.6
7	Osaka	Osaka	6 (Cfa)	17.1	6.1	28.3	147.8	91.2	207.5
8	Yamaguchi	Yamaguchi	6 (Cfa)	15.6	4.7	26.9	158.6	87.5	202.6
9	Kagoshima	Kagoshima	7 (Cfa)	18.6	9.1	28.5	162.9	109.0	207.3
10	Naha	Okinawa	8 (Cfa)	23.3	18.0	29.0	163.9	97.9	233.1

Dfb, Dfa and Cfa indicate the climate zones according to the Koppen-Geiger climate classification (Kottek et al. 2006).

Two design variable are adopted in optimization. The WWR in the optimizations varies from 20 % to 60 % with a 10 % increment to avoid unrealistic window areas in design practice. The relationship

between the CO<sub>2</sub> emissions and the WWR for a north-facing orientation of Sapporo in the small-scale building with medium internal gains under lighting power density of 5 W/m<sup>2</sup> when Double Low-E glazing, Double Clear, and Double Ref-A-H glazing are simulated is shown in figure 2. 24. The impact of glazing type on optimal WWR distribution can be clearly observed from the Double Low-E glazing and Double Ref-A-H glazing. The optimal WWR distribution of Double Low-E glazing belongs to pattern (iii). Whereas, the optimal WWR distribution for Double -Ref-A-H is classified into pattern (i). In addition, the increase in CO<sub>2</sub> emissions is 11 % (above the acceptable level of 5 %) when the optimal WWR value of Double Ref -A-H glazing is assigned to the case of Double-Low-E glazing. Thus, glazing type is selected as another design variable in the optimizations. The thermal characteristics of the U-value and the solar heat gain coefficient (SHGC) are used to describe the glazing type (Kim et al. 2014). In total, 14 types of glass are selected, as shown in Table 2. 10.

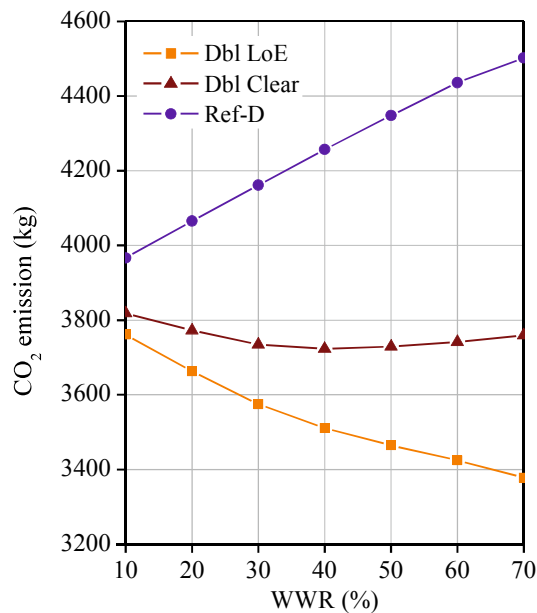


Figure 2.24. The impact of glazing type on optimal WWR configuration (north-facing orientation of Sapporo in small-scale building with medium internal gains under lighting power density of 5 W/m<sup>2</sup>)

Table 2. 10. Selected glazing types (the values in the parentheses indicate the light-to-solar Gain ratio, which is defined as the visible transmittance (VT) divided by the solar heat gain coefficient (SHGC)).

U-value (W/m <sup>2</sup> •K)	SHGC			
	0.2	0.4	0.6	0.75
1.0	A1 (1.1)	A2 (1.5)	A3 (1.2)	-
1.8	B1 (1.1)	B2 (1.2)	B3 (1.3)	B4 (1.0)
2.7	C1 (0.8)	C2 (0.7)	C3 (1.2)	C4 (1.1)
3.2	-	D2 (0.7)	D3 (1.2)	D4 (1.1)

A1.Trp LoE Film (44) Bronze 6mm/13mm Arg; A2.Trp LoE Film (66) Clr 6mm/13mm Arg; A3.Trp LoE (e5=.1) Clr 3mm/13mm Arg; B1.Trp LoE Film (44) Bronze 6mm/6mm Air; B2.Dbl LoE (e2=.1) Tint 6mm/13mm Air; B3.Dbl LoE (e2=.1) Clr 6mm/13mm Air; B4.Dbl Elec Abs Bleached 6mm/13mm Air; C1.Dbl Ref-A-H Clr 6mm/6mm Air; C2.Dbl Ref-D Clr 6mm/13mm Air; C3.Dbl Green 3mm/13mm Air; C4.Dbl Clr 3mm/13mm Air; D2.Dbl Ref-D Clr 6mm/6mm Air; D3.Dbl Green 3mm/6mm Air; D4.Dbl Clr 3mm/6mm Air.

The optimal WWR distribution under variable design conditions only displays three patterns as described above. Thus, three corresponding options are recommended in this study: a smaller WWR, a moderate WWR, and a larger WWR. The optimization results are processed according to the following procedure to show recommended WWR for different cases: (1) if the optimal WWR is calculated as 20 %, then the recommended WWR belongs to pattern (i): the smaller the WWR is, the lower the CO<sub>2</sub> emissions are; (2) if the optimal WWR value calculated is within the range of 30-50 %, then the recommended WWR is pattern (ii): an appropriate WWR (in the range of 30-50 %) exists to minimize the CO<sub>2</sub> emissions; and (3) if the optimal WWR is calculated as 60 %, then the recommended

WWR is classified as pattern (iii): the larger the WWR is, the lower the CO<sub>2</sub> emissions are. Then, the recommended WWR maps are generated according to the processed optimization results to provide preliminary information for default WWR value setting.

#### 2.3.2.2 Recommended WWR maps.

The recommended WWR maps created by the proposed method are shown in section. Figure 2. 25 presents the map of recommended WWR when the combined lighting power density is 10 W/m<sup>2</sup>. For each location, a disconnected circle is used to show the information of recommended WWR. The four portions of the disconnected circle represent the four main orientations: top stands for north, bottom for south, left for west, and right for east. Three different colors (black, gray, and white) are used to distinguish the recommended WWR options: black corresponds to “as the WWR decreases, the CO<sub>2</sub> emissions decrease”, gray to “an appropriate WWR exists (30-50 %) at which CO<sub>2</sub> emissions are minimized”, and white to “as the WWR increases, the CO<sub>2</sub> emissions decrease”. It can be observed that a larger WWR default value is recommended for most locations under the current lighting load from the viewpoint of building operation; this is especially true for buildings located in zones 1-5 of the Japanese climate regions, regardless of window orientation. For buildings located in zones 7-8 of the Japanese climate regions, the largest default value of WWR is still suggested for the south-, north-, and west- facing orientations. However, this finding is invalid for the eastern façade in these zones; instead, a moderate default value of WWR (in the range of 30-50 %) is suggested for optimal building performance. The maximum WWR of 40 % suggested by American National Standards Institute (ANSI)/American Society of Heating, Refrigerating and Air-Conditioning Engineers (ASHRAE)/Illuminating Engineering Society (IES) standard 90.1-2010 is therefore helpful for the eastern façade in these zones (ASHRAE 2010). Furthermore, buildings in Tokyo in zone 6 show the same recommended WWR default value as those in zones 1-5, and the results of Osaka and Yamaguchi



are identical to those of zones 7-8. Thus, the climate should be carefully examined for buildings located in zone 6 of the Japanese climate region, which has relatively complex climate conditions.

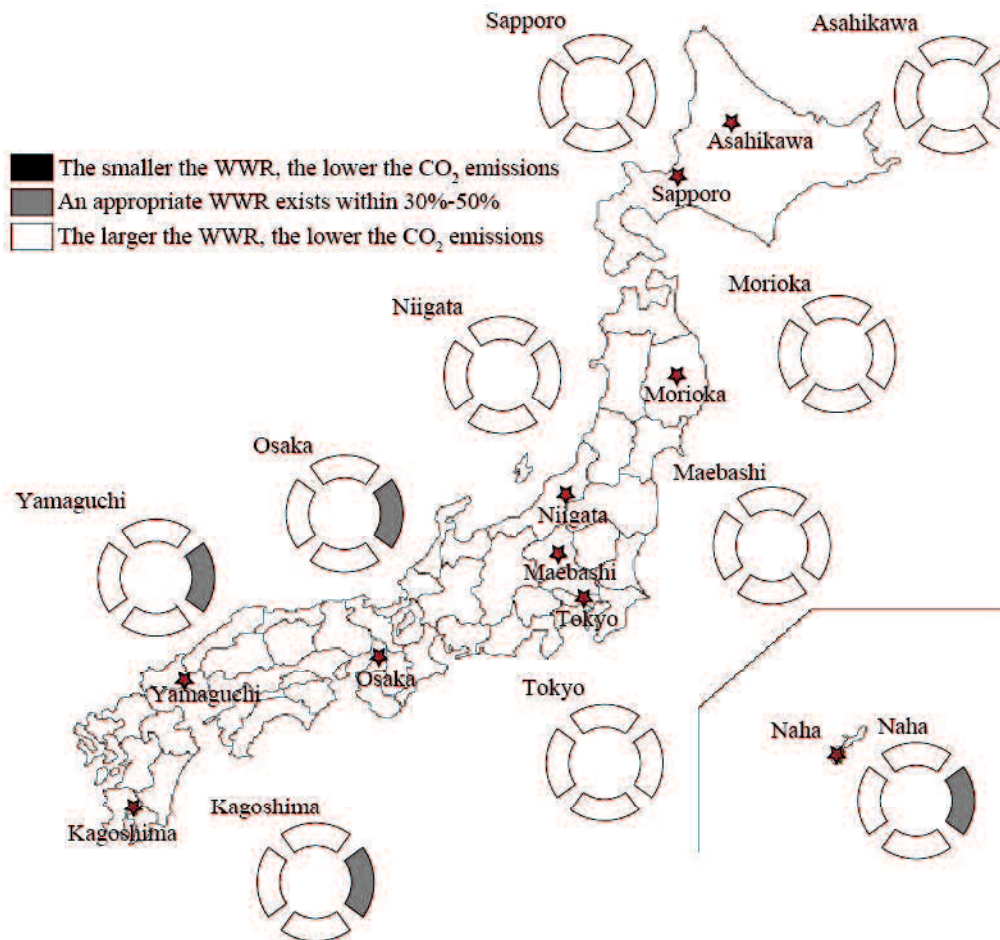


Figure 2. 25. Recommended WWR map for a lighting power density of 10 W/m<sup>2</sup> (The four disconnected circle sections represent the four main orientations: top stands for north, bottom for south, left for west, and right for east).

The active schedule controlling the raising and lowering of blind and the clear weather condition during morning are considered to be the major reasons for a smaller recommended WWR for the east-facing orientations in zones 6-8 of the Japanese climate regions and Tokyo. To increase the awareness of daylighting utilization, the inside blind in the simulation is supposed to be controlled by solar

radiation during the occupied period (9:00-18:00). The blind is off in exception of the occupied period. An oversized window area will cause an excessive increase in solar gain and thermal gain through the eastern facade occupied in the morning. Similar results were also observed in a previous study that focused on optimizing the properties of glazing and an internal woven roller shade (Singh et al. 2015). Accordingly, it is important to keep the creation conditions of recommended WWR maps consistent with the actual using status of buildings.

Figure 2. 26 presents the recommended WWR map for a combined lighting power density of 5 W/m<sup>2</sup>. The potential for lighting energy savings through daylight use decreases due to the decreased artificial lighting demand. Thus, the advantage of adopting a larger window area diminishes. Although the largest window area remained the best solution for all four orientations of buildings located in the cold climate zones 1-3 of the Japanese climate regions, the recommend default value of WWR clearly decreased in locations with a temperate and warm climate. This change is attributed to the excessive solar and thermal gains that occur through an oversized window area in these zones. For zones 4-7 of the Japanese climate regions, the default WWR value should be carefully selected according to window orientation. A larger WWR default value is recommended only for the northern façade. A moderate default value (in the range of 30-50 %) is suggested for the southern and western facades, while the minimum WWR default value is the best choice for the eastern façade. Finally, a glass facade is not suggested for buildings located in zone 8 of the Japanese climate regions, which is characterized by a warm climate and high amounts of sunshine. A smaller WWR default value is recommended for the south-, east-, and west- facing orientations. A moderate window size is allowed for the northern façade to obtain better performance.

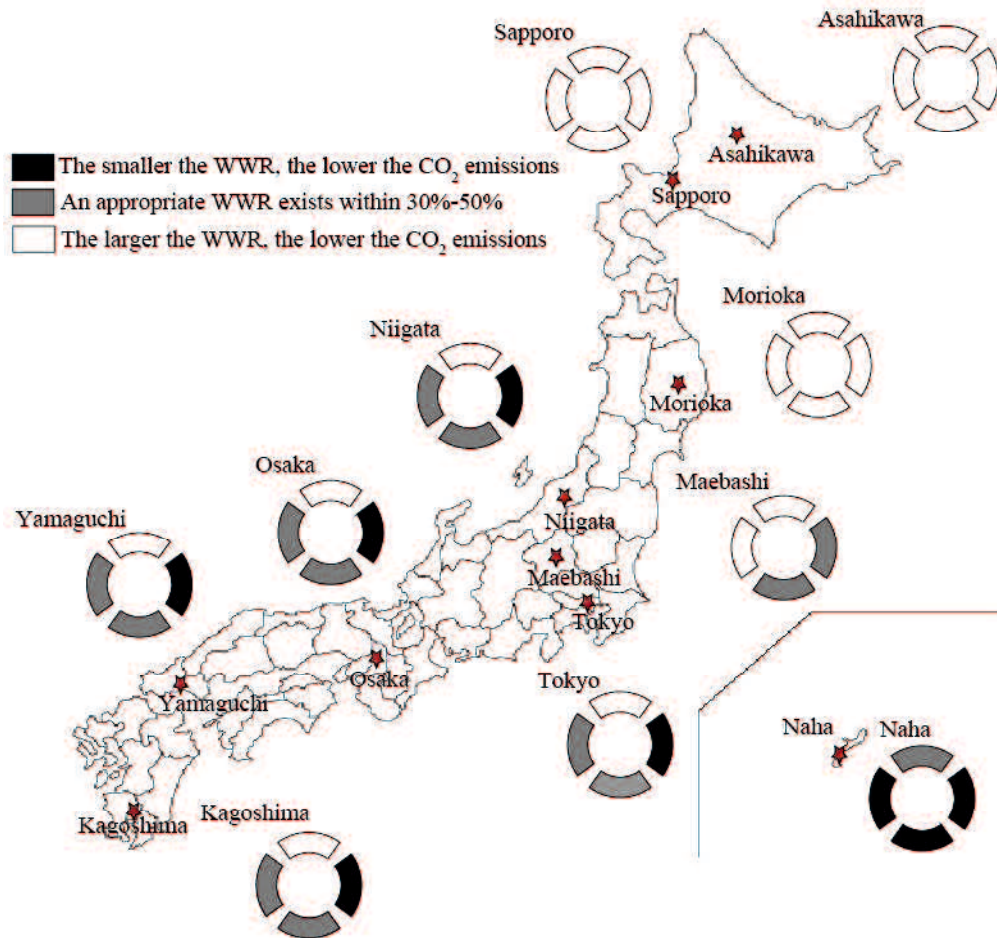


Figure 2.26. Recommended WWR map for a lighting power density of 5 W/m<sup>2</sup> (The four disconnected circle sections represent the four main orientations: top stands for north, bottom for south, left for west, and right for east).

The optimal WWR values presented in this section depend on the individual glazing type. However, WWR is the focus of this study because WWR is decided first in the design process. Glazing type is a design parameter that can be discussed and modified in the following design stages (Hiyama & Wen 2015). Thus, the glazing types corresponding to the optimal WWR are not discussed here; the relevant information is presented in Table 2. 11 and 2.12.

Table 2. 11. Optimal glazing types for a lighting power density of 10 W/m<sup>2</sup>.

	South	North	East	West
1. Asahikawa	A3	A3	A2	A2
2. Sapporo	A3	A3	A2	A3
3. Morioka	B3	A3	A2	A2
4. Niigata	B3	B3	A2	A2
5. Maebashi	D3	B3	D3	B3
6. Tokyo	D3	B3	D3	C3
7. Osaka	D3	B3	D3	C3
8. Yamaguchi	D3	B3	D3	C3
9. Kagoshima	D3	D3	D3	D3
10. Naha	D3	D3	D3	D3

Table 2. 12. Optimal glazing types for a lighting power density of 5 W/m<sup>2</sup>.

	South	North	East	West
1. Asahikawa	A3	A3	A2	A2
2. Sapporo	A3	A3	A2	A2
3. Morioka	A2	A2	A2	A2
4. Niigata	B3	A2	A2	A2
5. Maebashi	D3	A2	A2	A2
6. Tokyo	D3	A2	A2	A2
7. Osaka	D3	A2	A2	A2
8. Yamaguchi	D3	A2	A2	A2
9. Kagoshima	D3	D3	B1	D3
10. Naha	D3	D3	B1	D3

## 2.4 Summary

For successful energy efficient building design, design performance modeling (DPM), defined as the energy/performance simulations in the concept and schematic design stages, should be actively integrated into the design process. However, this integration is not an easy task because some design parameters required as input data are still undetermined in the early design stage. Window-to-wall ratio (WWR) is part of the required input data for discussing the building shape and configuration in the very beginning of the design process. In this paper, a methodology for creating maps of recommended WWR was proposed in section 2.2 to assign appropriate default values in DPM. This was accomplished using integrated thermal and daylighting simulations in section 2.3.1 and optimizations in section 2.3.2. The maps inform architects about the direction of default value: a

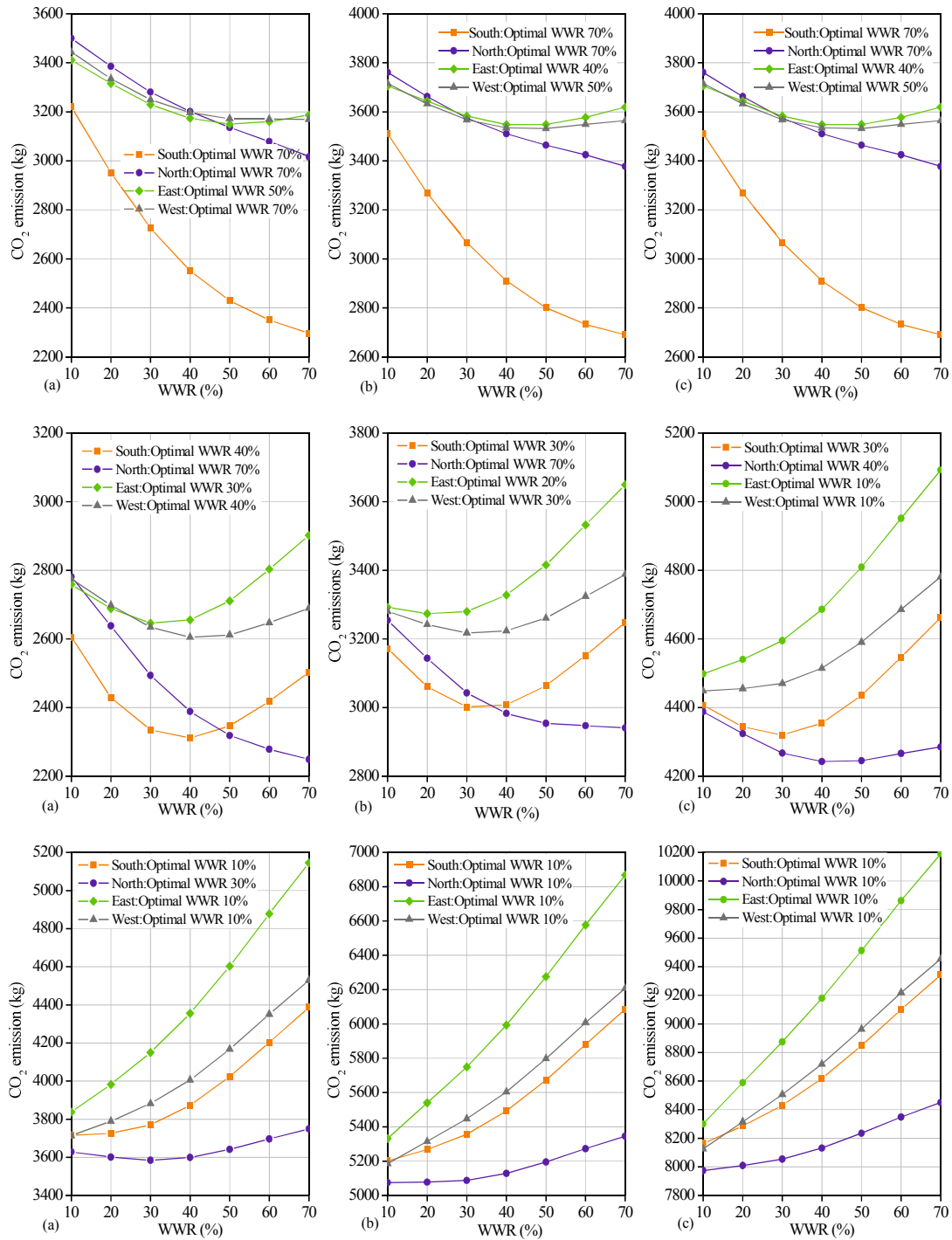
smaller WWR, a moderate WWR, or a larger WWR. The main findings of this study are summarized as follows:

- (1) This study was conducted to create maps of recommended WWR for open office in Japan. The possible distribution of optimal WWR under different design conditions of lighting power density, climate, window orientation, internal gains, and building scale were summarized as three overall patterns according to the integrated simulations: (i) the smaller the WWR is, the lower the CO<sub>2</sub> emissions are; (ii) an appropriate WWR value exists (in the range of 30-50 %) to minimize the CO<sub>2</sub> emissions; and (iii) the larger the WWR is, the lower the CO<sub>2</sub> emissions are. Both the exact optimal WWR value and the distribution of optimal WWR were verified to be influenced by lighting power density, climate, window orientation, and building scale. The impact of internal gains on the distribution of optimal WWR was observed for the future lighting load of 5 W/m<sup>2</sup>. However, the exact optimal WWR values increased by only 10 % when the internal gains increased to a higher level.
- (2) Quantitative evaluation was performed to determine the impact of each design condition on the optimal WWR configuration. This evaluation was conducted by examining the increase in CO<sub>2</sub> emissions when the determined optimal WWR was adopted in cases with variable design conditions. Quantitative evaluation indicated that the optimal results determined for medium internal gains and a small-scale building were sufficiently robust for a building with variable internal gains and building scale. However, the conditions of lighting power density, climate, and window orientation showed strong impacts on the optimal WWR configuration. Thus, the optimization results of 10 locations in four main orientations under two lighting power densities were processed according to the patterns of optimal WWR distribution to generate the maps of recommended WWR in Japan for current (10 W/m<sup>2</sup>) and future (5 W/m<sup>2</sup>) lighting conditions.
- (3) For the current lighting condition, a larger WWR default value was always recommended for

cities located in zones 1-5 and Tokyo, which is located in zone 6 of the Japan climate regions, regardless of window orientation. For the remaining locations, a moderate default value of WWR (30-50 %) was suggested for the eastern façade.

- (4) The recommended WWR tended to decrease as the lighting efficiency further improved, especially in the temperate and warm climate zones 4-8 of the Japan climate regions. A moderate or smaller default value should be carefully assigned according to window orientation. In addition, glass façade was not suggested to be installed for the east-facing orientation in these zones.

## Appendix A





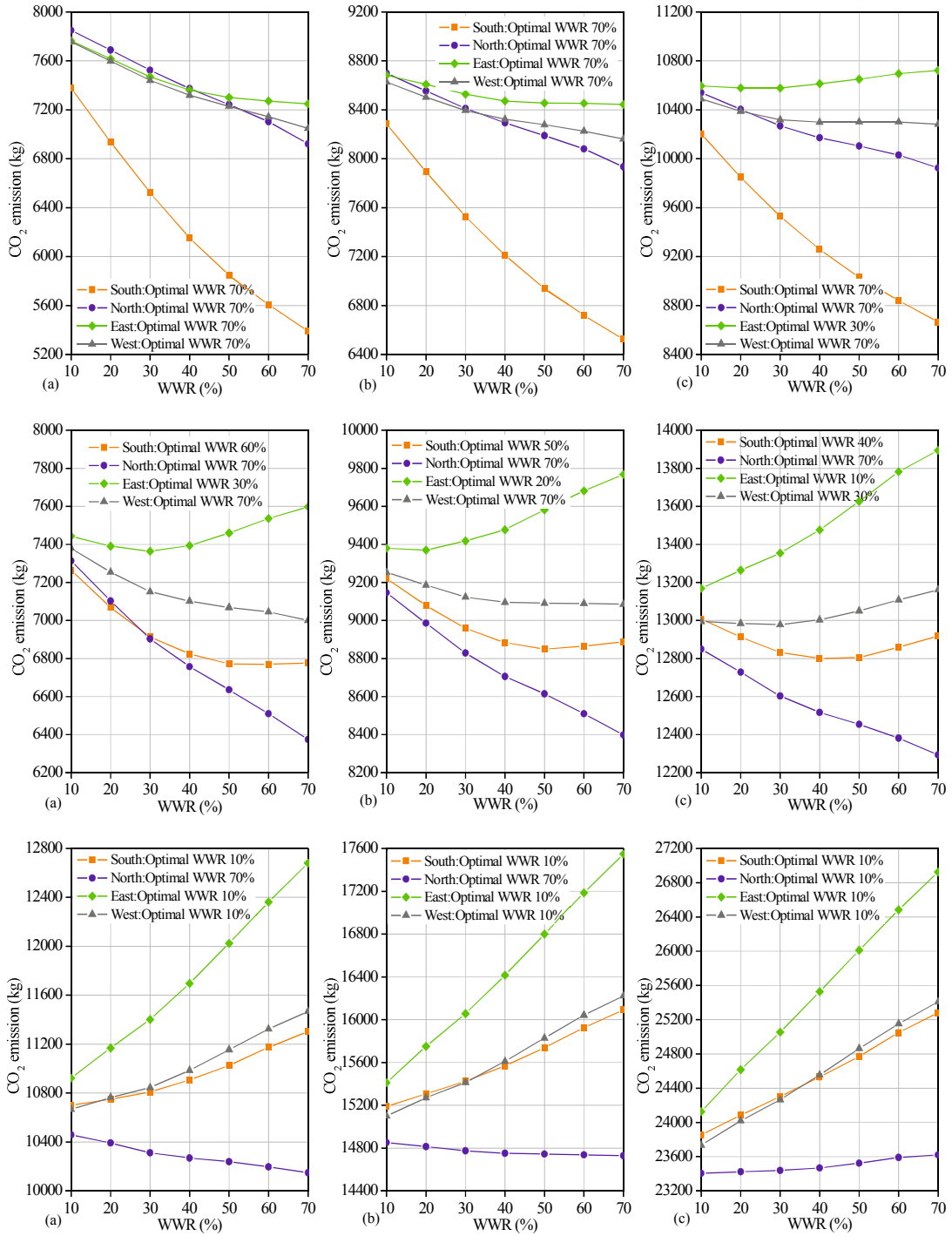


Figure 2. A. 2. Distribution of optimal WWR in a large-scale building (Double Low-E glazing; Lighting power density of 5 W/m<sup>2</sup>; Top: Sapporo, Middle: Tokyo, Bottom: Naha; (a) Low internal gains, (b) Medium internal gains, (c) High internal gains).

## Appendix B

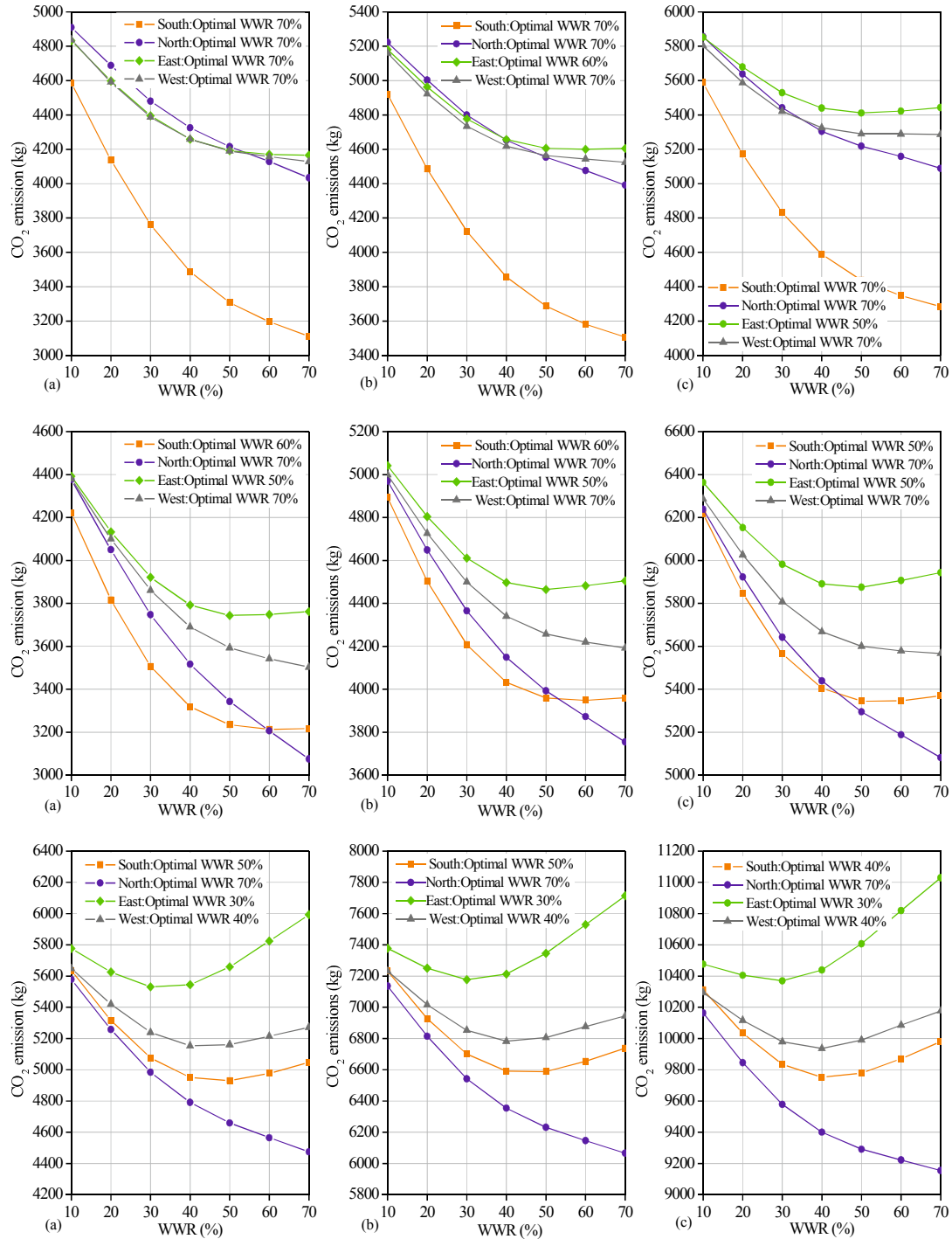


Figure 2. B. 1. Distribution of optimal WWR in a small-scale building (Double Clear glazing; Lighting power density of 10 W/m<sup>2</sup>; Top: Sapporo, Middle: Tokyo, Bottom: Naha; (a) Low internal gains, (b) Medium internal gains, (c) High internal gains).

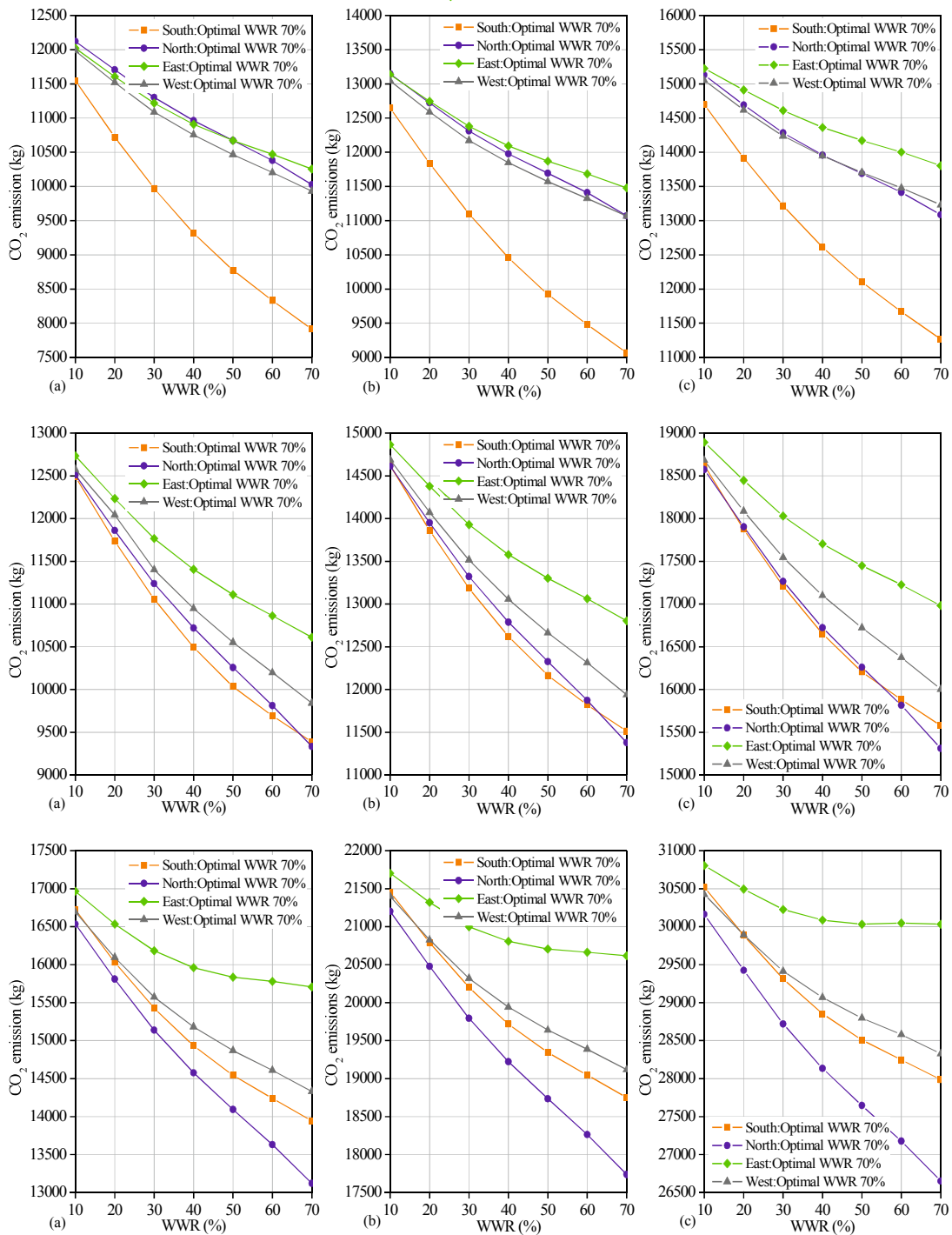


Figure 2. B. 2. Distribution of optimal WWR in a large-scale building (Double Clear glazing; Lighting power density of 10 W/m<sup>2</sup>; Top: Sapporo, Middle: Tokyo, Bottom: Naha; (a) Low internal gains, (b) Medium internal gains, (c) High internal gains).

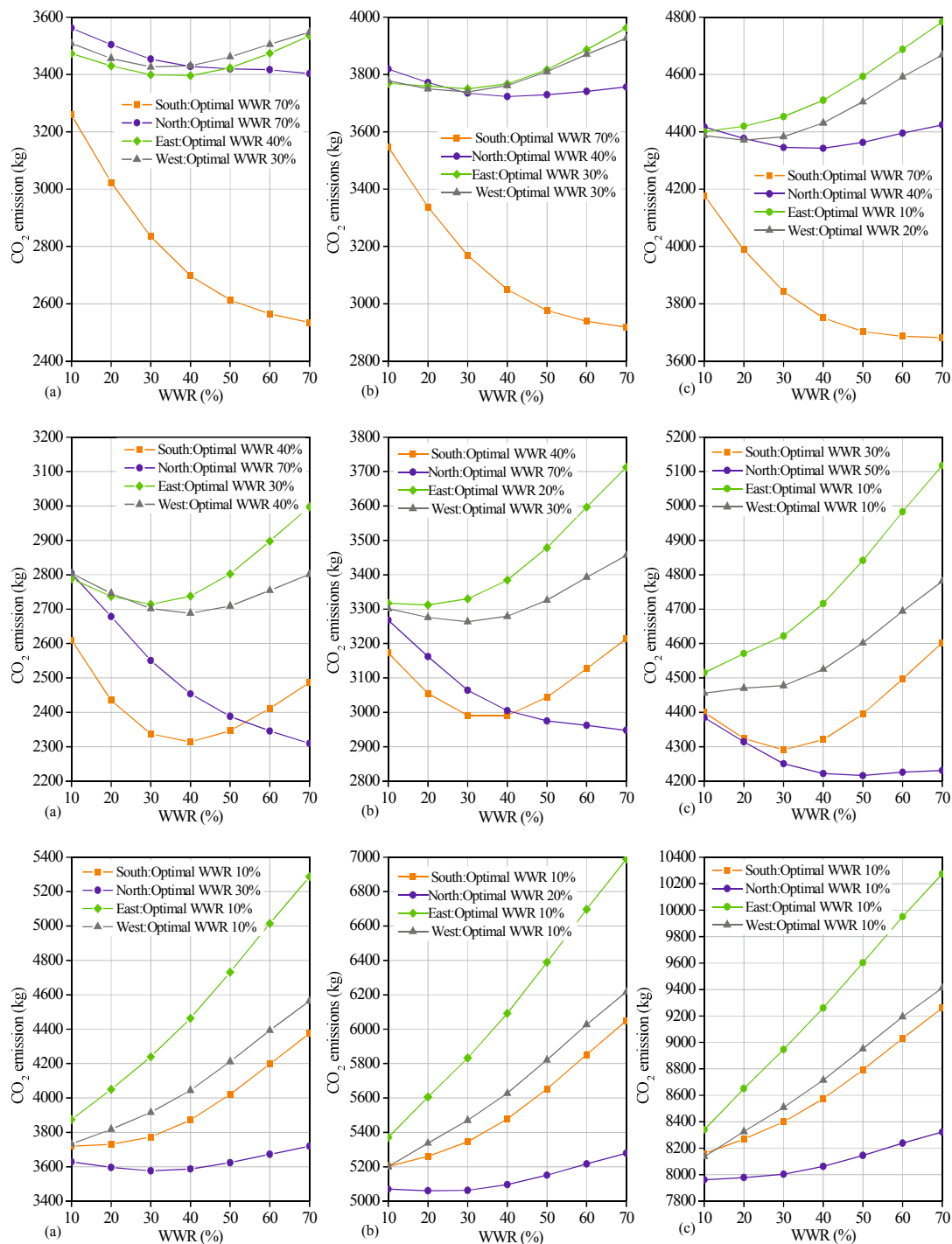


Figure 2. B. 3. Distribution of optimal WWR in a small-scale building (Double Clear glazing; Lighting power density of  $5 \text{ W/m}^2$ ; Top: Sapporo, Middle: Tokyo, Bottom: Naha; (a) Low internal gains, (b) Medium internal gains, (c) High internal gains).

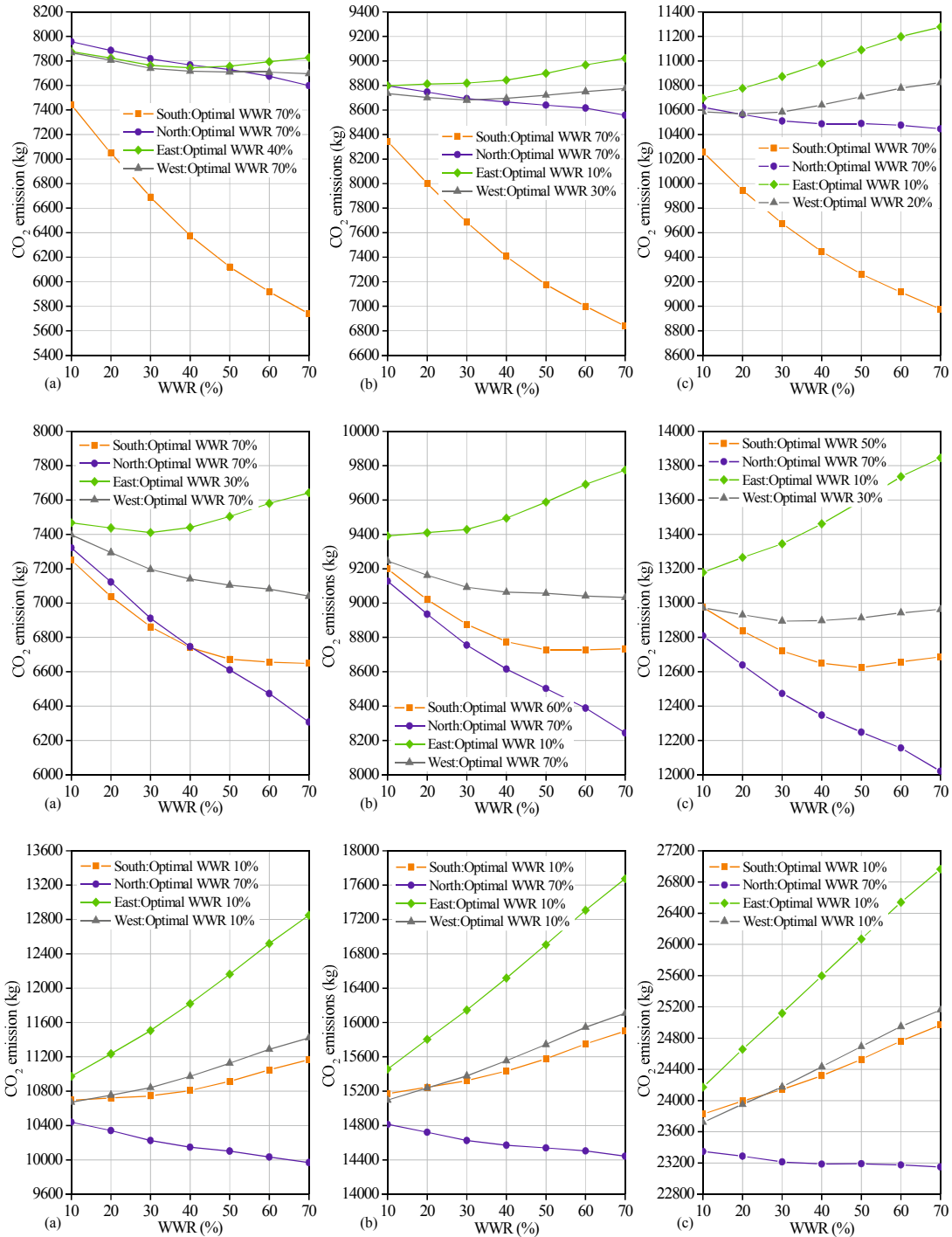


Figure 2. B. 4. Distribution of optimal WWR in a large-scale building (Double Clear glazing; Lighting power density of 5 W/m<sup>2</sup>; Top: Sapporo, Middle: Tokyo, Bottom: Naha, (a) Low internal gains, (b) Medium internal gains, (c) High internal gains).

## Appendix C

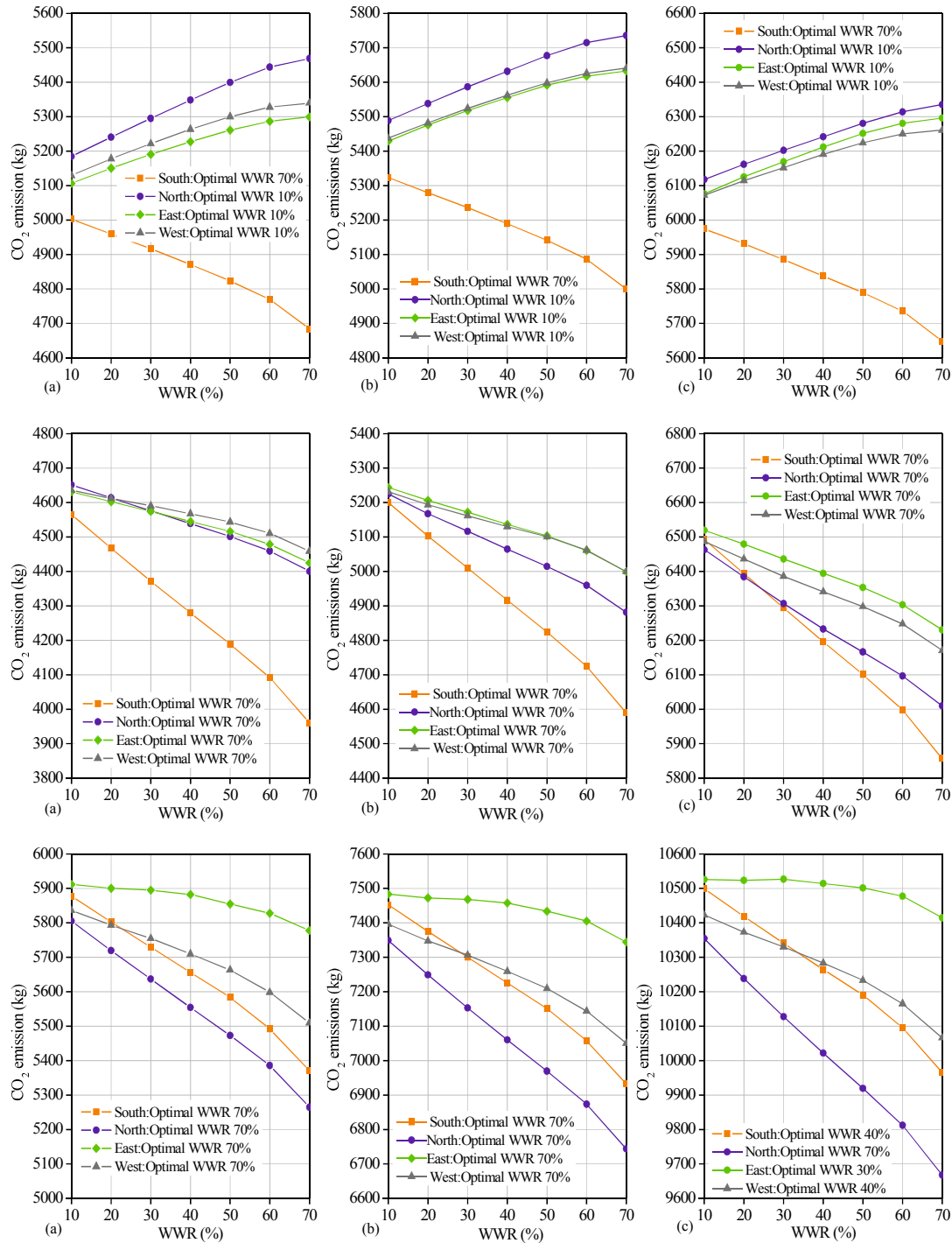


Figure 2. C. 1. Distribution of optimal WWR in a small-scale building (Double Ref-A-H glazing; Lighting power density of 10 W/m<sup>2</sup>; Top: Sapporo, Middle: Tokyo, Bottom: Naha, (a) Low internal gains, (b) Medium internal gains, (c) High internal gains).

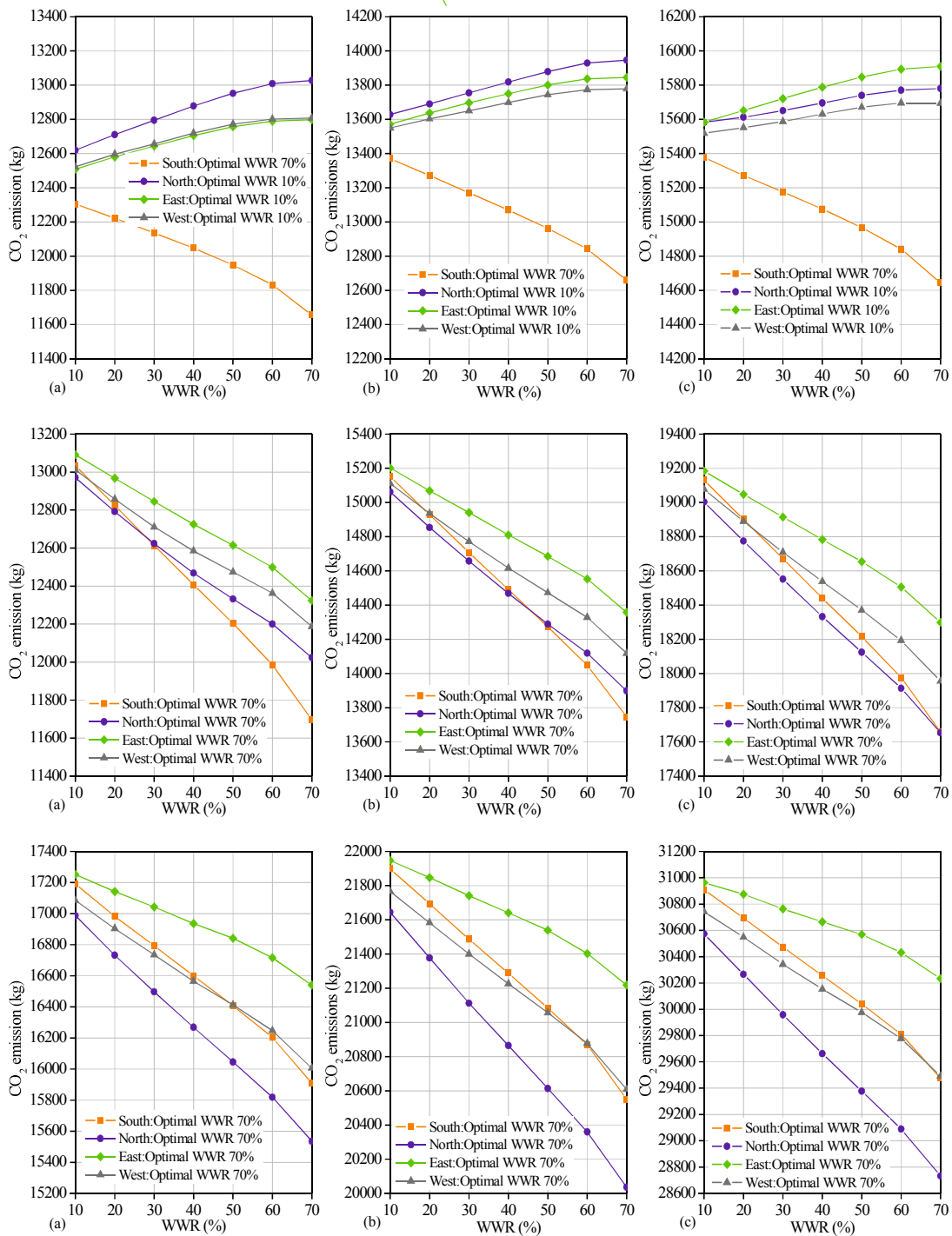


Figure 2. C. 2. Distribution of optimal WWR in a large-scale building (Double Ref-A-H glazing; Lighting power density of 10 W/m<sup>2</sup>; Top: Sapporo, Middle: Tokyo, Bottom: Naha; (a) Low internal gains, (b) Medium internal gains, (c) High internal gains).

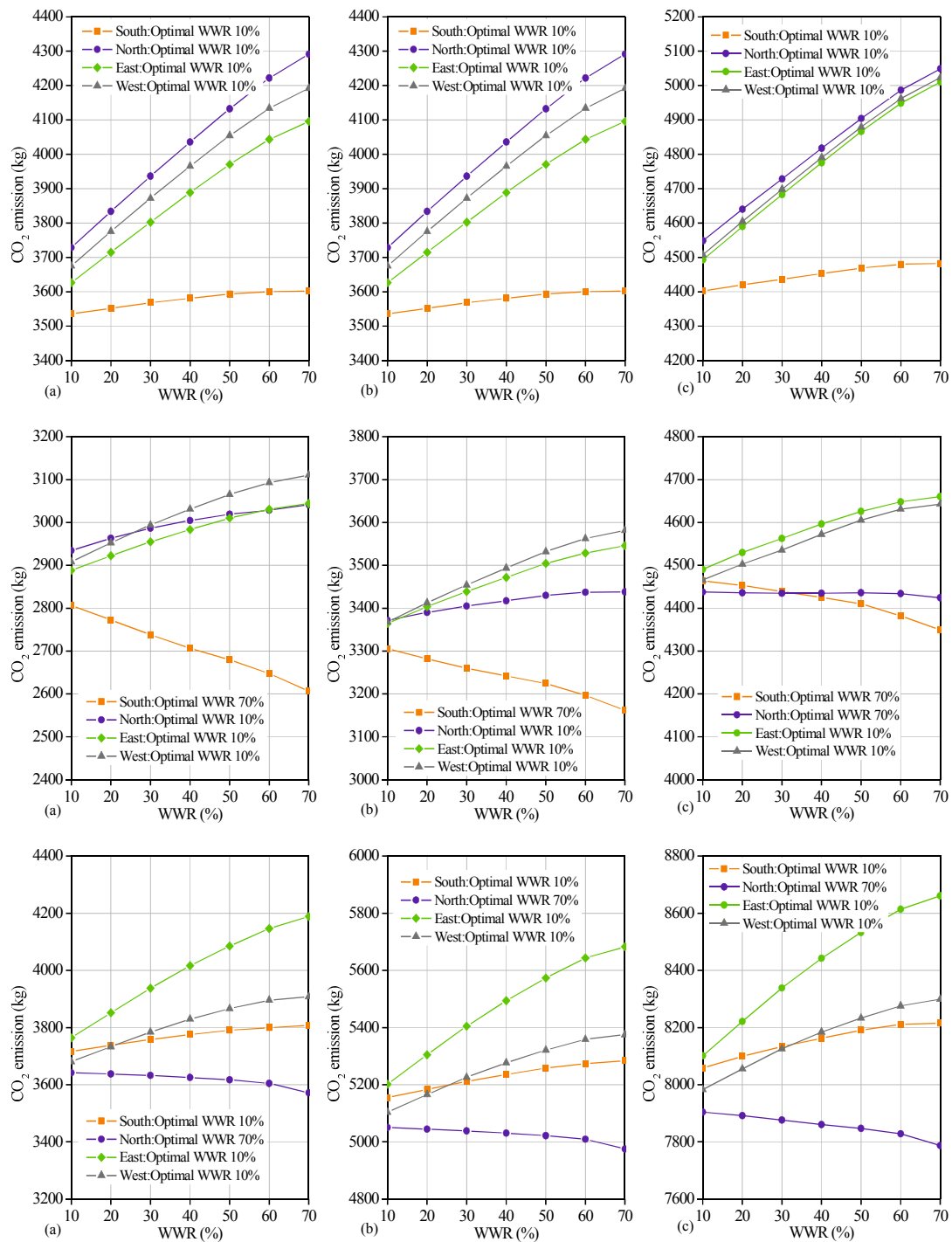


Figure 2. C. 3. Distribution of optimal WWR in a small-scale building (Double Ref-A-H glazing; Lighting power density of 5 W/m<sup>2</sup>; Top: Sapporo, Middle: Tokyo, Bottom: Naha; (a) Low internal gains, (b) Medium internal gains, (c) High internal gains).



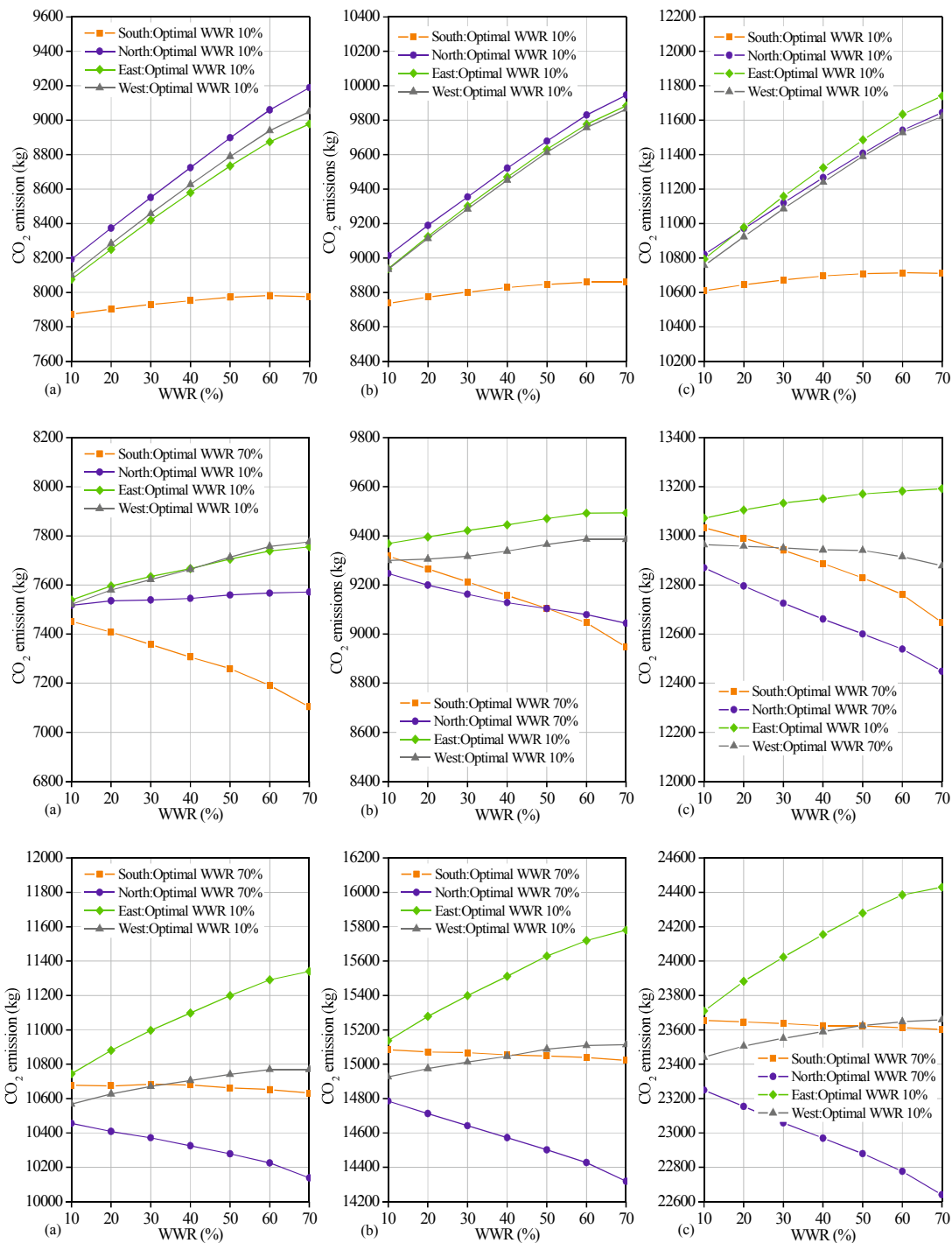


Figure 2. C. 4. Distribution of optimal WWR in a large-scale building (Double Ref-A-H glazing; Lighting power density of 5 W/m<sup>2</sup>; Top: Sapporo, Middle: Tokyo, Bottom: Naha; (a) Low internal gains, (b) Medium internal gains, (c) High internal gains).

## References

- Alrubaih, M.S. et al., 2013. Research and development on aspects of daylighting fundamentals. *Renewable and Sustainable Energy Reviews*, 21, pp.494–505.
- ARINAMI, Y. et al. 2013. Study on the evaluation of cross ventilation performance of detached house by effective air change rate and effective opening area of windows ratio. *Architectural Institute of Japan*. 78 (685), pp. 277-284.
- ASHRAE Inc, ANSI/ASHRAE/IEC Standard 90.1-2010: Energy standard for buildings except low-rise residential buildings.
- Cerezo, C., Dogan, T. & Reinhart, C., 2014. Towards standardized building properties template files for early design energy model generation. In *2014 ASHRAE/IBPSA-USA: Building Simulation Conference, Atlanta, GA, September 10-12, 2014*. pp. 25–32.
- Crawley, D.B. et al., 2001. EnergyPlus: creating a new-generation building energy simulation program. *Energy and Buildings*, 33(4), pp.319–331.
- Fernandes, L.L. et al., 2015. Angular selective window systems: Assessment of technical potential for energy savings. *Energy and Buildings*, 90, pp.188–206.
- Galasiu, A.D., Atif, M.R. & MacDonald, R.A., 2004. Impact of window blinds on daylight-linked dimming and automatic on/off lighting controls. *Solar Energy*, 76(5), pp.523–544.
- Ghisi, E. & Tinker, J.A., 2005. An Ideal Window Area concept for energy efficient integration of daylight and artificial light in buildings. *Building and Environment*, 40(1), pp.51–61.
- Goia, F., 2016. Search for the optimal window-to-wall ratio in office buildings in different European climates and the implications on total energy saving potential. *Solar Energy*, 132, pp.467–492.
- Goia, F., Haase, M. & Perino, M., 2013. Optimizing the configuration of a facade module for office buildings by means of integrated thermal and lighting simulations in a total energy perspective. *Applied Energy*, 108, pp.515–527.

Grynning, S. et al., 2013. Windows in the buildings of tomorrow: Energy losers or energy gainers?

*Energy and Buildings*, 61, pp.185–192.

Hiyama, K. et al., 2014. A new method for reusing building information models of past projects to

optimize the default configuration for performance simulations. *Energy and Buildings*, 73,

pp.83–91.

Hiyama, K., 2014. Assigning Robust Default Values in Building Performance Simulation Software

for Improved Decision-Making in the Initial Stages of Building Design. *The Scientific World*

*Joiurnal*.

Hiyama, K. & Wen, L., 2015. Rapid response surface creation method to optimize window geometry

using dynamic daylighting simulation and energy simulation. *Energy and Buildings*, 107,

pp.417–423.

JIS A 9110: 2011 照明規基準總則

Kim, S.-H. et al., 2014. A study on the proposes of energy analysis indicator by the window elements

of office buildings in Korea. *Energy and Buildings*, 73, pp.153–165.

Kim, S.Y. & Kim, J.J., 2007. The impact of daylight fluctuation on a daylight dimming control

system in a small office. *Energy and Buildings*, 39(8), pp.935–944.

Kottek, M. et al., 2006. World map of the Köppen-Geiger climate classification updated.

*Meteorologische Zeitschrift*, 15(3), pp.259–263.

Lee, J.W. et al., 2013. Optimization of building window system in Asian regions by analyzing solar

heat gain and daylighting elements. *Renewable Energy*, 50, pp.522–531.

Li, D.H.W. et al., 2010. An analysis of energy-efficient light fittings and lighting controls. *Applied*

*Energy*, 87(2), pp.558–567.

Li, D.H.W. et al., 2014. Study of daylight data and lighting energy savings for atrium corridors with

lighting dimming controls. *Energy and Buildings*, 72(February 2012), pp.457–464.

- M. Hiraoka, S. Hiromoto, H. Komoda, S. Tabuchi, S. Tanabe, T. kai, S. Hashimoto, A. N., 2011. Performance Evaluation of Multi-split Type Air-conditioning System and Advancing Knowledge of HVAC Design. *The society of Heating, Air-Conditioning Sanitary Engineers of Japan*, 169, pp. 13-20.
- Ma, P., Wang, L.-S. & Guo, N., 2015. Maximum window-to-wall ratio of a thermally autonomous building as a function of envelope U-value and ambient temperature amplitude. *Applied Energy*, 146, pp.84–91.
- M Grinberg, A.R., 2013. Architecture & energy in practice: implementing an information sharing workflow. In *Proceedings of BS 2013: 13th Conference of International Building Performance Simulation Association, Chambéry, France, August 26-28*. pp. 121–128.
- Ochoa, C.E. et al., 2012. Considerations on design optimization criteria for windows providing low energy consumption and high visual comfort. *Applied Energy*, 95, pp.238–245.
- Persson, M.L., Roos, A. & Wall, M., 2006. Influence of window size on the energy balance of low energy houses. *Energy and Buildings*, 38(3), pp.181–188.
- Pino, A. et al., 2012. Thermal and lighting behavior of office buildings in Santiago of Chile. *Energy and Buildings*, 47, pp.441–449.
- Ramos, G. & Ghisi, E., 2010. Analysis of daylight calculated using the EnergyPlus programme. *Renewable and Sustainable Energy Reviews*, 14(7), pp.1948–1958.
- Shen, H. & Tzempelikos, A., 2013. Sensitivity analysis on daylighting and energy performance of perimeter offices with automated shading. *Building and Environment*, 59, pp.303–314.
- Singh, R., Lazarus, I.J. & Kishore, V.V.N., 2015. Effect of internal woven roller shade and glazing on the energy and daylighting performances of an office building in the cold climate of Shillong. *Applied Energy*, 159, pp.317–333.
- States, U., 2012. ICEE 2012.

- Susorova, I. et al., 2013. The effect of geometry factors on fenestration energy performance and energy savings in office buildings. *Energy and Buildings*, 57, pp.6–13.
- Takamoto, Y. Next-generation energy saving reference, *The society of Heating, Air-conditioning Sanitary Engineers of Japan* 74 (2000) pp.543-550.
- Takizawa, H. Hyojyun-mondai no teian (Office-yo hyojyun-mondai). 15th thermal symposium, Architectural Institute of Japan. 1984.
- Tian, C. et al., 2010. A generalized window energy rating system for typical office buildings. *Solar Energy*, 84(7), pp.1232–1243.
- Wang, X. et al., 2017. Energy-saving analysis for the Modern Wing of the Art Institute of Chicago and green city strategies. *Renewable and Sustainable Energy Reviews*, 73(February 2016), pp.714–729.
- Wang, Z. & Tan, Y.K., 2013. Illumination control of LED systems based on neural network model and energy optimization algorithm. *Energy and Buildings*, 62, pp.514–521.
- Wen, L. & Hiyama, K., 2016. INFLUENCE OF DESIGN CONDITIONS ON THE DISTRIBUTION OF OPTIMAL WINDOW TO WALL RATIO FOR A TYPICAL OFFICE BUILDING IN JAPAN. *In in Proceedings of Building Simulation and Optimization 2016: Third IBPSA - England Conference, Newcastle*. pp. 60–67.

### 3.

## **A method for creating response surface to provide information on optimal window geometry**

Window geometries, such as window width and window height, have significant impacts on building performance. Building designs are multi-objective optimization processes in which unquantified values, such as the design preferences of architects or clients, are included as objective functions along with building performance. In this context, showing architects the response surface between window geometries and building performance is useful for their decision making. To support the assignment of window geometries in DPM, a rapid method for creating response surface is proposed using dynamic daylighting simulation and energy simulation. In the proposed procedure, the number of dynamic daylighting simulations is reduced by creating a link between the daylight factor (DF) and daylight autonomy (DA). In addition, the proposed procedure allows for the estimation of electric lighting energy savings with high resolution by integrating dynamic daylighting simulation tools into energy simulation tools. Case studies are conducted to create the response surfaces using the dynamic daylighting and energy simulation software of DAYSIM and EnergyPlus. The impact of COPs for the cooling and heating systems on the features of the response surface can be easily analyzed. Higher COP results in a narrower selectable design range in cases where the same percentage of acceptable ranges for building performance degradation is employed (window height from 1.2-2m to 1.4-2m, window width from 30–100 % to 60–100 %). The method was validated with detailed dynamic daylighting simulation outputs. The error caused by the proposed procedure (below 1 %) was negligible compared with the error caused by the selection of the daylight simulation algorithm (approximately 5 %).

### **3.1 General context**

With the design progress, the default WWR value mentioned in Chapter 2 can be replaced by the actual design value. As the design progresses, more specific window information will be required by DPM besides the rough window area of WWR. Therefore, chapter 3 focus on the approach development to support the assignment of window geometry, i.e., window width and height. To obtain information about links between building shapes and building performance, many studies on optimization have been conducted (Suga et al. 2010) (Nguyen et al. 2014) (Caruso & Kämpf 2015) (Méndez Echenagucia et al. 2015) (Harmathy et al. 2016). One difficulty in this type of study is how to address multiple objectives in a real building design process. In addition, the design preferences of architects and clients should be included in the numerous objectives, which increases the difficulty of multi-objective optimizations because it is difficult to quantify these design preferences. Moreover, design preferences tend to be weighted more heavily than building performance in the real design processes. In this context, it is somewhat ineffective to show architects a single optimal solution based on results from a building performance simulation or optimization alone to help their decisions making. Energy modelers who perform energy simulations should offer multiple and various design alternatives for architects and clients to find “an optimal solution” with consideration of both the design preference and building performance. At the same time, information on the sensitivity of each design parameter should also be provided to evaluate the robustness of the design candidates offered by the energy modelers.

In these contexts, showing architects the response surfaces between building shapes and building performance is an effective measure to offer information on multiple design candidates and the parameter sensitivities (Manzan & Padovan 2015). However, the creation of response surfaces tends to be time consuming because an enormous number of calculations are necessary to explore the surface features. With this background, the authors are developing methods that can create response surfaces

between building shapes and building performance in a feasible and timely manner. This paper describes one of the methods for creating a response surface between window geometry and building energy consumption.

Architects should understand which parameters have high sensitivities toward building performance (Singh & Kensek 2014). Response surface helps architects understand to what extent they can widen or narrow the window size without significantly decreasing the building performance. In the assumed design process in this study, the building geometry is studied first because most architects attach importance to the visual design. Then, the surface properties will be discussed to optimize the building performance. In terms of fenestration, the WWR is studied first, followed by the glazing properties (M Grinberg 2013).

### **3.2 Method for creating response surface**

Window geometry is an important factor which significantly impact the daylighting performance and the cooling/heating loads. In addition, the amount of electric lighting energy which varies with the daylight illuminance through the windows also influence the internal heat load (internal gain from lighting) in energy simulations. Therefore, in cases where window geometries are treated as design parameters, energy simulations to calculate cooling/heating loads should be integrated with daylighting simulations. EnergyPlus(Crawley et al. 2001) an energy simulation tool, allows the energy simulation and daylighting simulation to be integrated (Winkelmann & Selkowitz 1985). Two daylighting sensors in each zone can be set to measure the daylight illuminances and control the outputs of electric lighting. However, EnergyPlus has no capacity of dealing with such cases in which higher resolutions of daylight calculation with more sensor locations are demanded. In such cases, another daylighting simulation tool is necessary. In this study, DAYSIM (Reinhart & Walkenhorst



2001) is used as a dynamic simulation tool to calculate daylight with high resolution. The proposed response surface in this study is created by combining the outputs from energy simulation software of EnergyPlus and dynamic daylighting software of DAYSIM. This method is not limited to these two simulation software applications; any energy simulation tool and daylighting simulation tool can be adopted to replace them in the response surface creation.

### **3.2.1 Dynamic daylighting simulation**

DAYSIM is a validated RADIANCE-based (Ward & Rubinstein 1988) daylighting analysis software application that models the annual amount of daylight in and around a building. It outputs various performance indicators, including daylight autonomy (DA), useful daylight illuminance (UDI), continuous daylight autonomy (cDA), annual glare, and electric lighting energy use. Among these outputs, cDA is an index that can relate energy savings to electric lighting (Reinhart et al. 2006). The electric lighting energy consumption can be easily estimated with cDA, given a target illuminance and an energy coefficient for electric lighting. The daylighting calculation tends to be time consuming. DAYSIM was developed for use in real design processes. For this purpose, the time for calculation in DAYSIM appears to be sufficiently feasible for building design practice (Stouffs et al. 2013).

However, in order to create the response surface, an enormous number of calculations are necessary. The key problem then becomes how to reduce the number of calculations with regard to the proposed method for creating response surfaces. In this study, the number of calculations for cDA using dynamic daylighting simulation software of DAYSIM is limited to only one. In this one time daylighting simulation, the link between the daylight factor (DF) and cDA is obtained. To create a response surface, the variation in DF induced by the change of window geometry is calculated from energy simulation in which time consumption is relatively less. The variation in the cDA is estimated using the link

between cDA and the DF which are obtained from the one time daylighting simulation. Electric lighting energy consumption is then calculated by integrating the estimated cDA into an evaluation equation. The calculation time of response surfaces creation is largely reduced by this proposed procedure.

### **3.2.2 Energy simulation**

EnergyPlus is adopted to calculate the variation in the heat flow through the windows which is caused by the change of the windows geometry. In this process, the calculation does not include the lighting control systems. The variation in window geometry in this calculation process is represented as window-to-wall ratio (WWR) because that the impacts of the location, height and spacing interval of the window on the cooling/heating load are negligible in comparison with the impacts on the electric lighting energy savings due to daylight use. The number of calculations using EnergyPlus depends on the resolution of the WWR. In the case study referenced hereafter, nine calculations are performed using EnergyPlus.

### **3.2.3 Estimation on the total electric energy consumption**

The total energy consumption including cooling, heating, and electric lighting is calculated from Eq. (3-1). The impact of energy savings with respect to electric lighting due to daylight use on the cooling/heating load is estimated using cDA and outputs from EnergyPlus including  $L_c$ ,  $L_h$ ,  $L'_c$ , and  $L'_h$ . In this equation, the first term describes the annual electric consumption of the lighting system. The second term describes the annual electric consumption of the cooling system. During the cooling period, the electric lighting usage is equal to the internal heat load and it becomes the cooling load.

Daylighting can reduce the cooling load by reducing the electric lighting usage. The effect of daylighting is roughly estimated with  $L'_c$  and  $cDA$ . The third term describes the annual electric consumption of the heating system. During the heating period, the electric lighting usage can alternate with the heat supply from the heating system and can contribute to reducing the heating load. The effect of the heat supply by electric lighting usage is roughly estimated with  $L'_h$  and  $cDA$ . The validity of this proposed rough estimation method is evaluated in later sections.

$$Q = (100 - cDA) / 100 \times E \times I \times 365 \times 5 / 7 \times P + (L_c - L'_c \times cDA / 100) / COP_c + (L_h + L'_h \times cDA / 100) / COP_h \quad (3-1)$$

where  $E$  is the lighting energy to obtain the unit illuminance ( $W/(m^2lx)$ );  $I$  is the target illuminance redefined for the artificial lighting design ( $lx$ );  $P$  is the working period (period during which sufficient illuminance is required) (h);  $L_c$  is the annual cooling load calculated from EnergyPlus without the lighting control system ( $W h/m^2$ );  $L_h$  is the annual heating load calculated from EnergyPlus without the lighting control system ( $W h/m^2$ );  $L'_c$  is the sum of the cooling load results from electric lighting usage ( $W h/m^2$ );  $L'_h$  is the sum of the electric lighting energy consumption during the heating period ( $W h/m^2$ );  $COP_c$  is the coefficient of performance for the cooling system (–);  $COP_h$  is the coefficient of performance for the heating system (–). The simulation method is summarized in the following flow chart as shown in Figure 3.1. The specific explanations of response surface, DF and  $cDA$  can be found in Appendix A.

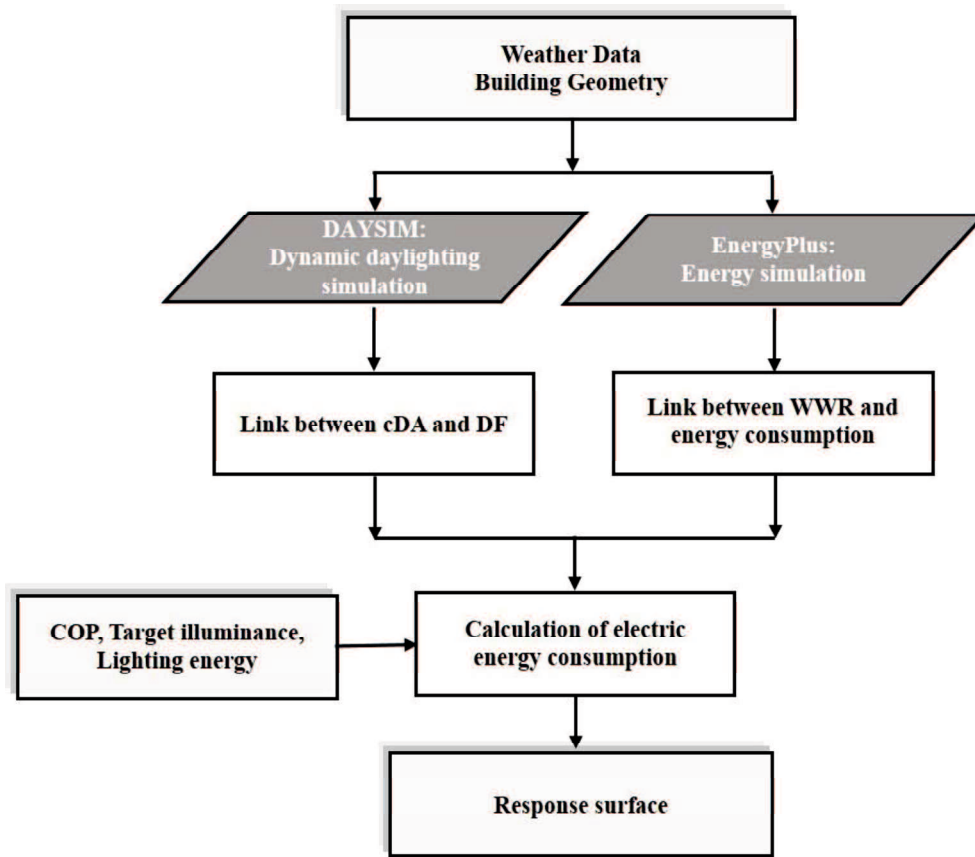


Figure 3.1. Flow chart of the calculation steps for creating response surface.

### 3.3 Case studies

#### 3.3.1 Basic condition

Figure 3.2 illustrates the outline of the building model adopted in the case study. The model building is a three-story office building. In the calculation process, only the second floor which is in the middle of the building is considered to determine the simulation results. The office area in each floor is  $18.0 \times 10.8 \text{ m}^2$ , and the core for staircase in each floor is  $18.0 \times 3.6 \text{ m}^2$ . The floor height is 2.8 m. Windows with internal blind are assumed to be only set on the facade facing south.

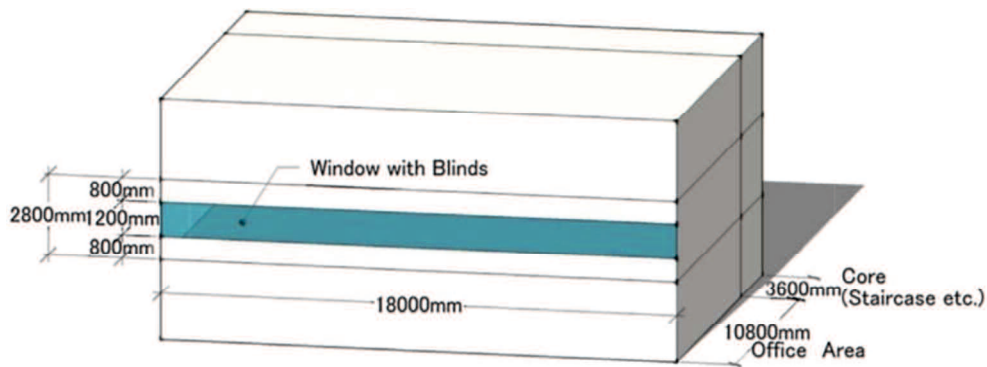


Figure 3.2. Outline of the building model adopted in case study.

The window geometry including window width and height is treated as the design variable in case study. The window height varies from 0.8 to 2.0 m. The window width is represented as a percentage value. It is decided from the sum of the window width divided by the sum of the wall width. The percentage varies from 10 % to 100 %. In this study, it is assumed that the impact of window spacing on the DF is not large, whereas the window height has a significant impact on the DF. For example, four types of window geometry (A, B, C, and D) are displayed in Figure 3.3.

With regard to type A, the window height is 1.2 m, and the window width accounts for 100 % of the wall width (ribbon window). With regard to type B, the window height is 2 m, and the window width is the same type A which accounts for 100 % of the wall width (ribbon window). With regard to type C, the window height is 1.2 m, and the window width accounts for 51 % (9.2 m/18 m) of the wall width. With regard to type D, the window height is 2.0 m, and the window width is 51% (9.2 m/18 m). These four types are chosen to set two levels for both parameters of window width and window height. The sill height of the windows is fixed at 0.8 m. The windows are equipped with internal Venetian blinds featuring with high-reflectivity slats. The blinds are closed if the transmitted direct sunlight is above 50 W/m<sup>2</sup> (Reinhart et al 2006). The expanded AMEDAS weather data in Tokyo is used as the weather data of the simulations.

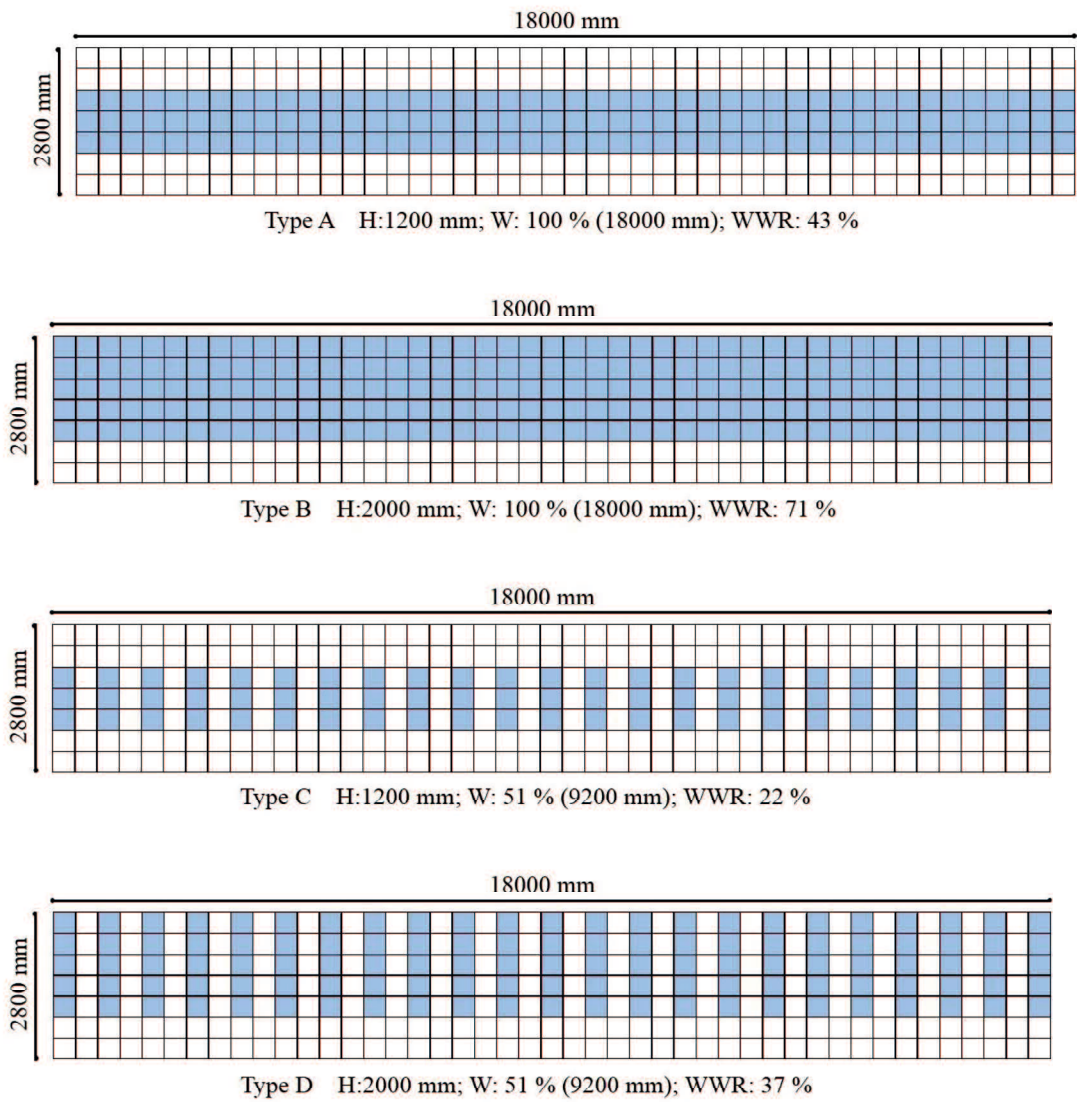


Figure 3.3 Redefined window geometry types for case study.

### 3.3.2 Dynamic daylighting simulation

First, the link between DF and cDA is calculated using DAYSIM program. In this calculation, the window of type A which the height of ribbon window is 1.2 m as shown in Figure 3.3 is used. The illuminance sensor is arrayed on the center line which is vertical to the south facing facade with the windows. The distance between the two sensors is 0.4 m as shown in the Figure 3. 4. The distance between first sensor (near the window) and window, and the distance between last sensor (near the internal partition) and the internal partition are 0.2 m. In total, 27 illuminance sensors in the central line are set for this simulation. The height of the working plane in which illuminance sensors are installed is defined as 0.8 m above the floor. The simulation conditions for DAYSIM are shown in Tables 3.1 and 3.2. The parameters in Table 3.1 are defined for the simulation algorithm that influences the simulation accuracy and calculation load. The parameters in Table 3.2 are used to describe the surface properties of the simulation model. With regard to the calculation of the cDA, the target illuminance is set at 400 lx following Japanese Industrial Standards that order a illuminance of 300–750 lx for working spaces in office buildings. The working hours are set as Monday through Friday from 8:00 to 19:00. Figure 3.5 shows the link between the DF and cDA calculated in this procedure using the A type window. The x- axle is the DF, and y-axle is the cDA.

Table 3.1. Utilized radiance simulation parameters.

Ambient bounces	Ambient division	Ambient sampling	Ambient accuracy	Ambient resolution	Direct sampling
5	1000	20	0.1	300	0.2

Table 3.2. Material properties of the investigated model.

Building element	Material description
Ceiling	80% diffuse reflectance
Walls	60% diffuse reflectance
Floor	30% diffuse reflectance
Venetian blinds	90% diffuse reflectance
Window	72% visual transmittance
External ground	25% diffuse reflectance

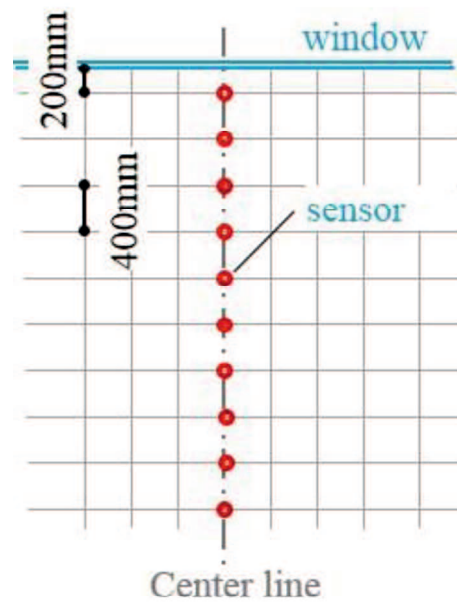


Figure 3.4. The location of illuminance sensors for calculating the link between the DF and cDA.



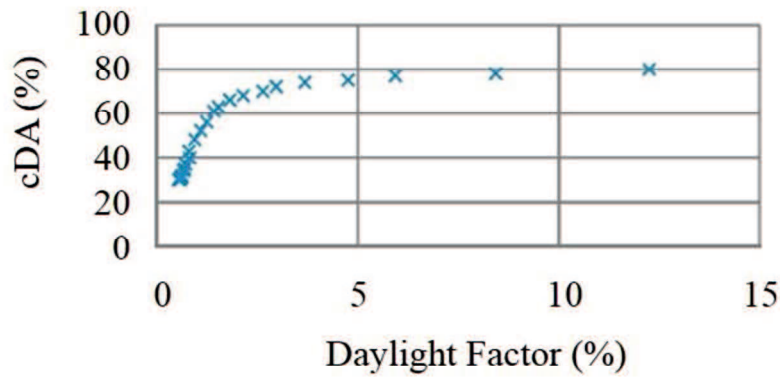


Figure 3.5. Link between the DF and cDA calculated using the type A window geometry (point diagram between the cDA and DF are analyze by DAYSIM).

In the next step, the response surface between the window geometry and cDA is created. First, the variation in the DF which caused by the variation in the window geometry is calculated. The DF is calculated using illuminance sensors with intervals of 1.2 m in both the x-direction and the y-direction as shown in Figure 3.6. In this study, DAYSIM program is used again to calculate the variation in DF which caused by window geometry change. The time consumption of DF calculation is greatly reduced because of that DF is static metric under a specific overcast weather condition. Other simple methods and simulation tools (e.g., Ecotect™ (Reeves et al 2012)) to calculate the DF can be replaced with DAYSIM in this procedure. The cDA at each point is estimated from the link between the DF and cDA (Figure 3.5). Figure 3.7 illustrates the estimated response surface of the average cDA in the model.

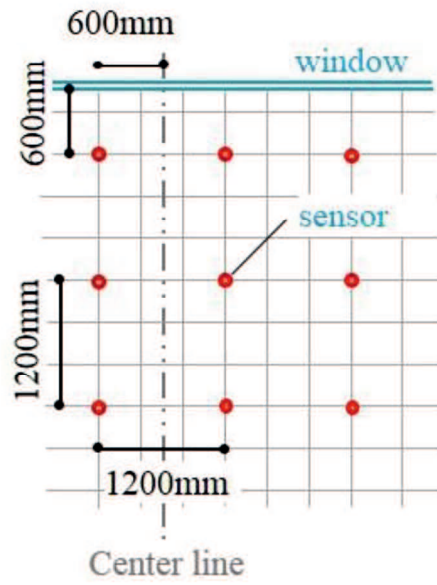


Figure 3.6. The location of illuminance sensors for calculating the variation in DF due to the change in window geometry.

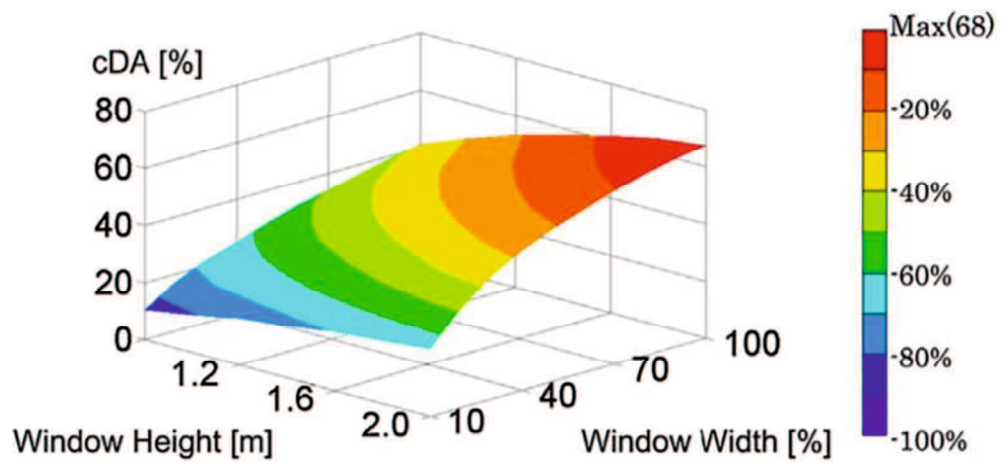


Figure 3.7. Response surface between the window geometry and cDA.

### 3.3.3 Energy simulation

The energy simulation is performed using the application of EnergyPlus. The WWR is treated as the design variable in energy simulation. The calculation numbers of energy simulation depend on the resolution of the design variable of WWR. In the case study, the WWR varies from 0 % to 80 % at intervals of 10 %. Therefore, nine energy simulations are performed. The lighting control is not implemented in energy simulation because the energy saving effect for artificial lighting systems is estimated using the cDA at a later stage. Table 3.3 shows the calculation conditions including envelop properties and settings of HVAC systems, which are based on a model office frequently used in simulations for academic studies of building performance in Japan (Takizawa 1984). Figure 3.8 shows the response surface between the window geometry and cooling load created using the energy simulation results. The heating load is negligible compared with the cooling load in this case study (up to 1 kW/m<sup>2</sup>). Therefore, the response surface between the window geometry and heating load is not shown.

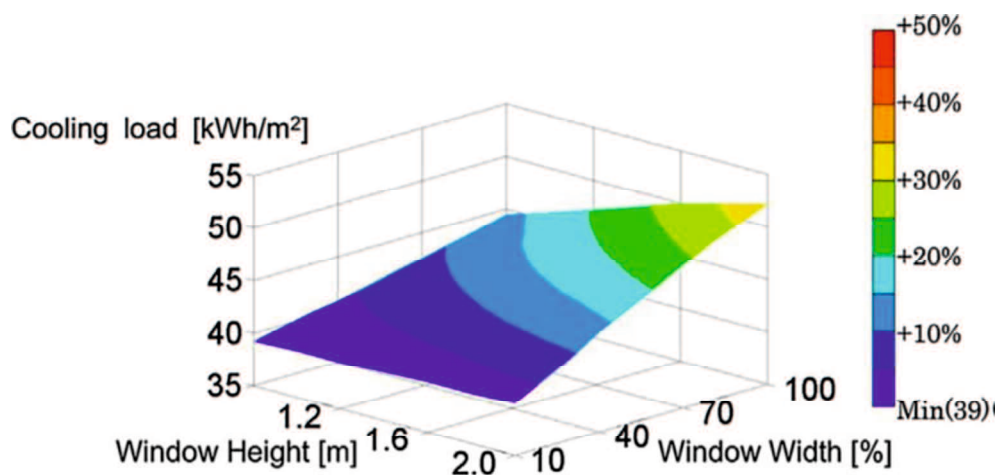


Figure 3.8. Response surface between the window geometry and cooling load.

Table 3.3 Conditions for energy simulation.

External wall	U-value: 0.79 W/m <sup>2</sup> K (Outer) Tile: 8 mm, mortar: 20 mm, concrete: 150 mm, foam-polyurethane: 25 mm, gypsum plastering:13 mm (Inner)
Internal partition	U-value: 2.28 W/m <sup>2</sup> K (Outer) Mortar: 20 mm, concrete: 150 mm, mortar:20 mm (Inner)
Floor	U-value: 0.67 W/m <sup>2</sup> K (Outer) Concrete (Lightweight): 60 mm, form polyurethane: 25 mm, asphalt: 10 mm, concrete:150 mm, air-gap, plasterboard: 9 mm, fiberboard:12 mm (Inner)
Window	Low-e double glazing, U-value: 2.5 W/m <sup>2</sup> K, SHGC: 0.60 Window shading (inside): blind with high-reflectivity slats
Occupancy	Density: 0.2 person/m <sup>2</sup> , metabolic rate:123×0.9 W/person Clothing: 1.00 clo (Winter), 0.50 clo (Summer) Schedule (Weekdays): 0%–8:00–70%–12:00–35%–13:00–70%–17:00– 35%–18:00–17%–19:00–0% Schedule (Weekends): 0%
Internal heat	Office equipment: 25 W/m <sup>2</sup> Schedule (Weekdays): 0%–8:00–50%–12:00–25%–13:00–50%–17:00– 25%–18:00–0% Schedule (Weekends): 0%
Lighting	Energy: 2.0 W/m <sup>2</sup> –100 lx* , radiant fraction: 0.42, visible fraction: 0.18, Target illuminance: 400 lx Schedule (Weekdays): 0%–8:00–100%–19:00–0% Schedule (Weekends): 0%
Cooling	Set-point temperature: 28.0 °C, schedule:off-8:00-on-19:00-off
Heating	Set-point temperature: 20.0 °C, schedule:off-8:00-on-19:00-off
Ventilation	7.0 l/s person

### 3.3.4 Total electric energy consumption

The total electric energy consumption for cooling, heating and electric lighting is calculated by inputting the simulation outputs from Sections 3.3.1 dynamic daylighting simulation and 3.3.2 energy simulation to Eq. (3-1). In this case study, the lighting energy  $E$  is set at  $0.02 \text{ W}/(\text{m}^2 \text{ lx})$ , target illuminance  $I$  is set at  $400 \text{ lx}$ , and the working period  $P$  is set at  $11 \text{ h}$  (from 8:00 until 19:00).

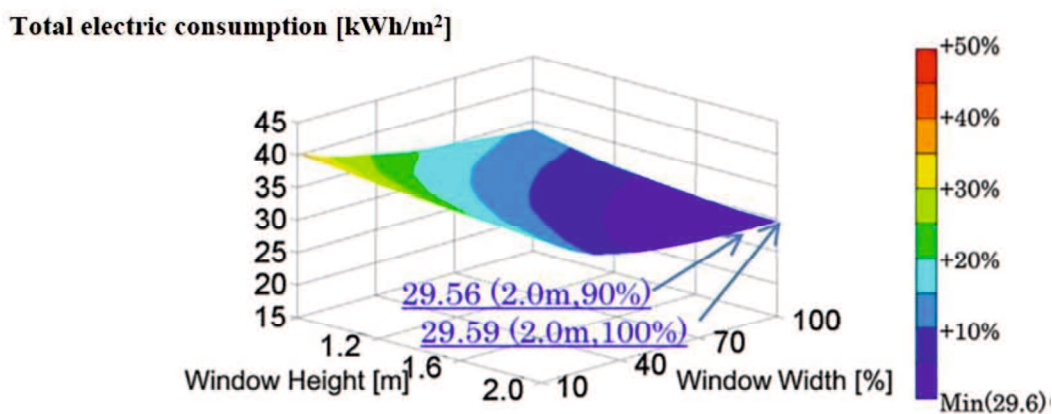


Figure 3.9. Response surface between the window geometry and the total electric energy consumption when the COPs of heating/ cooling system are 2.0.

Figure 3.9 shows the response surface between the window geometry and electric energy consumption including the electricity consumptions from heating, cooling, and lighting when the COPs for both the cooling and heating systems are both set at 2.0. The minimum value of total electric energy consumption ( $29.56 \text{ kWh}/\text{m}^2$ ) is observed when the window height is  $2.0 \text{ m}$  and the window width is  $90 \%$  of the total wall width. Assuming that  $10\%$  of building performance degradation is acceptable based on this optimal preference in the design practice, the window height can be set in the range between  $1.2$  to  $2.0 \text{ m}$ . In addition, the window width can be set in the range between  $30 \%$  and  $100 \%$  of the total wall. Architects or clients can then choose their favorite window geometries with

consideration of building performance degradation.

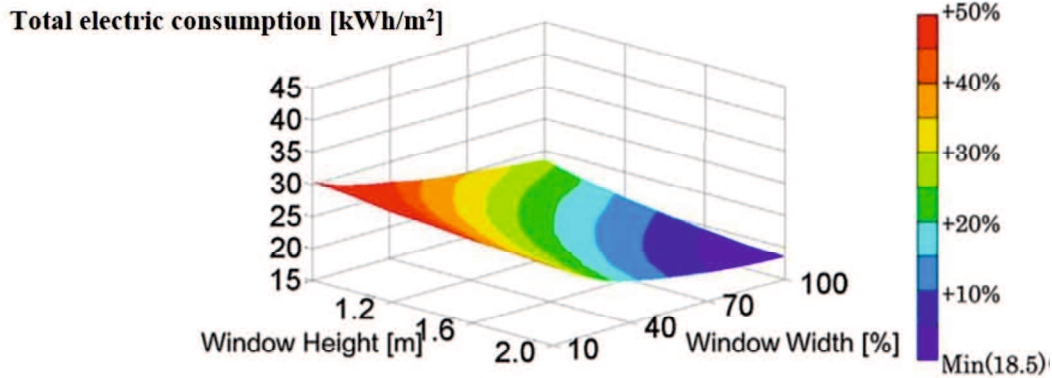


Figure 3.10. Response surface between the window geometry and the total electric energy consumption when the COPs of heating/cooling system are 4.0.

Figure 3.10 shows the response surface when the COPs for both the cooling and heating systems are all set at 4.0. The minimum value of total electric energy consumption (18.5 kWh/m<sup>2</sup>) is observed when the window height is 2.0 m and the window width is 100 % of the wall width. The optimal solution of the window geometry is not significantly changed compared with the case in which the COPs of heating and cooling systems are set at 2.0. However, the acceptable range of window geometry design under the 10 % degradation is significantly changed. The acceptable ranges for the window width are 60–100 % of the wall, for window height becomes 1.4–2.0 m, respectively. Increasing the heating and cooling systems COPs causes decreased electric energy usage for cooling and heating, whereas the amount of variation in electric lighting usage is not influenced by the change of COPs values. The ratio of building performance degradation to window geometry change then becomes relatively large compared with the total electric energy consumption. Consequently, the acceptable range of window geometry is narrowed. With the proposed measure, energy modelers can

offer useful information about the flexibilities of building design, which can help architects to decide their optimal design under the building performance guarantee.

### 3.4 Validation of the proposed method

#### 3.4.1 Estimation of cDA using the link between DF and cDA

To validate the proposed cDA estimation method using the link between DF and cDA, dynamic daylighting simulations using DAYSIM are performed with various window geometries: types B, C and D (see Figure 3.3). Table 3.4 lists the results calculated by DAYSIM program and those results estimated by the link between the DF and cDA proposed. It can be observed that the difference between these two estimation methods is small. Therefore, even the different window system is employed, the variation in the cDA caused by the variation of the window geometry can be estimated by the link obtain from the simple window model of type A.

Table 3.4. Comparison of the DAYSIM results and the estimated results by the link between the DF and cDA which is obtained from the result of the type A window geometry.

Window type	WWR (%)	cDA (%)	
		Estimated*	DAYSIM**
Type B	71%	67	67
Type C	22%	34	37
Type D	37%	51	52

\*: "Estimated (cDA)" shows the space average cDA using the method explained in Section 3.2.1.

The link between the DF and cDA obtained from the calculation results of the type A window (Figure 3.3) is used for the cDA estimation for type B, C, D window.

\*\*:"DAYSIM (cDA)" shows the space average cDA from the simulation results of DAYSIM using the types B, C, and D windows.

### 3.4.2 Estimation of the total electric energy consumption using the proposed method

To validate the estimated total electric energy consumption using the proposed Eq. (3-1), new cases are tested. In these new cases, the numbers of sensor location for daylight illuminance measure is limited to 2, which is the maximum numbers of sensor location for the EnergyPlus program. The two sensors are located at the center line vertical to the facade installed with windows (Figure 3.11). The first sensor, which is the sensor for the interior zone, is located 7.8 m from the facade with windows. The lighting floor area ratio handled by the first sensor is 66 %. The second sensor, which is the sensor for the perimeter zone, is located 3.0 m from the facade with windows. The lighting floor area ratio handled by the second sensor is 34 %.

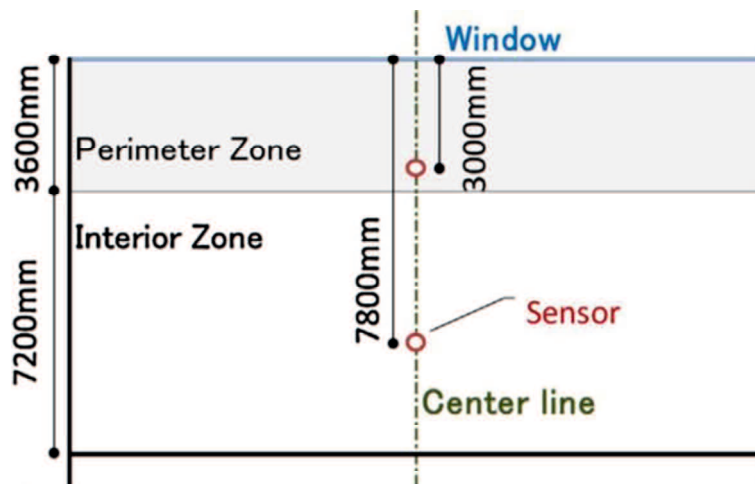


Figure 3.11. Two sensor locations in the cases for the validation.

Case 1 is the baseline case, in which the total electric energy consumption is calculated using EnergyPlus program alone in which the lighting control function according to the amount of daylight illuminance is on. Case 2 is designed to analyze the validity of Eq. (3-1). In this case, DAYSIM is not used. The cDA is calculated by the lighting control function in EnergyPlus program. First, the cDA at



the two sensor locations is calculated using EnergyPlus for each window type. Thus, the evaluated cDA values in case 1 and 2 are same. Conversely, with regard to the cooling/heating load, the calculation results from Section 3.3.2 are used. The cooling/heating load does not include the electric lighting savings effect due to daylight penetrate. This lighting saving effect is calculated using Eq. (3-1) in case 2. Thus, the validity of Eq. (3-1) can be evaluated in this procedure. Case 3 is designed to identify the difference in the results between DAYSIM and the daylighting calculation model in EnergyPlus program. In this case, the link between the DF and cDA at the two sensor locations is calculated using DAYSIM with the model of the type A window geometry (Figure 3.3). The next step is the same as that in Sections 3.3.2 and 3.3.3. In this section, the COPs for the cooling and heating systems are set at 4.0.

Table 3.5 presents the estimated results of cases 1, 2, and 3. The differences between cases 1 and 2 are small. This is true for all the four window geometry types of A, B, C, and D. In this context, a rough estimation of the impact of electric lighting energy savings due to daylight penetrate on the cooling/heating load using the proposed Eq. (3-1) does not cause significant problems in this study. Conversely, the differences in total electric energy usage between cases 1 and 3 when the window types A and C are adopted are relatively distinct. These differences are caused by the differences in cDA. DAYSIM can lead to a more accurate cDA results than the daylight function in EnergyPlus due to the assumption employed in the simulations. This means that the improved accuracy of the calculation algorithm for daylight is relatively important. In this context, the proposed method in this Chapter still has significance in terms of making it possible to combine different software applications for energy simulation and daylighting simulation.

Table 3.5. Comparisons among the estimations for each window type.

Type A (H: 1.2 m, W: 100 %, WWR: 43 %)

	cDA	Total electric energy consumption [kWh/m <sup>2</sup> ]
Case 1	53.9	21.1
Case 2		21.0
Case 3		22.6

Type B (H: 2.0 m, W: 100 %, WWR: 71 %)

	cDA	Total electric energy consumption [kWh/m <sup>2</sup> ]
Case 1	65.6	19.4
Case 2		19.1
Case 3		19.5

Type C (H: 1.2 m, W: 51 %, WWR: 22 %)

	cDA	Total electric energy consumption [kWh/m <sup>2</sup> ]
Case 1	33.4	25.5
Case 2		25.4
Case 3		26.8

Type D (H: 2.0 m, W: 51 %, WWR: 37 %)

	cDA	Total electric energy consumption [kWh/m <sup>2</sup> ]
Case 1	45.5	22.9
Case 2		22.9
Case 3		23.0

Case 1: the baseline case, in which the total electric energy consumption is calculated using EnergyPlus alone with the lighting control function according to the amount of daylight illuminance.

Case 2: case for evaluating the validity of Eq. (3-1). cDA is calculated by the lighting control function in EnergyPlus. Therefore, the value is same as in Case 1. In addition, the total electric

energy usage is calculated by Eq. 3-1 explained in Section 3.2.3.

Case 3: case for evaluating the difference in the results between DAYSIM and the daylighting calculation model in EnergyPlus. In case 3, the cDA is calculated by DAYSIM, while the cDA in case 2 is calculated by Energy Plus.

### **3.4 Summary**

Window geometries have significant impacts on building performance with respect to energy efficiency and daylight penetration. Because building facades are generally discussed during the early stages of building design, simulation-based decision support during these stages is in high demand. However, this is not an easy task because building designs are generally multi-objective problems. In addition, the design preferences of architects and clients should also be included in the objective functions. The fact that such preferences are unquantified values increases the difficulty of the problems. In these contexts, response surfaces between window geometries and building performance are useful to provide architects with information not only on the optimal solution but also on the range of building performance degradation due to their various design preferences. In this manner, architects can find Pareto-optimal solutions with considerations of both building performance and design preferences.

An enormous number of simulations are necessary to create the response surface. However, decision-making procedures should be conducted in a feasible and timely manner. The question then becomes how to reduce the number of simulations to a certain calculation cost to provide a response surface that can support decision making. In this study, utilization of the link between the DF and cDA defined in Section 3.2.1 and the specific example shown in Section 3.3.1 is proposed to reduce the number of dynamic daylighting simulations. With this method, daylighting simulations with high

resolution that integrate electric lighting energy savings into energy simulations can be incorporated into the optimization procedure. In the case studies, DAYSIM and EnergyPlus were used to create response surfaces between the window geometries and total electric energy consumption. The impact of COPs for the cooling/heating systems on the features of the response surface could be easily determined. A higher COP was shown to narrow the selectable design range in the case where the same percentage of acceptable ranges for building performance degradation is employed.

The error caused by employing the proposed method was analyzed by comparing the results with detailed simulation results. Regarding the use of the link between the DF and cDA, the estimated cDA in the proposed method was compared with simulation outputs using DAYSIM. The differences were negligible. With respect to the method for integrating cDA into energy simulation outputs, the validity was evaluated through detailed results simulated by EnergyPlus alone with the lighting control function using two sensor locations. These differences were also negligible. Furthermore, the results demonstrated that the differences caused by the difference in the simulation algorithm for the daylighting calculation are relatively significant compared with the error due to the proposed procedure. In this context, the proposed study also has significance to enable the combination of different daylighting simulation tools with energy simulations. Furthermore, this coupling can remove the constraints on the number of lighting sensors, in which only two lighting sensors were integrated into the validation process because of the limitation of the daylighting function in EnergyPlus.

## **Appendix (Explanation of the terms used in this Chapter):**

### **A.1. Response surface**

The response surface method (RSM) (Box & Wilson 1951) is frequently used as a sensitivity analysis tool for multi-attribute decision analysis (Bauer et al 1999). In this paper, the three-dimensional contour showing the sensitivity of the window geometries to the building performance is defined as the “response surface”.

### **A.2. Daylight factor (DF)**

The concept of Daylight Factor (DF) was developed in the United Kingdom in the early 20th century. It is generally considered as a static metric. Daylight Factor is a ratio that represents the amount of illumination available indoors relative to the illumination present outdoors at the same time under overcast skies. Daylight Factor is typically calculated by dividing the horizontal work plane illumination indoors by the horizontal illumination on the roof of the building being tested and then multiplying by 100.

*Source: <http://patternguide.advancedbuildings.net/using-this-guide/analysis-methods/daylight-factor> (accessed at April, 2017).*

### **A.3. Daylight Autonomy (DA)**

Daylight Autonomy was originally proposed by the Association Suisse des Electriciens in 1989 and was improved by Christoph Reinhart between 2001-2004. It is commonly referred as a dynamic daylight metrics. Daylight Autonomy is represented as a percentage of annual daytime hours that a given point in a space is above a specified illumination level. Daylight Autonomy is typically calculated by dividing the hours which the indoor illumination meet the predefined illumination threshold by the annual total occupied hours and then multiplying by 100.

Source:<http://patternguide.advancedbuildings.net/using-this-guide/analysis-methods/daylight-autonomy> (accessed at April, 2017).

#### A.4. Continuous Daylight Autonomy (cDA)

Continuous Daylight Autonomy (cDA) was proposed by Zach Rogers in 2006 as a basic modification of Daylight Autonomy. Continuous Daylight Autonomy awards partial credit in a linear fashion to values below the user defined threshold. However, DA does not award the partial credit. The diagrams of DA and cDA are shown in Figure A.1.

Source:<http://patternguide.advancedbuildings.net/using-this-guide/analysis-methods/continuous-daylight-autonomy> (accessed at April, 2017).

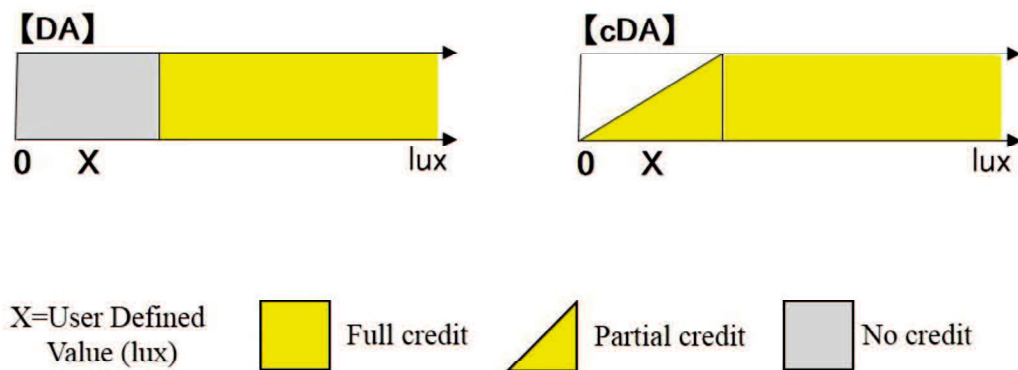


Figure 3. A.1. The diagrams of DA and cDA

## Reference:

- Bauer, K.W., Parnell, G.S., Meyers, D.A., 1999. Response surface methodology as a sensitivity analysis tool in decision analysis, *J. Multi-Criter. Decis. Anal.* 8(1999) 162–180.
- Box, G.E.P., Wilson, K.B., 1951. On the experimental attainment of optimum conditions, *J. R. Stat. Soc. Ser. B: Methodological* 13 (1951) 1–45.
- Caruso, G. & Kämpf, J.H., 2015. Building shape optimization to reduce air-conditioning needs using constrained evolutionary algorithms. *Solar Energy*, 118, pp.186–196.
- Crawley, D.B. et al., 2001. EnergyPlus: creating a new-generation building energy simulation program. *Energy and Buildings*, 33(4), pp.319–331.
- Harmathy, N., Magyar, Z. & Folic, R., 2016. Multi-criterion optimization of building envelope in the function of indoor illumination quality towards overall energy performance improvement. *Energy*, 114, pp.302–317.
- Manzan, M., Padovan, R., 2015. MultiMulti-criteria energy and daylighting optimization for an office with fixed and moveable shading devices, *Adv. Build. Energy Res* 9 (2015) 238-252.
- M Grinberg, A.R., 2013. Architecture & energy in practice: implementing an information sharing workflow. In *Proceedings of BS 2013: 13th Conference of International Building Performance Simulation Association, Chambéry, France, August 26-28*. pp. 121–128.
- Méndez Echenagucia, T. et al., 2015. The early design stage of a building envelope: Multi-objective search through heating, cooling and lighting energy performance analysis. *Applied Energy*, 154, pp.577–591.
- Nguyen, A.-T., Reiter, S. & Rigo, P., 2014. A review on simulation-based optimization methods applied to building performance analysis. *Applied Energy*, 113, pp.1043–1058.
- Reeves, T., Olbina, S., Issa, R., 2012. Validation of building energy modeling tools: Ecotect TM, Green Building Studio TM and IES<VE>TM, in: Simulation Conference (WSC), In: *Proceedings*

*of the 2012 Winter, 2012*, pp. 1–12

- Reinhart, C.F. & Walkenhorst, O., 2001. Validation of dynamic RADIANCE-based daylight simulations for a test office with external blinds. *Energy and Buildings*, 33(7), pp.683–697.
- Reinhart, C. F., Mardaljevic, J., & Rogers, Z. (2006). Dynamic Daylight Performance Metrics for Sustainable Building Design. *LEUKOS—J. Illum. Eng. Soc.* North Am 3 (2006)7–31
- Singh, S., Kensek, K., 2014. Early design analysis using optimization techniques in design/practice. *In: ASHRAE/IBPSA-USA Building Simulation Conference, Atlanta, GA, 2014*, pp.284-291.
- Stouffs, R. et al., 2013. Semi-transparent building integrated photovoltaic facades. *In: Proceedings of the 18th International Conference on Computer-Aided Architectural Design Research in Asia (CAADRIA 2013), (CAADRIA)*, pp.127–136.
- Suga, K., Kato, S. & Hiyama, K., 2010. Structural analysis of Pareto-optimal solution sets for multi-objective optimization: An application to outer window design problems using Multiple Objective Genetic Algorithms. *Building and Environment*, 45(5), pp.1144–1152.
- Takizawa, H., 1984. Hyojyun-mondai no teian (Office-yo hyojyun-mondai), in: 15th Thermal Symposium, Architectural Institute of Japan, 1984.
- Ward, G.J. & Rubinstein, F.M., 1988. A new technique for computer simulation of illuminated spaces. *Journal of the Illuminating Engineering Society*, 17(1), pp.80–91.
- Winkelmann, F.C. & Selkowitz, S., 1985. Daylighting simulation in the DOE-2 building energy analysis program. *Energy and Buildings*, 8(4), pp.271–286.



## 4.

# **Target air change rate and natural ventilation potential maps for assisting with preliminary natural ventilation design**

To achieve the desired free-cooling effect, the preliminary design of natural ventilation should be combined with discussions of building shape during the early design stages. In an earlier study (Hiyama & Glicksman 2015), a method for supporting strategic design of natural ventilation was developed that relies on the target air change rate and natural ventilation potential. The authors defined target air change rate as an air change rate at which the increase in cooling effect from natural ventilation reaches the maximum value. Our final purpose is to create the world target air change rate maps. It is necessary to confirm the robustness of target air change rate under the conditions of representative building model and construction specification in advance of the maps creation for a country. In this Chapter, case studies are firstly conducted to examine the robustness of the target air change rate by using a typical Chinese office building model with representative operation conditions in five climate zones of China. The impacts of insulation level, thermal capacity, and window-to-wall ratio (WWR) on target air change rate are investigated. Then, the target air change rate and natural ventilation potential maps in China are created to inform rough natural ventilation strategies in the early design stages. According to the evaluation results, simple natural ventilation strategies are sufficient for buildings with relatively low internal gains to realize the required small target air change rate, regardless of climate conditions. Under moderate internal gains condition, well organized and examined natural ventilation strategies are required in the Hot Summer and Warm Winter zone and

Temperate zone. However, these strategies are particularly suggested for cities in the Temperate zone with warm climate due to the higher cooling potential. Moreover, elaborate natural ventilation design is recommended for buildings in cold climate when the internal gains are increased to a high level.

## **4.1 General statement**

To improve the indoor air quality and the user satisfaction of non-residential buildings, fresh outdoor air is needed to dilute the contaminated indoor air. The exploitation of natural ventilation can reduce the energy consumption associated with auxiliary ventilation devices. Moreover, considerable free-cooling effects can be obtained for various climate conditions through successful natural ventilation design (Chou et al. 2008) (Ji et al. 2009) (Yik & Yu Fat Lun 2010) (Al-Obaidi et al. 2014) (Oropeza-Perez & Østergaard 2014a) (Oropeza-Perez & Østergaard 2014b) (Taleb 2015) (Ai et al. 2016). Thus, natural ventilation design attracts a lot of attention related to the increasing energy consumption of the building sector and the requirements of indoor environments (Li & Jones 2000) (Axley 2001) (Abdullah & Wang 2012) (Abdellatif & Al-Shamma'a 2015) (Chen et al. 2016). Etheridge reviewed relevant research on natural ventilation in nine areas including steady envelope flow models, steady flow characteristics of openings, unsteady envelope flow models, internal air motion, zonal models and stratification, contaminant transport, age of air, CFD and its applications, scale modelling, full-scale measurements during the past fifty years. In his study, the importance of design process improvement and natural ventilation strategies selection was emphasized to minimize the risk of design failure (Etheridge 2014). Design decisions, such as building shape and opening configuration, that are made in the early design stages significantly influence the performance of natural ventilation. Therefore, the design strategies for natural ventilation should be combined with discussions of building shape and sketch during the early design stages because the configurations of atrium and

ventilation shafts affect the performance of natural ventilation (Holford & Hunt 2003) (Khan et al. 2008).

In the most recent twenty years, extensive climate analysis research, which largely impacts the applicability of passive heating and cooling strategies, has been conducted to promote passive design (Tejero-González et al. 2016). In the field of natural ventilation, Ghiaus proposed a method for assessing the energy saving potential of natural ventilation using the free-running temperature (Ghiaus & Allard 2006). Artmann attempted to evaluate the suitability of climate for night-time ventilation based on the degree-hours approach (Artmann et al. 2007). The concept of natural ventilation hours, which considers both outdoor climate conditions and ambient air quality, was proposed by Tong to examine the regional feasibility of natural ventilation (Tong et al. 2016). These rapid evaluation methods are very useful for addressing the most fundamental question of whether climate conditions are suitable for using natural ventilation. However, it is difficult to obtain additional information regarding appropriate natural ventilation strategies that effectively utilize the available natural ventilation potential when performing these climate analysis. For natural ventilation design, remarkable cooling effects cannot be obtained from insufficient natural ventilation strategies. Conversely, an excessive natural ventilation strategy, i.e., mixed-mode, would result in unnecessary initial costs and labor associated with the complex design (Salcido et al. 2016).

In this context, the authors developed a preliminary design method for natural ventilation using the criteria of target air change rate and natural ventilation potential in an earlier study (Hiyama & Glicksman 2015). The authors defined the target air change rate as the maximum gradient of the cooling effect increase from natural ventilation. Only the climate data and internal gains data are needed to evaluate the proposed design criteria. Therefore, these design criteria are helpful for determining a rough natural ventilation strategy during the early design stages, which are characterized by uncertainty and lacking information. The ultimate purpose of our study is to verify the availability

of the proposed design method that uses the criteria of target air change rate and natural ventilation potential. Additionally, world target air change rate and natural ventilation potential maps are created. Therefore, in this paper, a convincing sensitivity investigation is firstly conducted to examine the robustness of the target air change rate by using a typical Chinese office building model with representative operation conditions in five climate zones of China. The impacts of insulation level, thermal capacity, and window-to-wall ratio (WWR) on the target air change rate are examined. In addition, the target air change rate and natural ventilation potential maps from China are shown to provide architects with information for determining appropriate natural ventilation strategies in the early design stages. Notably, the cooling effects that occur related to night-time ventilation and mixed-mode (hybrid) systems are beyond the scope of this study.

China is selected as the object of this study due to its significantly increasing energy consumption and CO<sub>2</sub> emissions corresponding with rapid economic and industrial development. The building sector in China accounts for approximately 46 % of the total energy consumption according to perspective of life cycle evaluations (Zhang et al. 2015). This ratio has continued to increase at a stable rate in recent years. On the other hand, a large number of newly constructed commercial buildings in China have resulted in an energy saving opportunity due to the adoption of passive natural ventilation design.

## **4.2 Theory**

### **4.2.1 Definition of the target air change rate**

The authors defined target air change rate as an air change rate at which the increase in cooling effect from natural ventilation reaches the maximum value. The red column represents the rise in cooling effect when air change rate of natural ventilation increases 1ac/h. The increment of cooling

effect reaches the maximum value when the air change rate increases to 3 ac/h. Thus, 3 ac/h is defined as the target air change rate under such conditions.

The extra increase in the amount of air change achieved by the complex design and additional costs does not contribute to the increase in free-cooling effect. Thus, the target air change rate can be used as a design benchmark for determining appropriate natural ventilation strategies, through which the maximum energy saving effect can be obtained and the requirement of cost effectiveness can also be satisfied. Additionally, the available free-cooling effect at an infinite air change rate is regarded as the natural ventilation potential.

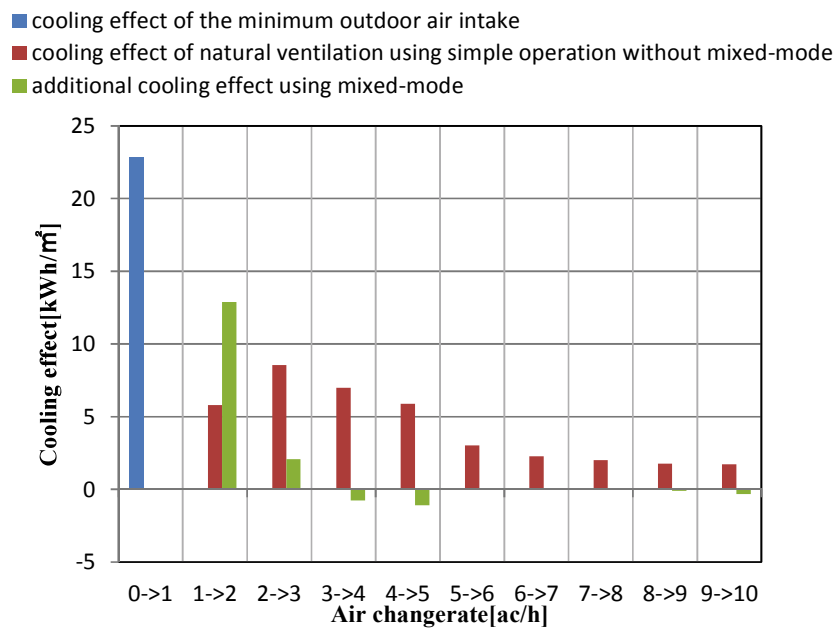


Figure 4.1. Definition of target air change rate using a simulation result

#### 4.2.2 Simple method for estimating the target air change rate

The target air change rate is decided when the cooling effect from natural ventilation reaches saturation. However, the portion of the cooling effect combined with the mechanical system (mixed-mode) is excluded from the evaluation. Mixed-mode is defined as a mode when air conditioner and the natural ventilation are operated at the same time and the same place as shown in Figure 4.2. In this study, the climate conditions and indoor usage conditions are used to determine the suitability of natural ventilation at a particular time step. The suitability of the climate for natural ventilation is decided by two parameters, outdoor dry-bulb temperature and dew point temperature. The upper threshold of the outdoor dry-bulb temperature is the 90 % acceptability of the optimal comfort temperature in naturally ventilated buildings and is defined by the adaptive comfort model in ASHAR-55 (Eqs. 4-1 and 4-2) (De Dear & Brager 2002). In addition, the dew point temperature is confined within 17 °C for the sake of humidity control (ASHRAE 2009).

$$t_{comf} = 0.31 \times t_{a,out} + 17.8 \quad (4-1)$$

$$t_{up} = t_{comf} + 2.5 \quad (4-2)$$

where  $t_{comf}$  (°C) is the optimum comfort temperature in a naturally ventilated building,  $t_{a,out}$  (°C) is the monthly average outdoor dry-bulb temperature, and  $t_{up}$  (°C) is the upper threshold of the outdoor dry-bulb temperature for natural ventilation.

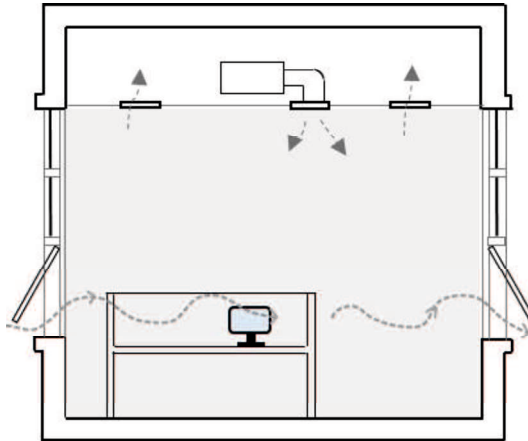


Figure 4.2. The image of a mixed-mode (air condition and operate window simultaneously turn on).

The indoor usage conditions refer to whether the internal gains of the building can be fully offset by the cooling effect obtained solely from natural ventilation (see Eq. (4-3)).  $Q_{in}$  in Eq. (4-3) represents the specific internal gains and is defined as the combination of gains from solar and indoor activities. The negative value of  $m_{i,j}$  indicates that the cooling effect induced by natural ventilation can fully offset the specific heat gains  $Q_{in}$  and indicates that the indoor conditions are suitable for natural ventilation. Natural ventilation mode (operable windows are open and air-conditioning system is off as shown in Figure 4.3) begins once the predefined climate conditions and indoor usage conditions are both satisfied. Otherwise, air-conditioning mode (operable windows are closed and air-conditioning system is on as shown in Figure 4.4) is used.

$$m_{i,j} = Q_{in} - \frac{iH\rho C_p(t_{up} - t_{out,j})}{3600} \quad (4-3)$$

where  $Q_{in}$  (Wh/m<sup>2</sup>) is the specific internal gains,  $i$  (ac/h) is the air change rate,  $H$  (m) is the ceiling

height,  $\rho$  ( $\text{kg/m}^3$ ) is the density of air,  $C_p$  ( $\text{J/kg K}$ ) is the specific heat of dry air, and  $t_{out,j}$  ( $^{\circ}\text{C}$ ) is the outdoor temperature at the time step  $j$ .

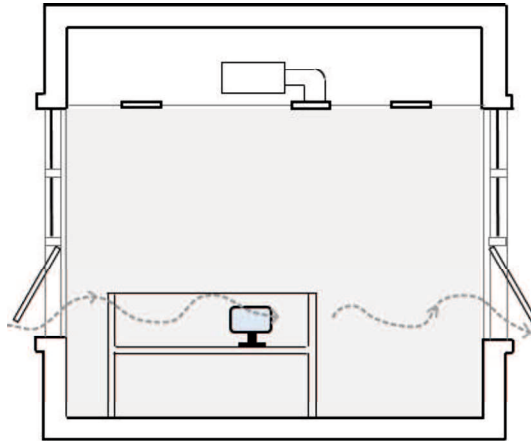


Figure 4.3. The image of natural ventilation mode (air conditioner is off and operate window is open).

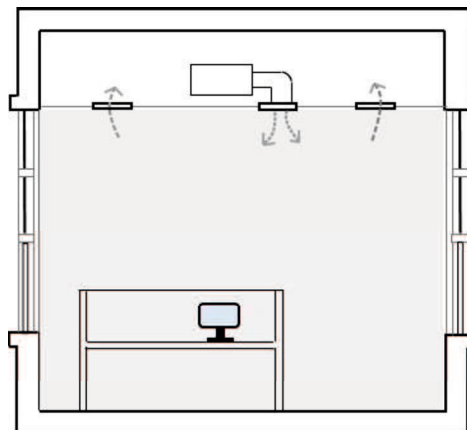


Figure 4.4. The image of air conditioner mode (air conditioner is on and operate window is off).



The hourly and annual cooling loads required to be processed by air-conditioning systems are calculated using Eqs. (4-4) and (4-5), respectively. The cooling effect of air change at the rate of 1 ac/h is not considered in the evaluation because this amount of air change is approximately equal to the required minimum amount of fresh air in office buildings. The cooling effect used to determine the target air change rate is evaluated from the decrease in cooling load from the baseline, as shown in Eq. (4-6). The baseline is the cooling load at the minimum required amount of air change (1 ac/h). As the air change rate  $i$  increases, the target air change rate can be determined when  $E_{nat,i}$  reaches the maximum value. Finally, the natural ventilation potential is defined as the available cooling effect when the air change rate is infinite, as shown in Eq. (4-7).

$$L_{i,j} = \begin{cases} 0 & \text{Natural ventilation : on / air - conditioning : off} \\ \left( Q_{in} - \frac{MH\rho C_p (T_{up} - T_{out,j})}{3600} \right) \times T & \text{Natural ventilation : on / air - conditioning : on} \end{cases} \quad (4-4)$$

$$L_i = \sum_j L_{i,j} \quad (4-5)$$

$$E_{nat,i} = L_{min} - L_i \quad (4-6)$$

$$E_p = E_{nat,\infty} \quad (4-7)$$

where  $L_{i,j}$  (Wh/m<sup>2</sup>) is the cooling load when the air change rate is  $i$  ac/h at time step  $j$ ,  $M$  is the required minimum air change rate (1 ac/h),  $T$  is the time interval (1 h),  $L_i$  (Wh/m<sup>2</sup>) is the annual cooling load at  $i$  ac/h,  $E_{nat,i}$  (Wh/m<sup>2</sup>) is the cooling effect obtained when only using natural ventilation at  $i$  ac/h,  $L_{min}$  (Wh/m<sup>2</sup>) is the baseline cooling load at 1 ac/h, and  $E_p$  (Wh/m<sup>2</sup>) is the cooling potential from natural ventilation.

### **4.2.3 Application of the target air change rate in preliminary design of natural ventilation**

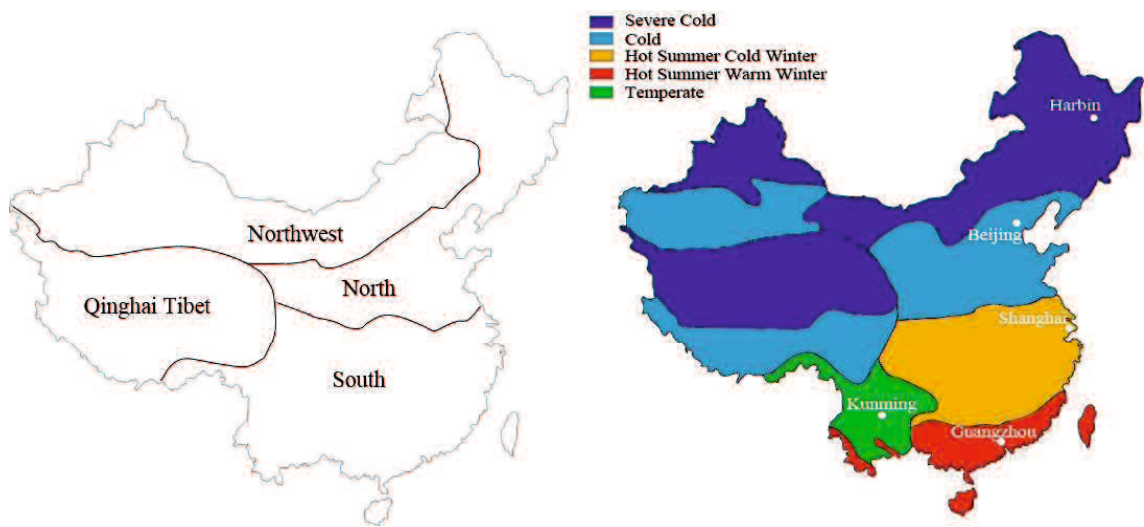
The strategic design of natural ventilation in the early design stages can be roughly divided into three categories based on the magnitude of the target air change rate: (i) Simple natural ventilation strategies (i.e., single-sided ventilation) are suggested to obtain the combined effects of remarkable free-cooling with reasonable initial costs when the target air change rate is relatively small ( $\leq 3$  ac/h). (ii) Well organized and examined natural ventilation strategies are necessary to achieve the desired target air change rate, and 10 ac/h is defined as the boundary for this category. It is because that the air change rate of 10 ac/h is considered as a realizable level through available natural ventilation strategies (Axley 2001). (iii) Complex mixed-mode natural ventilation strategies must be considered to attain the target air change rate of more than 10 ac/h. However, the cost effectiveness and design risks should be considered carefully in this category.

## **4.3 Validating the robustness of the target air change rate using a case study of China**

### **4.3.1 Basic simulation conditions**

Only climate and internal gains data are necessary to evaluate the target air change rate and natural ventilation potential described in section 4.2. To further verify the feasibility of using the target air change rate as a design criterion, sensitivity analysis is used and described in this section. The influences of construction thermal capacity, envelope insulation level, and WWR on the target air change rate are examined using a typical Chinese office building model with the representative operation conditions. Due to the obvious differences in the terrain and topography and the locations of land and sea, various types of climate, including temperate monsoon climate in the north, temperate

continental climate in the northwest, plateau-mountain climate in the southwest, and subtropical monsoon climate in the south exist in China, as shown in Figure 4.5 (a) (People’s Education Press 2015). Therefore, sensitivity analysis must be conducted for different climate conditions. China is divided into five major climate zones according to the design standards for commercial buildings (GB50189 2015). Figure 4.5 (b) shows the five climate zones of Severe Cold, Cold, Hot Summer and Cold Winter, Hot Summer and Warm Winter, and Temperate zones. Harbin, Beijing, Shanghai, Guangzhou, and Kunming are chosen as the representative cities in these five major climate zones (see Figure 4.5 (b)). For these five cities, the hourly Chinese Standard Weather Data (CSWD) provided by Tsinghua University and the China Meteorological Bureau are used in the sensitivity analysis (China Meteorological Bureau 2005).



(a) Geographical regions in China

(b) Climate zones in China

Figure 4.5. Geographic and climate divisions in China.

The climate characteristics and the upper limit of envelope U value in each city are summarized in Table 4.1. Figure 4.6 shows a typical Chinese office building modeled in the simulation program of

EnergyPlus (Crawley et al. 2001). It is an eighteen story open office building with a floor area of 1500 m<sup>2</sup>, and the geometry of the building were originally collected by Chinese design institutes (Feng et al. 2014). Table 4.2 shows the simulation conditions that refer to the design guidelines of GB50189.

#### **4.3.2 Variable design conditions**

The variable design conditions and their corresponding modifications are given below.

- Heavyweight and lightweight structures are used to examine the impacts of construction thermal capacity. The thermal capacities of heavyweight and lightweight structures are 213.7 kJ/m<sup>2</sup> K and 65.2 kJ/m<sup>2</sup> K, respectively. The compositions of heavyweight structures from the outer side to the inner side are brick tile, mortar, ESP expanded polystyrene, concrete block (heavyweight), and gypsum plastering. The compositions of lightweight structures from the outer side to the inner side are brick tile, mortar, ESP expanded polystyrene, concrete block (lightweight), and gypsum plastering.
- Three different WWR values of 20 %, 40 %, and 60 % are used in the simulation to consider the influences of opening area.
- In addition to the typical internal gains shown in Table 4.2, high level internal gains with twice the typical density of occupants, lighting, and plug load values are also available in the simulation.
- For each selected city, the simulated high and low insulation levels are shown in Table 4.3. In each climate zone, both the high and low insulation levels meet the design guidelines listed in Table 4.1.
- Moreover, an additional case with an adiabatic envelope and no glazing is simulated for the five representative cities.

In total, 130 cases are simulated by combining the modifications of the three variable design

conditions. For each case, the design variable is the air change rate. To obtain the target air change rate, the objective function of simulation is the hourly cooling load (the specific procedures for calculating target air change rate are shown in Appendix A). The tenth floor in the middle of the model is selected as the analysis object.

Table 4.1. Climate characteristics and the required U values of envelopes in five representative cities.

City	Climate zone	Latitude	Climate characteristics		Upper limit of U value (W/m <sup>2</sup> K)	
			ATCM	ATHM	External Wall	Roof
Harbin	Severe Cold	45.75	-18.7	22.8	0.38	0.28
Beijing	Cold	39.93	-3.8	26.4	0.5	0.45
Shanghai	Hot Summer Cold Winter	31.40	4.5	27.5	0.6	0.4
Guangzhou	Hot Summer Warm Winter	23.22	13.9	28.8	0.8	0.5
Kunming	Temperate	25.02	8.4	20	-	-

Note: ATCM=average temperature in the coldest month, and ATHM=average temperature in the hottest month. The U value of the climate zone of Kunming is not required.

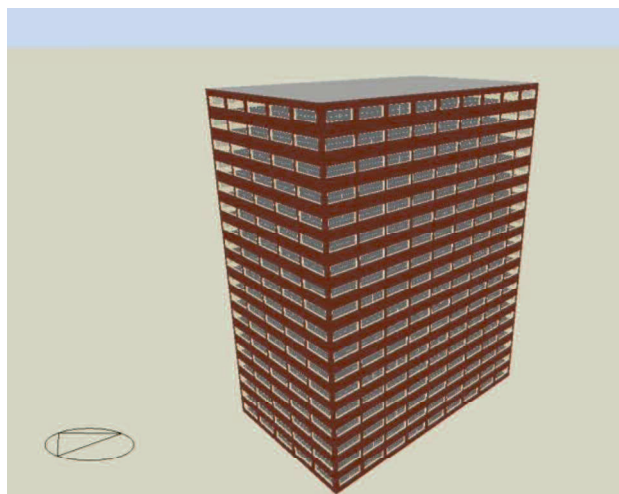


Figure 4. 6. Typical office building model used in this study.

**Table 4.2. Simulation conditions.**

Building geometry	Floor area: 1500 m <sup>2</sup> (30 m×50 m); Floor height: 3.5 m; Ceiling height: 2.5 m
Occupant	Density: 0.1 person/m <sup>2</sup> 0 %-7:00-10 %-8:00-50 %-9:00-95 %-12:00-80 %-14:00-95 %-18:00-30 %-20:00
Plug load	Density: 15 W/m <sup>2</sup> 0 %-7:00-10 %-8:00-50 %-9:00-95 %-12:00-50 %-14:00-95 %-18:00-30 %-20:00
Lighting	Density: 2.25 W/m <sup>2</sup> 100 lx; Target illuminance: 400 lx 0 %-7:00-10 %-8:00-50 %-9:00-95 %-12:00-80 %-14:00-95 %-18:00-30 %-20:00
Natural Ventilation	T <sub>indoor</sub> >22 °C and T <sub>outdoor</sub> <T <sub>indoor</sub> ; Occupied period: 7:00-19:00
Cooling	Set-point temperature: 26 °C; Schedule: OFF-7:00-ON-19:00-OFF
Window shading	Blind with high reflectivity slats (inside); solar set point: 120 W/m <sup>2</sup>

**Table 4.3. U value of the external wall in each selected city (W/m<sup>2</sup> K).**

	Severe Cold (Harbin)	Cold (Beijing)	Hot Summer Cold Winter (Shanghai)	Hot Summer Warm Winter (Guangzhou)	Temperate (Kunming)
High insulation	0.27	0.37	0.47	0.55	0.55
Low insulation	0.37	0.47	0.58	0.70	0.70

Note: glazing used for high insulation is double low E glazing (U value=1.8 W/m<sup>2</sup> K, SHGC=0.6); glazing used for low insulation is double glazing (U value=2.7 W/m<sup>2</sup> K, SHGC=0.7).

### 4.3.3 Simulation results

Tables 4.4 and 4.5 show the evaluated target air change rates for cases with typical and high level internal gains, respectively. For both typical and high level internal gains, no distinctive variations in the target air change rate (at level of ±1 ac/h) are observed as the thermal capacity, insulation level, and WWR varied in the same city. Therefore, the reasonability of the target air change rate estimated based on a completely adiabatic condition without considering the impacts of heat conduction and window area is confirmed through the sensitivity analysis. Meanwhile, the robustness of the target air change rate as a criterion in early design stages characterized by rapid design changes is verified. From

the simulation results presented by Tong, the energy savings effect of natural ventilation did not obviously vary (within 8 %) with variations in plug load. In his analysis, the plug load varied from 10 W/m<sup>2</sup> to 20 W/m<sup>2</sup> at an increment of 5 W/m<sup>2</sup> (15 W/m<sup>2</sup> was the baseline load) (Tong et al. 2016). However, besides the plug load, the occupant and lighting served as internal gains components are very different among office buildings (Emmerich et al. 2011). Therefore, this study focuses on the impacts of the internal gains originating from the occupant, lighting, and plug load. The significant influences of internal gains on the target air change rate can be distinctively observed from the simulation results of Kunming listed in Tables 4.4 and 4.5. The target air change rates of Kunming under the typical internal gains condition are 3-4 ac/h. The design strategies suggested for naturally ventilated buildings in this case can be approximatively classified as category (i). However, the target change rates in Kunming increase to 6-7 ac/h when the internal gains are increased to the high level. For such cases, simple natural ventilation strategies are not sufficient for achieving the desired target air change rate. A well designed and examined natural ventilation strategy is necessary to realize a measurable cooling effect. This impact of internal gains on natural ventilation performance was also indicated by Yao, who developed a simple evaluation tool for assessing preliminary natural ventilation strategies (Yao et al. 2009). In addition, the impacts of climate on the target air change rate tend to become more intense with increasing internal gains.

Table 4.4. Target air change rates under the typical internal gains condition.

Structure	Insulation level	Window-to-wall ratio	Target ACH				
			Harbin	Beijing	Shanghai	Guangzhou	Kunming
Heavyweight	High	20 %	2	3	2	2	3
		40 %	3	3	2	3	3
		60 %	3	3	2	3	4
	Low	20 %	2	3	2	2	3
		40 %	2	3	2	3	3
		60 %	3	3	3	3	4
Lightweight	High	20 %	2	3	2	3	3
		40 %	3	3	2	3	3
		60 %	3	3	2	3	4
	Low	20 %	2	3	2	2	3
		40 %	3	3	2	3	4
		60 %	3	3	3	3	4
	Adiabatic	0	2	2	2	3	4

Table 4.5. Target air change rates under the high level internal gains condition.

Structure	Insulation level	Window-to-wall ratio	Target ACH				
			Harbin	Beijing	Shanghai	Guangzhou	Kunming
Heavyweight	High	20 %	3	3	3	4	6
		40 %	3	3	3	4	7
		60 %	3	2	3	4	6
	Low	20 %	3	3	3	4	6
		40 %	3	3	3	4	7
		60 %	3	3	3	4	6
Lightweight	High	20 %	3	3	3	4	6
		40 %	3	3	3	4	7
		60 %	3	3	3	4	6
	Low	20 %	3	3	3	4	6
		40 %	3	3	3	4	7
		60 %	3	3	3	4	7
	Adiabatic	0	2	3	3	5	7



## 4.4 Case study

### 4.4.1 Basic conditions for maps creation

The creation of maps is a visual and feasible approach for showing architects information regarding design parameters that depend on climate conditions (Wen & Hiyama 2017). Therefore, the target air change rate and natural ventilation potential maps in China are created using the proposed method, whose availability in China was verified in section 4.3. These created maps will inform architects of rough natural ventilation strategies in the early design stages when building shape and sketch are discussed. In this study, 36 major cities, including the provincial capitals and sub-provincial cities shown in Table 4.6, are selected to generate these maps. Additionally, the specific internal gains ( $Q_{in}$ ) adopted to evaluate the target air change rate and natural ventilation potential are 10 W/m<sup>2</sup>, 20 W/m<sup>2</sup>, 40 W/m<sup>2</sup>, and 80 W/m<sup>2</sup> (Emmerich et al. 2011). These maps are created considering various specific internal gains to provide design options for different projects. The other necessary parameters for evaluating the criteria of target air change rate and natural ventilation potential are listed in Table 4.7.

### 4.4.2 Target air change rate and natural ventilation potential maps in China

Figure 4.7 shows the target air change rate and natural ventilation potential maps created for buildings with minimum specific internal gains of 10 W/m<sup>2</sup>. The characteristics of such buildings are designed with high-efficiency lighting systems, minimum plug load, and low occupant density. A uniform target air change rate of 2 ac/h can be seen in all the selected locations regardless of climate conditions, as shown in Figure 4.7 (a). According to the classification of design strategies for naturally ventilated buildings described in section 4.2, simple natural ventilation strategies are sufficiently capable of realizing the relatively small target air change rate for buildings with minimum internal gains. Figure 4.7 (b) demonstrates the natural ventilation potential map under the specific internal gains of 10 W/m<sup>2</sup>. The maximum value of the color label represents the annual summation of the

specific internal gains during the occupied period of between 7:00 and 19:00. For most selected locations, the cooling effect potential from natural ventilation stays between 4380 and 8760 W/m<sup>2</sup>. The cooling effect potential of natural ventilation in the selected cities only accounts for 7-28 % of the annual specific internal gains (43800 W/m<sup>2</sup>). The cooling effect induced by the required minimum amount of fresh outdoor air (1 ac/h), which is excluded from the evaluation of natural ventilation potential, compensates for most of the specific internal gains. Thus, the cooling potential experiences no obvious increase, even when the amount of air change is large enough. Accordingly, the simplest natural ventilation strategies, such as single-sided natural ventilation with operable windows, are recommended for buildings with minimum internal gains to achieve high energy performance and cost-effectiveness.

Table 4.6. 36 Selected cities for the creation of maps.

No.	City	Longitude	Latitude	No.	City	Longitude	Latitude
1	Beijing	116.47	39.80	19	Nanchang	115.92	28.60
2	Changchun	125.22	43.90	20	Nanjing	118.80	32.83
3	Changsha	112.92	28.22	21	Nanning	108.22	22.63
4	Chengdu	104.02	30.67	22	Ningbo	120.65	28.03
5	Chongqing	106.47	29.58	23	Qingdao	119.18	36.75
6	Dalian	121.63	38.90	24	Shanghai	121.45	31.40
7	Fuzhou	119.28	26.08	25	Shenyang	123.45	41.73
8	Guangzhou	113.33	23.17	26	Shenzhen	114.10	22.55
9	Guiyang	106.73	26.58	27	Shijiazhuang	114.42	38.03
10	Haikou	110.35	20.03	28	Taiyuan	112.55	37.78
11	Hangzhou	120.17	30.23	29	Tianjin	117.07	39.08
12	Harbin	126.77	45.75	30	Urumqi	87.530	43.83
13	Hefei	117.23	31.87	31	Wuhan	114.13	30.62
14	Hohhot	111.68	40.82	32	Xiamen	118.07	24.48
15	Jinan	117.05	36.60	33	Xian	108.93	34.30
16	Kunming	102.68	25.02	34	Xining	101.75	36.72
17	Lanzhou	103.88	36.05	35	Yinchuan	106.22	38.48
18	Lhasa	91.130	29.67	36	Zhengzhou	113.65	34.72

Table 4.7. Parameters for evaluating the target air change rate and natural ventilation potential.

$\rho$	1.205 kg/m <sup>3</sup>
$C_p$	1006 J/kg K
Ceiling height	2.5 m
Occupied hours	7:00-19:00
Air change rate	1-10 ac/h

Figure 4.8 shows the target air change rate and natural ventilation potential maps when the specific internal gains of buildings are at the relatively low level of 20 W/m<sup>2</sup>. Compared with the maps acquired for the specific internal gains of 10 W/m<sup>2</sup>, the target air change rates of cities located in the Hot Summer and Warm Winter zone and the Temperate zone vary slightly from 2 ac/h to 3 ac/h. The target air change rates in the other cities are maintained at 2 ac/h, as shown in Figure 4.8 (a). All the selected locations still belong to the first category, in which simple natural ventilation strategies are recommended to realize the relatively small amount of air change. In the natural ventilation potential map shown in Figure 4.8 (b), the cooling effect potential of natural ventilation tends to slightly increase relative to the cooling effect potential when the specific internal gains are 10 W/m<sup>2</sup>. The percentage of the available cooling effect potential of natural ventilation divided by the total specific internal gains increased to 13 % and 55 %. Due to the smaller difference between indoor and outdoor temperatures in Kunming, further increasing the amount of air change based on the required minimum amount of air change (1 ac/h) is an effective approach for offsetting the internal gains. Therefore, Kunming in Temperate zone exhibits the highest cooling effect potential when the air change rate is large enough. In comparison with the Temperate zone, the lower cooling effect potential of natural ventilation in the Severe Cold and Cold zones likely occurred because the obvious temperature difference allows the required minimum amount of air change to completely compensate for internal gains during a long period. Consequently, increases in the cooling effect are terminated as the air

change rate increases. In addition, the cities near the Yangtze River Basin in the Hot Summer and Cold Winter zone (e.g., Chongqing, Wuhan, Changsha, Nanchang) and the cities selected from the Hot Summer and Warm Winter zone display relatively lower cooling effect potential due to the unfavorable hot-humid climate for the utilization of natural ventilation.

Figure 4.9 shows the target air change rate and natural ventilation potential maps for naturally ventilated buildings with specific internal gains of  $40 \text{ W/m}^2$ , which is similar to the standard level of internal gains in office buildings in China. According to the target air change rate map in Figure 4.9 (a), the categories of natural ventilation strategies are distinguished by the Yangtze River. The cities located south of the Yangtze River are characterized by a hot-humid climate and are classified into category (ii), in which the target air change rate is moderate (4-10 ac/h). This tendency is especially remarkable for the cities in the Hot Summer and Warm Winter zone and the Temperature zone. To realize the required larger target air change rates at these locations, careful considerations and examinations on the natural ventilation strategies are necessary during the initial design stages. The cities located north of the Yangtze River belong to category (i), with a target air change rate of less than 3 ac/h. In the natural ventilation potential map shown in Figure 4.9 (b), significant growth in the cooling effect potential of natural ventilation can be observed when the combined specific internal gains are increased to the standard level of  $40 \text{ W/m}^2$ . In the Severe Cold and Cold climate zones, higher potential is observed due to the favorable climate conditions for natural ventilation. This observation is especially true for the locations in the northwest and southwest due to the dry climate throughout the year. On the other hand, the cooling effect potential of Kunming and Haikou should be highlighted although the strategic design of natural ventilation in these two cities are all classified as category (ii). The cooling effect potential in Kunming reaches 74 % of the total annual internal gains. Due to this high potential, it is important to carefully organize the natural ventilation strategies for the projects located in the Temperate zone. Conversely, the cooling effect potential available from natural

ventilation only covers 16 % of the combined total annual internal gains in Haikou. Thus, it may be difficult to realize a measurable cooling effect through natural ventilation design due to the lower potential under such hot and humid climate conditions. In this case, architects should cautiously determine whether a complex natural ventilation strategy should be used due to the high cost, complex technology, and ineffectiveness of complex natural ventilation strategies for improving the indoor environment and realizing a larger target air change rate.

Figure 4.10 shows the target air change rate and natural ventilation potential maps for naturally ventilated buildings, with internal gains originated from high densities of lighting and plug load and a large number of occupants. The natural ventilation design strategies for all of the selected locations are included into category (ii), which is described in section 4.2, when the combined specific internal gains are  $80 \text{ W/m}^2$  in Figure 4.10 (a). Particularly, the cities located south of the Qinling Mountain-Huaihe River have a relatively larger target air change rate. The maximum target air change rate of 8-9 ac/h is observed in the Hot Summer and Warm Winter zone. Serious consideration of the natural ventilation strategies is necessary to achieve large target air change rates. Moreover, no areas are categorized into the third category, whose target air change rate exceeds 10 ac/h based on the evaluation results presented in this study. For various climate conditions in China, the measurable cooling effect can be realized by using available natural ventilation strategies (Axley 2001), even under high internal gains condition. Figure 4.10 (b) is a map marked with the cooling effect potential from natural ventilation when the combined internal gains are  $80 \text{ W/m}^2$ . The cooling effect potential in the Severe Cold and Cold zones distinctively increase in comparison with the results obtained at the general internal gains level of  $40 \text{ W/m}^2$ . It is demonstrated that the additional amount of air change is still required to compensate for higher internal gains, even in the cold climate conditions, where the difference between the indoor and outdoor temperatures is large. According to the target air change rate and natural ventilation potential maps, an elaborate natural ventilation design is particularly

recommended for the buildings located in the cold climate zone when the internal gains of the buildings are increased to a high level. Furthermore, the target air change rate and natural ventilation maps in Japan are shown in appendix B



(a) Target air change rates of 36 selected cities

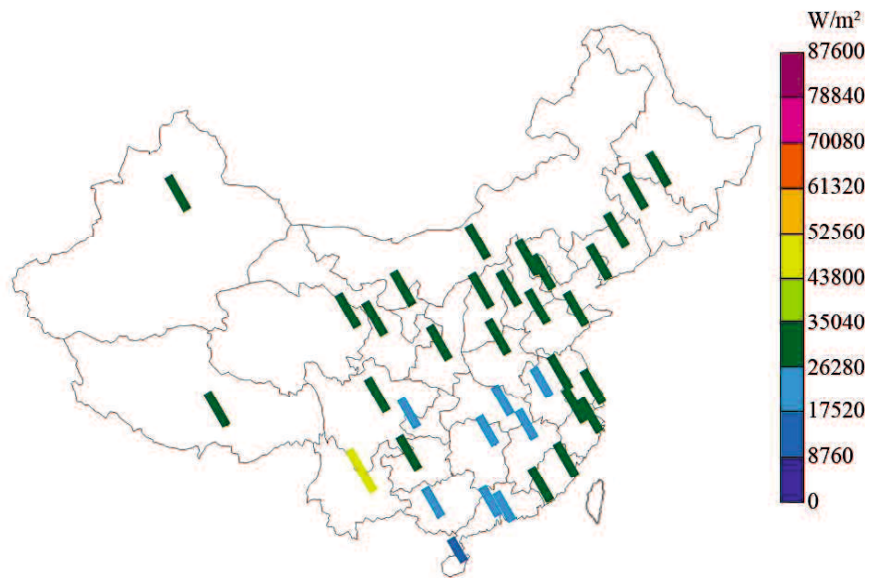


(b) Natural ventilation potentials of 36 selected cities; the highest value in the label represents the annual sum of the internal gains

Figure 4. 7. Maps with a specific internal gains of 10 W/m<sup>2</sup> in China.

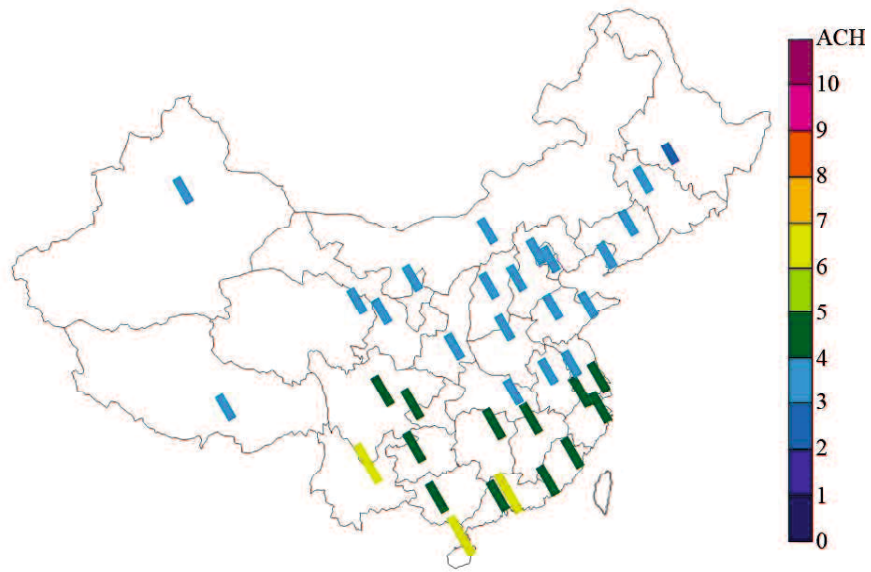


(a) Target air change rates of 36 selected cities



(b) Natural ventilation potentials of 36 selected cities; the highest values in the label represents the annual sum of the internal gains

Figure 4. 8. Maps with a specific internal gains of 20  $W/m^2$  in China.



(a) Target air change rates of 36 selected cities

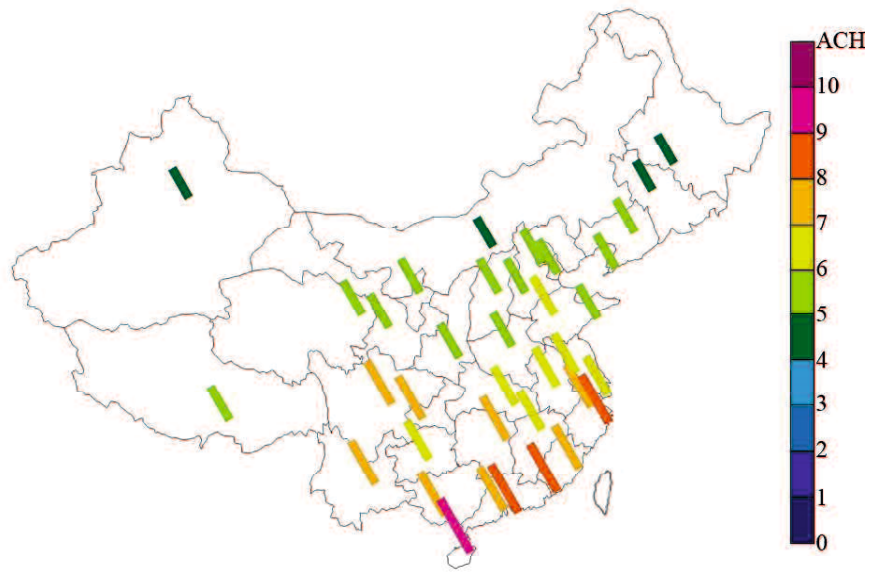


(a) Natural ventilation potentials of 36 selected cities; the highest value in the label

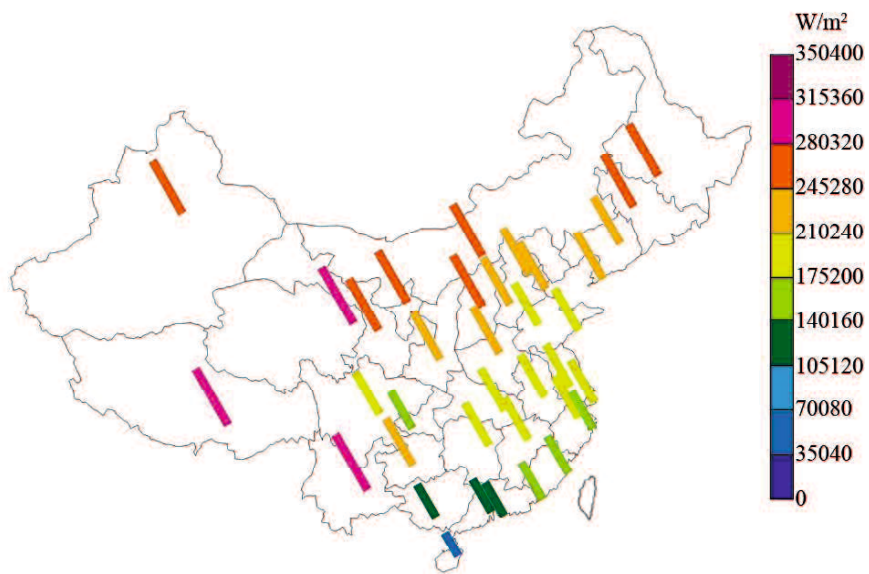
represents the annual sum of the internal gains

Figure 4. 9. Maps with a specific internal gains of  $40 W/m^2$  in China.





(a) Target air change rates of 36 selected cities



(b) Natural ventilation potentials of 36 selected cities; the highest value in the label

represents the annual sum of the internal gains

Figure 4. 10. Maps with a specific internal gains of 80 W/m<sup>2</sup> in China.

## 4.5 Summary

To facilitate the strategic design of natural ventilation in the early design stages, a preliminary design method using the target air change rate and natural ventilation potential was proposed in a previous study. The authors defined the target air change rate as the maximum point of the increasing gradient of the cooling effect from natural ventilation. The ultimate purpose of our study is to verify the availability of the proposed design method and to create world maps of the target air change rate and natural ventilation potential. In this paper, a more convincing sensitivity investigation is performed to further verify the robustness of the target air change rate as a design criterion in the early stages using a typical Chinese office building model with representative operation conditions in five climate zones of China. No distinctive variations in the target air change rate (at level of  $\pm 1$  ac/h) are observed as the thermal capacity, insulation level, and WWR varied in the same city. In addition, some specific findings based on the created target air change rate and natural ventilation potential maps in China are summarized as follows:

- (1) Simple natural ventilation strategies (category (i)), i.e., single-sided natural ventilation, are recommended for buildings with relatively low internal gains (such as 10 W/m<sup>2</sup> and 20 W/m<sup>2</sup>) to realize the required small target air change rate ( $\leq 3$  ac/h), regardless of the climate conditions. These simple options can simultaneously satisfy the requirements of high energy performance and the cost-effectiveness.
- (2) For buildings with moderate internal gains of 40 W/m<sup>2</sup>, the categories of design strategies for natural ventilation are distinguished by the Yangtze River. Well organized and examined natural ventilation strategies (category (ii)) are suggested for cities located south of the Yangtze River. This result is especially obvious for locations in the Hot Summer and Warm Winter zone and the Temperate zone. However, in comparison with the hot-humid climate in the Hot Summer and Warm Winter zone, careful consideration of the natural ventilation design is strongly

recommended for the cities located in the Temperate zone with a warm climate due to the higher cooling effect potential.

- (3) Careful natural ventilation design (category (ii)) in the early design stages is required in all the selected cities to achieve a moderate and realizable target air change rate of 4-10 ac/h when the internal gains are increased to the relatively high level of 80 W/m<sup>2</sup>. In addition, the increase in cooling effect potential of natural ventilation in the Severe Cold and Cold zones is very obvious. Therefore, it is more effective to elaborately organize the natural ventilation strategies for buildings in cold climate when the internal gains are increased.
- (4) According to the results of this study, no location is classified as category (iii), which corresponds to a target air change rate of more than 10 ac/h. A measurable cooling effect can be realized by using the available natural ventilation strategies under various climate conditions in China, even with high internal gains.

## Appendix A

$$E_{\min} = L_{bas} - L_{\min}$$

$$E_{nat,i} = L_{bas} - L_{sim,i} - E_{\min} = L_{\min} - L_{sim,i} \quad (i = 2, 3, \dots, 10)$$

$$L_{sim,i} = L_i + E_{mix,i}$$

$$E_{mix,i} = \sum_j p_{i,j}$$

$$p_{i,j} = \begin{cases} 0 & \text{air-conditioning : off} \\ q_{i,j} - q_{1,j} & \text{air-conditioning : on} \end{cases}$$

where:

$i$ : fixed air change rate through natural ventilation, which is the design variable [ac/h]

$E_{\min}$ : cooling effect of the minimum outdoor air intake [Wh/m<sup>2</sup>]

$E_{nat,i}$ : cooling effect of natural ventilation using simple operation without mixed-mode at  $i$  ac/h [Wh/m<sup>2</sup>]

$E_{mix,i}$ : additional cooling effect using mixed-mode at  $i$  ac/h [Wh/m<sup>2</sup>]

$L_i$ : cooling load at  $i$  ac/h [Wh/m<sup>2</sup>] (energy simulation output)

$L_{bas}$ : baseline cooling load [Wh/m<sup>2</sup>] (=L<sub>0</sub>)

$L_{\min}$ : cooling load at minimum air change rate [Wh/m<sup>2</sup>] (=L<sub>1</sub> =L<sub>sim, 1</sub>)

$L_{sim,i}$ : cooling load using simple operation without mixed-mode at  $i$  ac/h [Wh/m<sup>2</sup>]

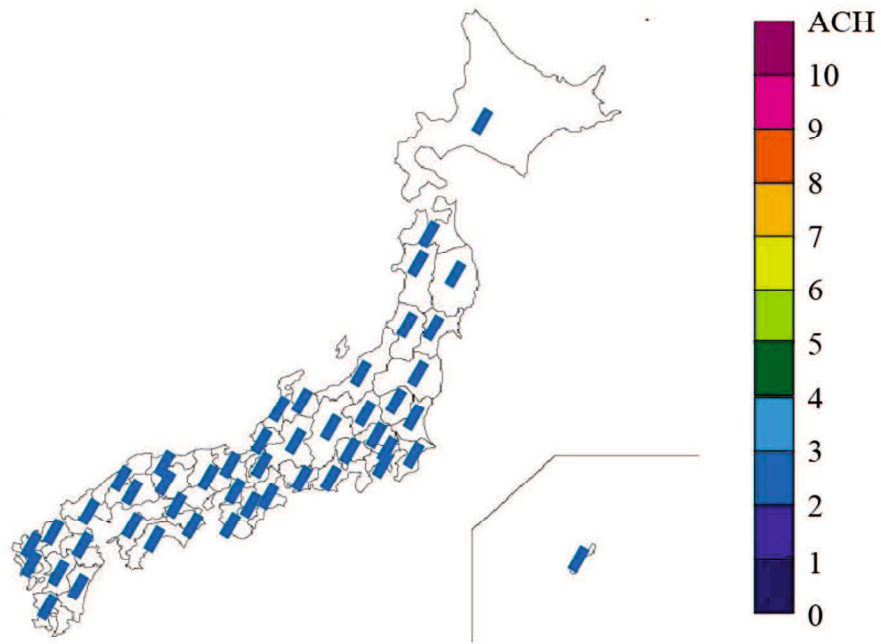
$P_{i,j}$ : hourly additional cooling effect using mixed-mode at  $i$  ac/h and at time step  $j$  [Wh/m<sup>2</sup>]

$q_{i,j}$ : hourly cooling effect due to the entry of outside air at  $i$  ac/h and at time step  $j$  [Wh/m<sup>2</sup>] (energy simulation output)

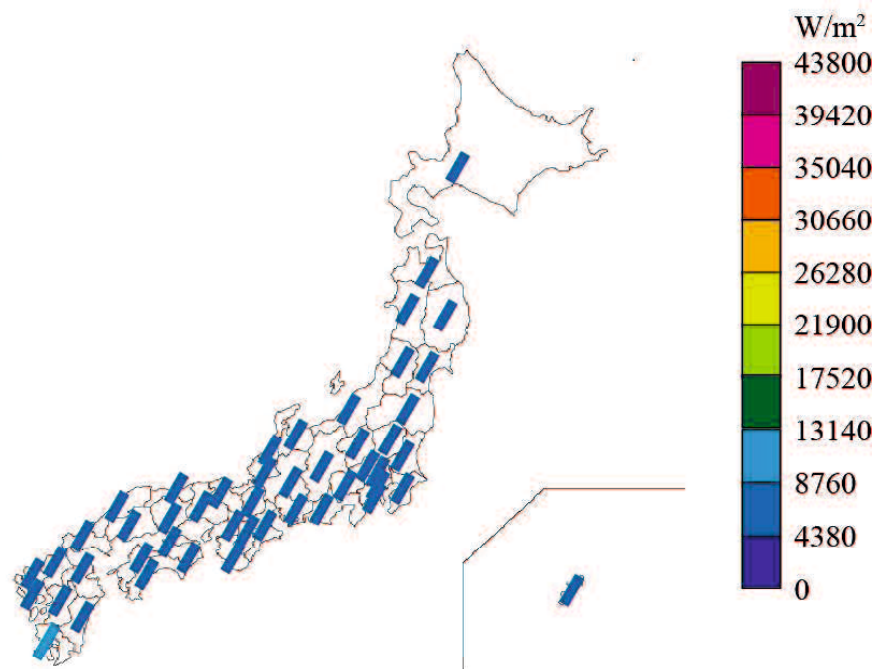
Appendix B

Table 4 B.1. Target air change rate and natural ventilation in 46 selected cities of Japan.

Internal Gain W/m <sup>2</sup>				10		20		40		80	
Location		longitude	latitude	Potential W h/m <sup>2</sup>	Target ACH	Potential W h/m <sup>2</sup>	Target ACH	Potential W h/m <sup>2</sup>	Target ACH	Potential W h/m <sup>2</sup>	Target ACH
Hokkaido	Sapporo	141.3	43.1	7633	2	34007	2	102874	3	174073	5
Aomori	Aomori	140.8	40.8	7744	2	35545	2	97966	3	163266	5
Akita	Akita	140.1	39.7	7235	2	33018	2	92782	3	156736	5
Iwate	Morioka	141.2	39.7	7032	2	32479	2	94450	3	162250	5
Miyagi	Sendai	140.9	38.3	7886	2	36303	2	98439	3	152526	6
Yamagata	Yamagata	140.3	38.3	7470	2	33705	2	93507	3	151266	5
Fukushima	Fukushima	140.5	37.8	7700	2	33761	2	90383	3	141808	6
Tochigi	Utsunomiya	139.9	36.5	8225	2	34801	3	87322	4	130099	7
Gunma	Maebashi	139.1	36.4	8118	2	33886	2	85346	4	129348	7
Ibaraki	Mito	140.5	36.4	8055	2	35617	3	89462	4	130360	7
Saitama	Urawa	139.6	35.9	7203	2	33824	2	86340	4	132874	7
Tokyo	Tokyo	139.8	35.7	8452	2	35896	3	86063	4	124437	7
Chiba	Chiba	140.1	35.6	8241	2	36946	3	88904	4	125966	7
Kanagawa	Yokohama	139.7	35.4	7830	2	35640	3	87966	4	124887	7
Niigata	Niigata	139.1	37.9	8179	2	34868	2	88111	3	141003	6
Toyama	Toyama	137.2	36.7	7797	2	34113	3	88295	3	134260	6
Nagano	Nagano	138.2	36.7	7409	2	30934	2	85696	3	144330	5
Ishikawa	Kanazawa	136.6	36.6	8812	2	35165	2	85805	4	135204	6
Fukui	Fukui	136.2	36.1	7938	2	32403	2	82848	3	132106	6
Yamanashi	Kofu	138.6	35.7	7623	2	33070	3	84370	4	126252	7
Gifu	Gifu	136.8	35.4	8337	2	33307	3	80186	4	118653	7
Aichi	Nagoya	137.0	35.2	7755	2	33117	3	81152	4	120332	7
Shizuoka	Shizuoka	138.4	35.0	9202	2	36108	3	81883	5	103529	9
Kyoto	Kyoto	135.7	35.0	8338	2	34445	3	82902	4	121407	6
Shiga	Otsu	135.9	35.0	7509	2	33969	2	86771	4	133690	7
Mie	Tsu	136.5	34.7	8137	2	36188	3	87390	4	121101	7
Nara	Nara	135.8	34.7	7089	2	32523	3	83809	4	125107	7
Hyogo	Kobe	135.2	34.7	8088	2	34909	3	83698	4	120400	7
Osaka	Osaka	135.5	34.7	8709	2	34824	3	80190	4	118851	7
Wakayama	Wakayama	135.2	34.2	8834	2	35590	3	79895	4	115187	8
Tottori	Tottori	134.2	35.5	7983	2	33131	3	82046	4	122957	6
Shimane	Matsue	133.1	35.5	7889	2	34561	2	85753	4	128760	7
Okayama	Okayama	133.9	34.7	7959	2	33869	2	82719	4	122295	7
Hiroshima	Hiroshima	132.5	34.4	8310	2	33059	3	79208	4	114252	7
Yamaguchi	Yamaguchi	131.5	34.2	8054	2	33265	3	80168	4	115333	7
Kagawa	Takamatsu	134.1	34.3	7986	2	34567	3	83093	4	119216	7
Tokushima	Tokushima	134.6	34.1	8781	2	35721	3	81642	4	112909	7
Ehime	Matsuyama	132.8	33.8	9022	2	35039	3	81320	4	111045	8
Kochi	Kochi	133.6	33.6	8956	2	33789	3	77772	4	93972	8
Fukuoka	Fukuoka	130.4	33.6	8991	2	36824	3	85280	4	109356	7
Saga	Saga	130.3	33.2	8216	2	32538	3	77040	4	109119	7
Oita	Oita	131.6	33.2	8465	2	35521	3	84306	4	111834	7
Kumamoto	Kumamoto	130.7	32.8	7802	2	30827	3	73879	4	103158	7
Nagasaki	Nagasaki	129.9	32.7	9511	2	36488	3	81604	4	105251	7
Miyazaki	Miyazaki	131.4	31.9	9801	2	34152	3	73819	4	86007	7
Kagoshima	Kagoshima	130.6	31.6	9758	2	34163	3	72443	4	88288	8
Okinawa	Naha	127.7	26.2	11224	3	31495	4	50057	6	18960	10

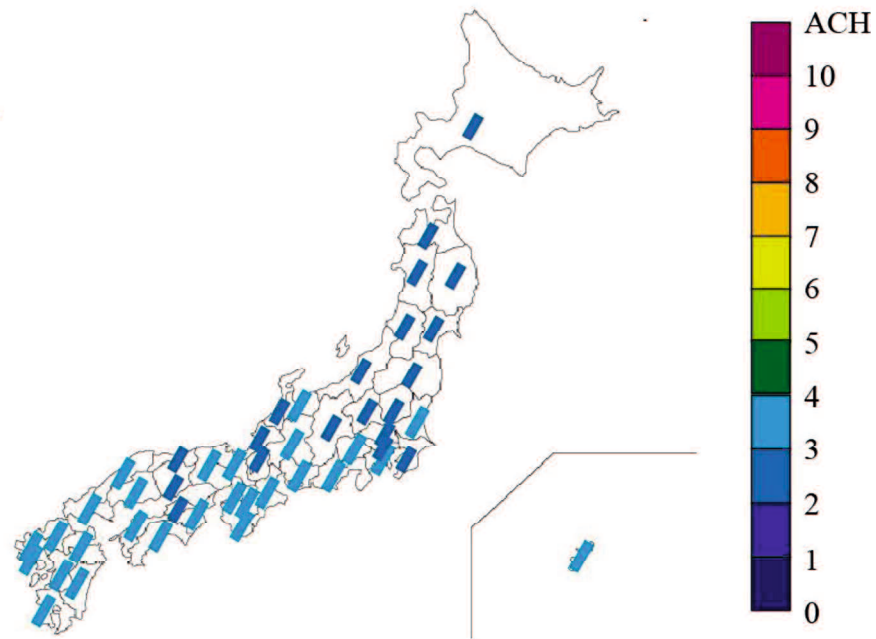


(a) Target air change rates map

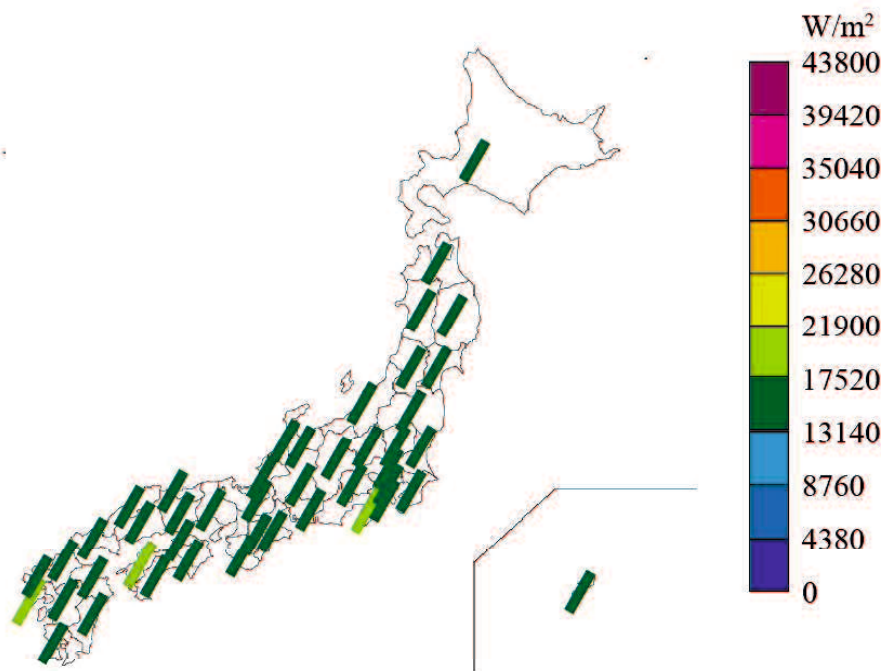


(b) Natural ventilation potentials map; the highest value in the label represents the annual sum of the internal gains

Figure 4. B. 1. Maps with a specific internal gains of 10 W/m<sup>2</sup> in Japan.

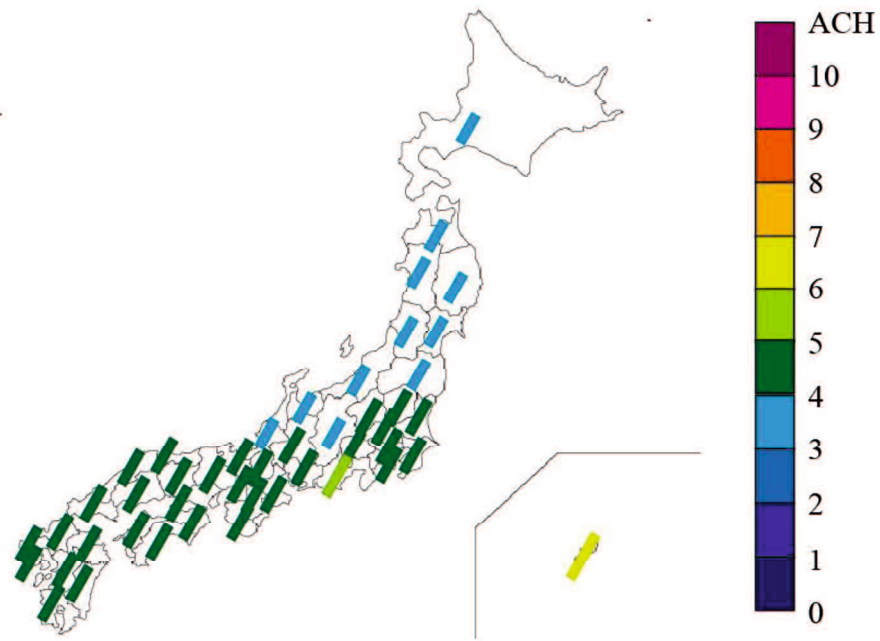


(a) Target air change rates map

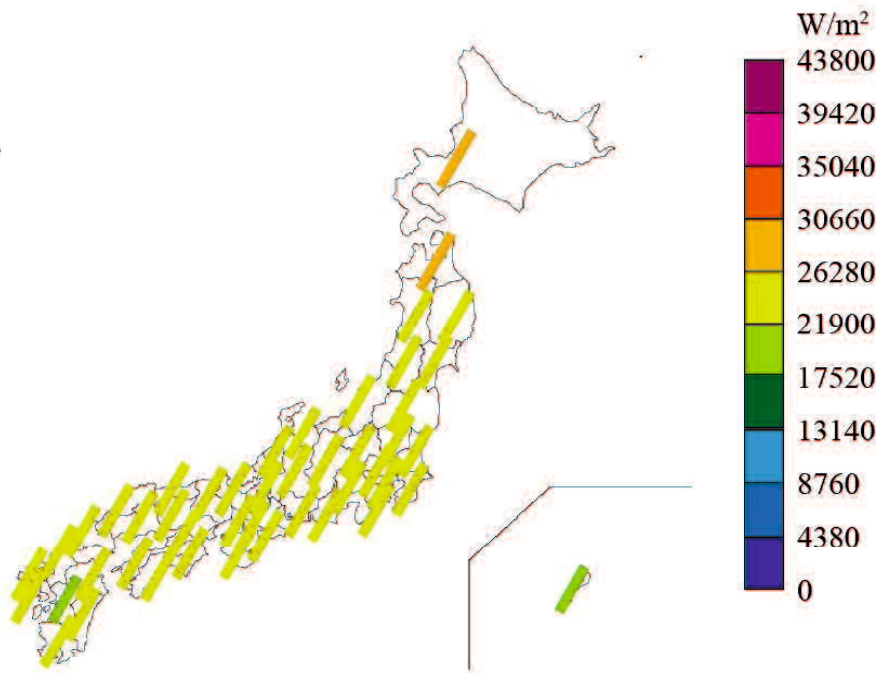


(b) Natural ventilation potentials map; the highest value in the label represents the annual sum of the internal gains

Figure 4. B. 2. Maps with a specific internal gains of 20 W/m<sup>2</sup> in Japan.



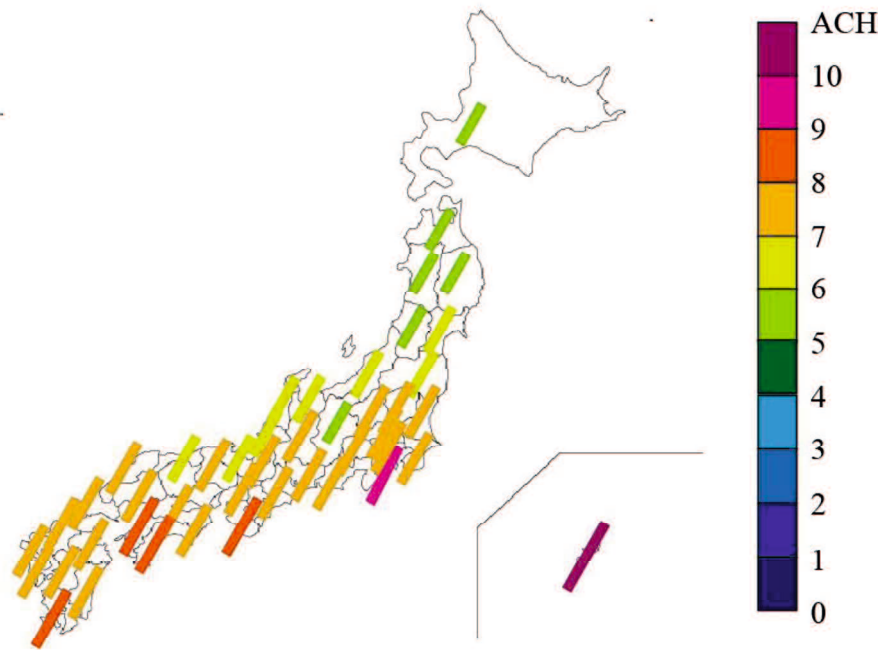
(a) Target air change rates map



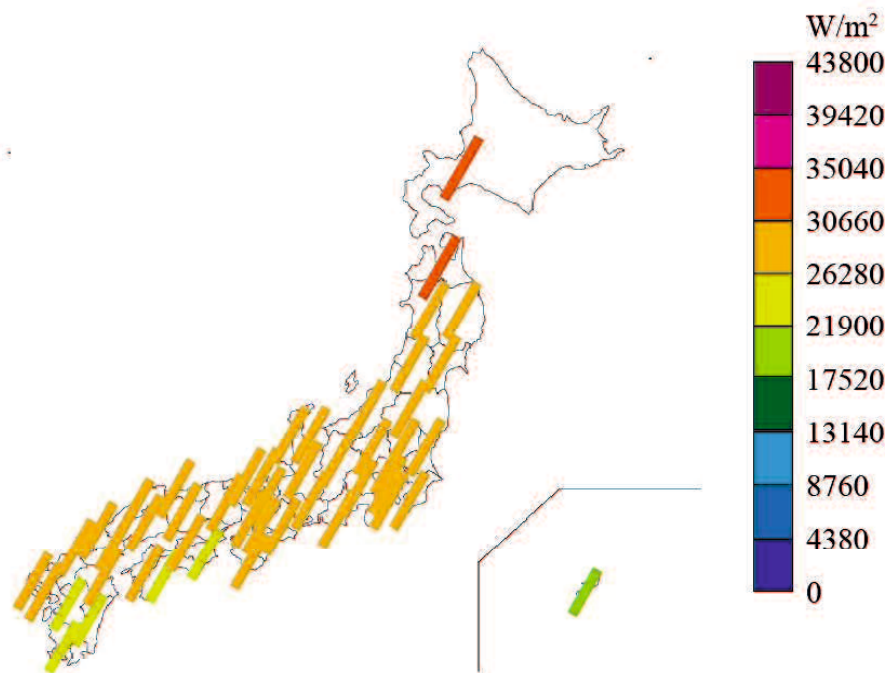
(b) Natural ventilation potentials map; the highest value in the label represents the annual sum of the internal gains

Figure 4. B 3. Maps with a specific internal gains of 40 W/m<sup>2</sup> in Japan.





(a) Target air change rates map



(b) Natural ventilation potentials map; the highest value in the label represents the annual sum of the internal gains

Figure 4. B. 4. Maps with a specific internal gains of 80 W/m<sup>2</sup> in Japan.

## References:

- Abdellatif, M. & Al-Shamma'a, A., 2015. Review of sustainability in buildings. *Sustainable Cities and Society*, 14(1), pp.171–177.
- Abdullah, A.H. & Wang, F., 2012. Design and low energy ventilation solutions for atria in the tropics. *Sustainable Cities and Society*, 2(1), pp.8–28.
- Ai, Z.T. et al., 2016. Ventilation of air-conditioned residential buildings : A case study in Hong Kong. *Energy and buildings*, 127, pp.116–127.
- Al-Obaidi, K.M., Ismail, M. & Abdul Rahman, A.M., 2014. A review of the potential of attic ventilation by passive and active turbine ventilators in tropical Malaysia. *Sustainable Cities and Society*, 10, pp.232–240.
- Artmann, N., Manz, H. & Heiselberg, P., 2007. Climatic potential for passive cooling of buildings by night-time ventilation in Europe. *Applied Energy*, 84(2), pp.187–201.
- ASHRAE. 2009. ASHRAE handbook – fundamentals.
- Axley, J.W., 2001. Application of Natural Ventilation for U. S. Commercial Buildings; Climate Suitability, Design Strategies, & Methods Modeling Studies. *Prepared for U.S. Department of Energy Office of Building Systems*, pp.1–161.
- Chen, X., Yang, H. & Sun, K., 2016. A holistic passive design approach to optimize indoor environmental quality of a typical residential building in Hong Kong. *Energy*, 113, pp.267–281.
- China Meteorological Bureau, Climate Information Center, Climate Data Office and Tsinghua University, Department of Building Science and Technology. 2005. China Standard Weather Data for Analyzing Building Thermal Conditions. Beijing: China Building Industry Publishing House.
- Chou, P.-C. et al., 2008. Natural Ventilation Efficiency in a Bedroom with a Central-Pivoting Window.

- Indoor and Built Environment*, 17(2), pp.164–172.
- Crawley, D.B. et al., 2001. EnergyPlus: creating a new-generation building energy simulation program. *Energy and Buildings*, 33(4), pp.319–331.
- De Dear, R.J. & Brager, G.S., 2002. Thermal comfort in naturally ventilated buildings: Revisions to ASHRAE Standard 55. *Energy and Buildings*, 34(6), pp.549–561.
- Emmerich, S.J., Polidoro, B. & Axley, J.W., 2011. Impact of adaptive thermal comfort on climatic suitability of natural ventilation in office buildings. *Energy and Buildings*, 43(9), pp.2101–2107.
- Etheridge, D., 2014. A perspective on fifty years of natural ventilation research. *Building and Environment*, 91, pp.51–60.
- Feng, W. et al., 2014. Evaluation of Energy Savings of the New Chinese Commercial Building Energy Standard. *The American Council for An Energy-Efficient Economy 2014 Summer Study on Energy Efficiency*, pp.121–132.
- GB50189---2015, Design standard for energy efficiency of public buildings. China P.R: Ministry of Housing and Urban-rural Development [In Chinese].
- Ghiaus, C. & Allard, F., 2006. Potential for free-cooling by ventilation. *Solar Energy*, 80(4), pp.402–413.
- Hiyama, K. & Glicksman, L., 2015. Preliminary design method for naturally ventilated buildings using target air change rate and natural ventilation potential maps in the United States. *Energy*, 89, pp.655–666.
- Holford, J.M. & Hunt, G.R., 2003. Fundamental atrium design for natural ventilation. *Building and Environment*, 38(3), pp.409–426.
- Ji, Y., Lomas, K.J. & Cook, M.J., 2009. Hybrid ventilation for low energy building design in south China. *Building and Environment*, 44(11), pp.2245–2255.

- Khan, N., Su, Y. & Riffat, S.B., 2008. A review on wind driven ventilation techniques. *Energy and Buildings*, 40(8), pp.1586–1604.
- Li, A. G. & Jones, P.J., 2000. Developments in Strategies Used for Natural and Mechanical Ventilation in China. *Indoor and Built Environment*, 9(2), pp.65–74.
- Oropeza-Perez, I. & Østergaard, P.A., 2014a. Energy saving potential of utilizing natural ventilation under warm conditions - A case study of Mexico. *Applied Energy*, 130, pp.20–32.
- Oropeza-Perez, I. & Østergaard, P.A., 2014b. Potential of natural ventilation in temperate countries - A case study of Denmark. *Applied Energy*, 114, pp.520–530.
- People's Education Press. 2015. Eighth Grade Geography. People's Education Press. Beijing: People's Education Press. [In Chinese].
- Salcido, J.C., Raheem, A.A. & Issa, R.R.A., 2016. From simulation to monitoring: Evaluating the potential of mixed-mode ventilation (MMV) systems for integrating natural ventilation in office buildings through a comprehensive literature review. *Energy and Buildings*, 127, pp.1008–1018.
- Taleb, H.M., 2015. Natural ventilation as energy efficient solution for achieving low-energy houses in Dubai. *Energy and Buildings*, 99, pp.284–291.
- Tejero-González, A. et al., 2016. Assessing the applicability of passive cooling and heating techniques through climate factors: An overview. *Renewable and Sustainable Energy Reviews*, 65, pp.727–742.
- Tong, Z. et al., 2016. Energy saving potential of natural ventilation in China: The impact of ambient air pollution. *Applied Energy*, 179, pp.660–668.
- Wen, L., Hiyama, K., and Koganei, M., A Method for Creating Maps of Recommended Window-to-Wall Ratios to Assign Appropriate Default Values in Design Performance Modeling: A case study of a typical office building in Japan. *Energy and Buildings*, in process.

- Yao, R. et al., 2009. Assessing the natural ventilation cooling potential of office buildings in different climate zones in China. *Renewable Energy*, 34(12), pp.2697–2705.
- Yik, F.W.H. & Yu Fat Lun, 2010. Energy Saving by Utilizing Natural Ventilation in Public Housing in Hong Kong. *Indoor and Built Environment*, 19(October), pp.73–87.
- Zhang, Y. et al., 2015. China's energy consumption in the building sector: A life cycle approach. *Energy and Buildings*, 94, pp.240–251.

## 5.

# Conclusions

Building design is challenged by the increasing demand of energy efficiency and indoor environment. The results of building performance simulations provide useful feedback which can guide the design towards better performance. Especially, building performance simulations are increasingly required to be integrated into the early design stages because that the design decisions made in these stages significantly impact the final performance of buildings. However, the numerous uncertainties on design variables during the early design stages complicate the integration of this early building performance simulation which is defined as design performance modeling (DPM) by American Institute of Architects (AIA). In addition, insufficient intelligence approaches which can be used to inform design decisions based on the analysis results also impedes the exertion of the effect of DPM in guiding the design towards better performance.

The main purpose of this thesis is to develop flexible approaches for facilitating the high accuracy and efficiency implementation of DPM towards performance-based design decisions making. To achieve this goal, we conduct the study in two aspects. The first aspect is to develop approaches for assigning robust default values, which are defined as tentative values, for the uncertain design parameters required by DPM for discussing a target design variable. The other aspect is to develop an efficient approach for assisting the implementation of DPM and informing the corresponding design decisions based on the modeling results. To determine the inputs this thesis selected to support their default values assignment in the first aspect of this study, a review study on ten simple building performance evaluation tools which are supposed to be adopted to perform DPM in this thesis is carried out in Chapter 1. To support the default WWR value assignment, the creation method of

recommended WWR maps is proposed in Chapter 2. Chapter 3 develops an efficient approach for performing DPM to assist the determination of optimal window geometry including window height, window width and window location in the floor. It is realized by the creation of response surface between window geometry and building performance. Chapter 4 describes a developing approach from an earlier study for supporting the data filling associated with natural ventilation for DPM through the creation of target air change rate maps. Chapter 5 summaries the key findings and the further work of our study.

## **5.1 Key findings of this study**

### **Object inputs selected to support their default values assignment**

The necessary inputs of ten simple tools and their organization measures are reviewed to find the inputs which are difficult to be accessed in the design practice. An additional criteria is that the inputs have a major impact on the evaluation results. As a consequence, window configuration including rough window area and window geometry, and natural ventilation information setting of air change rate and rough natural ventilation strategies are selected as the support objects of this thesis.

### **Approach for assigning the default value of rough window area: A method for creating recommended window-to-wall ratios (WWR) maps to provide information on optimal window area for DPM**

A methodology for creating maps of recommended WWR is proposed to assign appropriate default WWR values in DPM. This is accomplished using integrated thermal and daylighting simulations and optimizations. A case study is conducted to create recommended WWR maps in Japan. The novelty

of the proposed maps is to show architects with the recommended setting direction of WWR towards which building performance becomes better in contrast to global optimal default values.

The main findings in this Chapter are summarized as follows:

- The possible distribution of optimal WWR under different design conditions of lighting power density, climate, window orientation, internal gains, building scale, and glazing are summarized as three overall patterns according to the integrated simulations: (i) the smaller the WWR is, the lower the CO<sub>2</sub> emissions are; (ii) an appropriate WWR value exists (in the range of 30-50 %) to minimize the CO<sub>2</sub> emissions; and (iii) the larger the WWR is, the lower the CO<sub>2</sub> emissions are. When the double low-E glazing is adopted, both the exact optimal WWR value and the distribution of optimal WWR are verified to be influenced by lighting power density, climate, window orientation, and building scale. The impact of internal gains on the distribution of optimal WWR was observed for the future lighting load of 5 W/m<sup>2</sup>. However, the exact optimal WWR values increased by only 10 % when the internal gains increased to a higher level.
- Quantitative evaluation was performed to determine the impact of each design condition on the optimal WWR configuration. This evaluation was conducted by examining the increase in CO<sub>2</sub> emissions when the determined optimal WWR is adopted in cases with variable design conditions. Quantitative evaluation indicated that the optimal results determined for medium internal gains and a small-scale building are sufficiently robust for a building with variable internal gains and building scale. However, the conditions of lighting power density, climate, and window orientation showed strong impacts on the optimal WWR configuration. Thus, the optimization results of 10 locations in four main orientations under two lighting power densities are processed according to the patterns of optimal WWR distribution to generate the maps of recommended WWR in Japan for current (10 W/m<sup>2</sup>) and future (5 W/m<sup>2</sup>) lighting conditions.
- For the current lighting condition, a larger WWR default value was always recommended for



cities located in zones 1-5 and Tokyo, which is located in zone 6 of the Japan climate regions, regardless of window orientation. For the remaining locations, a moderate default value of WWR (30-50 %) was suggested for the eastern façade.

- The recommended WWR tended to decrease as the lighting efficiency further improved, especially in the temperate and warm climate zones 4-8 of the Japan climate regions. A moderate or smaller default value should be carefully assigned according to window orientation. In addition, glass façade was not suggested to be installed for the east-facing orientation in these zones.

### **Approach for assigning the implementation of DPM: A method for creating response surface to provide information on optimal window geometry**

A procedure for creating response surfaces between window geometries and building performance is developed to support the assignment of window geometry, i.e., window height and window width. It is achieved by combining the analysis results of dynamic daylighting simulation and energy simulation. The response surfaces can not only show architects with the optimal solution but also help architects to understand to what extent they can widen or narrow the window geometry without significantly decreasing the building performance. The novelty of the proposed procedure is to address the enormous number of simulation for exploring the surface features. It is realized by the adoption the link between daylight factor (DF) and continuous daylight autonomy (cDA). In case studies, the daylighting simulation tool of DAYSIM and energy simulation tool of EnergyPlus are used to create response surfaces. The impact of COPs for the cooling/heating systems on the features of the response surface can be easily determined. Higher COP results in a narrow selectable design range of window geometry in case where the same percentage of building performance degradation is acceptable.

The error caused by employing the proposed method is analyzed by comparing the results with detailed simulation results. Regarding the use of the link between the DF and cDA, the estimated cDA

in the proposed method is compared with simulation out-puts using DAYSIM. The differences are negligible. With respect to the method for integrating cDA into energy simulation outputs, the validity is evaluated through detailed results simulated by EnergyPlus alone with the lighting control function using two sensor locations. These differences are also negligible. Furthermore, the results demonstrated that the differences caused by the difference in the simulation algorithm for the daylighting calculation are relatively significant compared with the error due to the proposed procedure. In this context, the proposed study also has significance to enable the combination of different daylighting simulation tools with energy simulations. Moreover, this coupling can remove the constraints on the number of lighting sensors, in which only two lighting sensors are integrated into the validation process because of the limitation of the daylighting function in EnergyPlus.

**Approach for assigning the default value of air change rate for natural ventilation:  
Target air change and natural ventilation potential maps for assisting with  
preliminary natural ventilation design**

A method for supporting strategic design of natural ventilation that relies on the target air change rate was developed by the authors in an earlier study. The authors defined target air change rate as an air change rate at which the increase in cooling effect from natural ventilation reaches the maximum value. The availability of the proposed method is further verified by the application for China. The verified results are reported in this Chapter. Case studies are firstly conducted to examine the robustness of the target air change rate by using a typical Chinese office building model with representative operation conditions in five climate zones of China. The impacts of insulation level, thermal capacity, and window-to-wall ratio (WWR) on target air change rate are investigated. Then, the target air change rate and natural ventilation potential maps in China are created based on this verified method.

Some specific findings based on the created target air change rate and natural ventilation potential maps in China are summarized as follows:

- Simple natural ventilation strategies (category (i)), i.e., single-sided natural ventilation, are recommended for buildings with relatively low internal gains (such as 10 W/m<sup>2</sup> and 20 W/m<sup>2</sup>) to realize the required small target air change rate ( $\leq 3$  ac/h), regardless of the climate conditions. These simple options can simultaneously satisfy the requirements of high energy performance and the cost-effectiveness.
- For buildings with moderate internal gains of 40 W/m<sup>2</sup>, the categories of design strategies for natural ventilation are distinguished by the Yangtze River. Well organized and examined natural ventilation strategies (category (ii)) are suggested for cities located south of the Yangtze River. This result is especially obvious for locations in the Hot Summer and Warm Winter zone and the Temperate zone. However, in comparison with the hot-humid climate in the Hot Summer and Warm Winter zone, careful consideration of the natural ventilation design is strongly recommended for the cities located in the Temperate zone with a warm climate due to the higher cooling effect potential.
- Careful natural ventilation design (category (ii)) in the early design stages is required in all the selected cities to achieve a moderate and realizable target air change rate of 4-10 ac/h when the internal gains are increased to the relatively high level of 80 W/m<sup>2</sup>. In addition, the increase in cooling effect potential of natural ventilation in the Severe Cold and Cold zones is very obvious. Therefore, it is more effective to elaborately organize the natural ventilation strategies for buildings in cold climate when the internal gains are increased.
- According to the results of this study, no location is classified as category (iii), which corresponds to a target air change rate of more than 10 ac/h. A measurable cooling effect can be realized by using the available natural ventilation strategies under various climate conditions in China, even

with high internal gains

## 5.2 Further studies

According to the review study in Chapter 1, the data filling on window configuration, natural ventilation, and shading device are necessary when DPM is performed during the early design stage. The approaches developed in this thesis mainly focus on the default value assignment of window configuration and natural ventilation. The settings of shading device simultaneously impact the daylighting performance and cooling load in office building. It also significantly influences the results of DPM. Therefore, measures for supporting the data filling associated with shading device are scheduled to be carried out in the future study.

The recommended WWR maps presented in Chapter 2 is suitable for the office building designed with open concept. For the office building divided into small cells, the distribution of optimal WWR pattern requires further investigation. The relevant maps should be generated based on the overall distribution of optimal WWR originated from the simulation results adopting a standard cell as model.

Large cooling load appears in many office building even in winter due to the relatively higher internal gains. The evaluation method of target air change rate described in Chapter 4 majorly intends to examine the cooling effect from natural ventilation. The evaluation of the climate suitability of natural ventilation considers the upper limit of the outdoor temperature and the humidity control. The lower threshold of the outdoor temperature is not limited. The outdoor air with much significantly lower temperature gives rise to cold draft and further affects the comfortability of occupant. Accordingly, the limit conditions of climate suitability of natural ventilation would be improved to confirm the thermal comfort of occupant in further study.